

**CuInS<sub>2</sub> thin films using chemical methods for the  
fabrication of CuInS<sub>2</sub>/CdS solar cells**

*Thesis submitted to  
~~Cochin~~ University of Science and Technology  
for the award of the degree of*

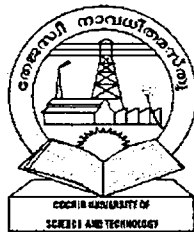
***Doctor of Philosophy***

By

Bini.S

Department of Physics  
Cochin University of Science and Technology  
Kochi-682 022, India.

2003



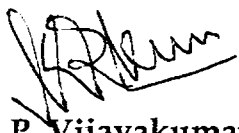
Department of Physics  
Cochin University of Science and Technology  
Cochin – 682 022

---

### CERTIFICATE

Certified that the work presented in this thesis entitled “**CuInS<sub>2</sub> thin films using chemical methods for the fabrication of CuInS<sub>2</sub>/CdS solar cells**” is based on the bonafide research work done by Ms. Bini S under my guidance, at the Department of Physics, Cochin University of Science and Technology, Cochin – 682 022, and has not been included in any other thesis submitted previously for the award of any degree.

Cochin - 22  
08.05.2003

  
Prof. K. P. Vijayakumar  
(Supervising Guide)

## DECLARATION

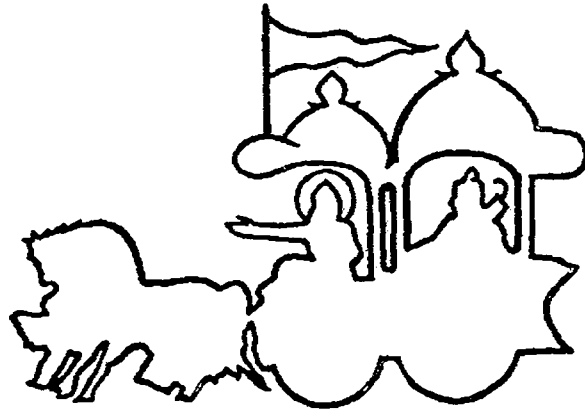
---

Certified that the work presented in this thesis entitled “**CuInS<sub>2</sub> thin films using chemical methods for the fabrication of CuInS<sub>2</sub>/CdS solar cells**” is based on the original research work done by me under the guidance and supervision of Prof. K. P. Vijayakumar, Department of Physics, Cochin University of Science and Technology, Cochin - 22 and has not been included in any other thesis submitted previously for the award of any degree.

Cochin - 22  
08.05.2003



**Bini S.**



*“ Your right is to work only, but never to the fruit of that.  
Let not the fruit of action be your object,  
nor let your attachment be to inaction ”*

*(Bhagavadgita 2/47)*

## *Acknowledgement*

*At the outset may I express my sincere and heartfelt gratitude to Dr.K.P.Vijayakumar, my supervising guide for his smart guidance and timely motivations. Moreover, being the Head of the department, he was kind enough to provide all the facilities available at the Department.*

*Next I would like to thank Dr.C.Sudha Kartha whose encouragements and valuable advices were equally important for the timely completion of this work.*

*I am also thankful to Dr.N.Unnikrishnan Nair, Vice chancellor of CUSAT for providing necessary facilities and financial assistance in the form of fellowship.*

*I remember with gratitude the facilities provided by Prof. Elizabeth Mathai, Prof. K. P Rajappan Nair, Prof. M. Sabir and Prof. K. Babu Joseph, former Heads of the department of Physics, CUSAT.*

*During present work, a part of sample characterisation was done at Iwate University, Morioka, Japan, through our collaboration with Prof.Y. Kashiwaba. I take this chance to express my deep gratitude to Prof. Y. Kashiwaba. Also, I express my sincere thanks to Dr.T.Abe for carrying out XPS measurement, and Dr. Yasuhiro Kashiwaba , Sendai National College of Technology, Japan for thickness measurement. I am thankful to*

*Director, Sree Chitra Tirunal Institute of Medical Science & Technology for granting me permission for SEM analysis.*

*I acknowledge the assistance from UGC through DSA-COSIST scheme. Supports from Ministry of Non-conventional Energy Sources, DST, and ANERT are also gratefully acknowledged.*

*Words are insufficient to express my gratitude to my colleagues Ms. Bindu K, Ms. Teny Teresa John , Mr. Ram Kumar. S, Mrs. Syamala S.B, Mr. Paulraj M, Mrs.Rupa R. Pai, Mr. Wilson K.C, Mr. Ratheesh Kumar P.M, Ms. Beena Mary John, Mr.Arun B, and Mr.Sreekumar. I am thankful to my seniors and other research Scholars of this department for their moral support.*

*I am highly indebted to Sri. Chulliyarambil Balakrishnan, Manager, National H S S, Engandiyoor for his fatherly advices and motivations in the hour of need. Also I would be grateful to our principal Mr.V Premlal for his inspirations, and management committee for the support. I shall always remember with pleasure the help and co-operation extended by my colleagues.*

*I thank every members of my family for being always a source of inspiration. I appreciate their patience and understanding. They were the chief force behind the successful completion of this work.*

*Dedicated*  
*to*  
*my Parents, Teachers, Husband & Daughter*

# Contents

Preface	
List of publications	
Chapter 1	
Solar cells:An introduction .....	1
Chapter 2	
Review on copper indium sulfide films and cells .....	45
Chapter 3	
Preparation of $\text{CuInS}_2$ thin films starting from CBD $\text{Cu}_x\text{S}$ and CBD $\text{CdS}$ .....	90
Chapter 4	
Studies on $\text{CuInS}_2$ thin films prepared using chemical spray pyrolysis technique .....	141
Chapter 5	
Fabrication and characterisation of all-sprayed $\text{CuInS}_2/\text{CdS}$ solar cells.....	192
Chapter 6	
Summery and conclusion .....	218



## Preface

Today, in this time of scarcity of conventional energy sources, photovoltaics is viewed as an ideal way to produce eco-friendly power from a virtually inexhaustible source without noise or pollution. Based on semiconductor technology, solar cells operate on the principle that electricity will flow between two p and n type semiconductors when they are put in contact with each other and exposed to light (photons). When photons strike a solar cell, electrons are set free from the semiconductor atoms. These free electrons can be channeled to flow through the solar cell's built-in circuit, producing electricity. By linking a number of solar cells together, a useful flow of direct current (DC) electricity can be generated. Photovoltaic-generated electricity can be used as is, or stored in a battery for consumption in a later time, or converted to alternating current (AC) by an inverter.

In general, PV materials are categorized as either *crystalline* or *thin film* and are judged on two basic factors viz, efficiency (how much of the sun's light they transform into usable electricity) and economics (how difficult and how expensive they are to manufacture). The cost of PV systems is a key factor affecting large-scale applications and improvements in conversion efficiency will help to reduce the cost. Since the first photovoltaic panel was developed in 1954, the efficiency of solar cells has risen steadily. Because of the continuing improvements in PV technology, declining prices and new markets, the PV business is likely to grow by 20%-30% annually in the next few decades.

Lowering the cost of solar cell production is one of the most important intentions in photovoltaic research. To achieve this, it is necessary to develop new or improved thin-film materials with good photovoltaic properties and appropriate band gaps, that can be deposited rapidly and uniformly over large areas.

Semiconductor materials most frequently used in thin film technology are silicon, copper indium diselenide, or cadmium telluride. Amorphous silicon is the only thin-film technology that already has a substantial market share (15%), and it is generally believed to be the first thin-film technology that can compete with crystalline silicon. However, thin film silicon cells lack the ordered structure and inherent photovoltaic properties of crystalline silicon, and its present efficiency is 13.5%. CdTe is close to an ideal photovoltaic material with respect to its physical properties with a bandgap close to the optimum. Laboratory cells have already reached efficiencies over 16%. One major drawback is the high content of cadmium which gives rise to environmental concerns. Copper indium diselenide (CIS) is one of the most promising thin film materials today. With the incorporation of gallium,  $\text{Cu(In,Ga)Se}_2$  has reached the highest efficiencies of all thin film cells. The record laboratory efficiency recently announced by ENREL is an impressive 18.8%, small modules are at 14% and large modules at 11%-12%. This has motivated several research groups to carryover extensive research in CIS based cells. However, the optical bandgap of CIS (1.02 eV) is quite small. Moreover, selenium raises apprehension for consumers for ecological reasons. Therefore, elimination of selenium in the compound used is viewed as a major contribution to mitigate the negative environmental perception. One possibility is to substitute S to Se and prepare  $\text{CuInS}_2$  thin films.

$\text{CuInS}_2$ , which is the material for the present study has great potential for photovoltaic applications due to its optimum direct bandgap of 1.53eV and high absorption coefficient.  $\text{CuInS}_2$  can be obtained in both n and p-type so that fabrication of homojunction solar cells is possible. When they are paired with CdS, they are found to have a compatible lattice structure with acceptable lattice mismatches and differences in electron

affinities favorable for the formation of heterojunctions. The material has a number of additional potential advantages in comparison with CIS. These include the significantly reduced toxicity and abundance of its constituents, which makes it suitable for terrestrial as well as space applications. The highest conversion efficiency reported recently for  $\text{CuInS}_2$  based solar cells is 12.5%

$\text{CuInS}_2$  films have been prepared using different techniques such as vacuum evaporation, chemical vapor deposition, flash evaporation, rf sputtering, sulfuration of  $\text{CuIn}$  alloys, electrodeposition, chemical bath deposition and chemical spray pyrolysis (CSP). For economic reasons, it will be very interesting to deposit this film using a low-cost deposition technique. In our lab, we prepared  $\text{CuInS}_2$  thin films using chemical bath deposited (CBD)  $\text{Cu}_x\text{S}$  for the first time. This is quite new technique and has the potential of being low in cost, as the preparation of  $\text{Cu}_x\text{S}$  film is carried out by the simple and low cost chemical bath deposition technique at room temperature itself. This is a zero energy process as no substantial amount of energy is required for the process. Also we used spray pyrolysis, which is another low cost deposition technique, for preparing device quality  $\text{CuInS}_2$  thin films with good photo response. We could fabricate  $\text{CuInS}_2/\text{CdS}$  solar cells using these films.

This thesis contains results of the work done in the Thin Film Photovoltaic Division of the Dept. of Physics, CUSAT and is organized into six chapters, with introduction, conclusion and references. The chapter-wise description of the contents is given below.

**Chapter-1** is a general introduction to solar cells. It starts with a brief history of solar cells and describes principle and theory of solar cell operation. Later description of different solar cell structures and the various factors affecting its efficiency are also

included. Some important thin film solar cells are also mentioned in this chapter. The chapter ends mentioning the scope and importance of present work.

**Chapter-2** presents an exhaustive review on Copper indium sulfide films and  $\text{CuInS}_2$  based solar cells.

**Chapter-3** has two parts. The first part deals with the preparation of copper indium sulfide films using CBD copper sulfide films and advantages of this deposition technique are hinted. Experimental details and characterization of the films using XRD, absorption and transmission studies, XPS along with brief description of the different characterization techniques are also included.

Second part of this chapter describes an attempt to prepare copper indium sulfide films using copper sulfide films, which are prepared through the conversion of cadmium sulfide films. The important results, advantages and drawback of this method are highlighted.

**Chapter-4** mainly deals with the preparation and characterization of copper indium sulfide films using chemical spray pyrolysis. This technique is essentially suitable for the solar cell production, because large-area deposition of thin films with low cost is possible and it is one of the chemical techniques suitable for a molecular level design of thin films. Many groups were successful in preparing  $\text{CuInS}_2$  films using this technique. We prepared films by systematically varying the copper to indium ratio and copper to chalcogen ratio in the initial spray solution, at different substrate temperatures. Structural, electrical and optical characterization of all the films obtained was carried out. It is found that the chemical composition of the solution controls the film resistivity and photo response very much as it affects the stoichiometry of the film. We could optimize the composition of the solution to get good values of film resistivity and photo- response. We have selected the

best film in terms of photo response and electrical resistivity to fabricate solar cell structure with CdS.

**Chapter-5** describes the fabrication of CuInS<sub>2</sub>/CdS solar cells by an “all-spray” method. The bottom electrode SnO<sub>2</sub> is deposited at a temperature of 450<sup>0</sup>C. Over this, the absorber layer CuInS<sub>2</sub> is deposited at a temperature of 300<sup>0</sup>C and finally the window layer CdS is sprayed at the same temperature. Cells were fabricated by varying the thickness of both the window and absorber layer. The current-voltage characteristics of the cells fabricated are discussed and the cell conversion efficiencies are calculated.

**Chapter-6** is a summary of whole work done. The important results are highlighted. The chapter ends with a note on the environmental and safety aspects of the materials and the thin film deposition techniques used in the present work

## LIST OF PUBLICATIONS

### Journal/ conference papers

1. Preparation of  $\text{CuInS}_2$  thin films using CBD  $\text{Cu}_x\text{S}$  films.  
**S.Bini**, K.Bindu, M.lakshmi, C Sudha Kartha, K P Vijayakumar,  
Y.Kashiwaba,T.Abe  
*Renewable Energy* , 20(2000) 405
2.  $\text{CuInS}_2$  thin films using a new technique  
**S.Bini**, K.Bindu, M.lakshmi, C Sudha Kartha, K P Vijayakumar,T.Abe,  
Y.Kashiwaba,  
*Proceedings of the DAE Solid State Physics Symposium, Kurukshetra  
University, Kurukshetra, 41 Dec 27-31, (1998), 489*  
[Also presented at the 53<sup>rd</sup> meeting of the Tohoku branch of The Japan Society  
of Applied Physics, Dec, 1998, Sendai ,Tohoku University,Japan]
3. Electrical and structural characterisation of spray pyrolysed  $\text{CuInS}_2$  thin films  
**S.Bini**, K.Bindu, M.lakshmi, C Sudha Kartha, K P Vijayakumar  
*Workshop on Complete Cycle Charaterisation of Materials, Organised by  
MRSI, IGCAR Kalpakkam, Sep. 12-14, 2001*
4. Characterisation of spray pyrolysed indium sulfide thin films  
Teny Theresa John, **S Bini**, Y Kashiwaba, T Abe, Y Yasuhiro, C Sudha Kartha,  
K P Vijayakumar  
*(Accepted for publication in Semiconductor Science and Technology)*
5. Amorphous Selenium thin films prepared using CBD:Optimization of the  
deposition process and Characterization  
Bindu. K, Lakshmi. M, **Bini. S**, Sudha Kartha. C, Vijayakumar. K.P, Abe. T and  
Kashiwaba.Y  
*Semiconductor Science and Technology*, 17(2002)270
6. Chemical bath deposition of different phases of copper selenide thin films by  
controlling bath parameters  
M.lakshmi. K.Bindu, **S.Bini**, K P Vijayakumar, C Sudha Kartha,T.Abe,  
Y.Kashiwaba.  
*Thin Solid Films*, 370 (2000) 89

7. Reversible  $\text{Cu}_{2-x}\text{Se} \leftrightarrow \text{Cu}_3\text{Se}_2$  phase transformation in copper selenide thin film prepared by chemical bath deposition  
M. Lakshmi, K. Bindu, **S. Bini**, K.P. Vijayakumar, C. Sudha Kartha, T.Abe, Y.Kashiwaba  
*Thin Solid Films*, 386(2001)127
8. Structural and Optical absorption changes of chemically prepared  $\text{Cu}_{2-x}\text{Se}$  due to Indium diffusion  
K. Bindu, M. Lakshmi, **S. Bini**, C Sudha Kartha and K. P.Vijayakumar.  
*DAE, Solid State Physics Symposium, IGCAR, Kalpakkam, Dec 20 –24, 1998*
9. CBD – A technique to prepare different phases of Copper Selenide  
K. Bindu, M. Lakshmi, **S. Bini**, C Sudha Kartha and K. P.Vijayakumar.  
*Proceedings of the DAE Solid State Physics Symposium, Kurukshetra University, Kurukshetra, 41(1998) Dec 27 –31, 487*
10. Preparation of Pyrite ( $\text{FeS}_2$ ) Thin Films Using Chemical Bath Deposition Technique: An attempt  
M.Lakshmi, K.Bindu, **S.Bini**, C.Sudha Kartha, and K.P.Vijayakumar,  
*ANERT National Conference , Trivandrum ,Feb 1999.*

## Chapter-1

### SOLAR CELLS: AN INTRODUCTION

1.1 Introduction .....	3
1.1.1 Brief history of solar cells .....	5
1.2 Principle of solar cell operation .....	6
1.3 Solar Cell Structures .....	6
1.3.1 Semiconductor- semiconductor homojunctions .....	7
1.3.2 Semiconductor- Semiconductor heterojunctions .....	8
1.3.3 Schottky Barriers (Metal- Semiconductor heterojunctions) .....	9
1.3.4 Buried or heteroface junctions .....	11
1.3.5 Alternative device structures .....	12
1.4 Theory of semiconductor solar cell structures .....	13
1.4.1 Semiconducior-Semiconductor Homojunctions .....	13
1.4.1.1 Electrostatics of p-n junction .....	13
1.4.1.2 Junction Capacitance.....	15
1.4.1.4 More realistic photovoltaic model .....	21
1.4.2 Theory of Heterojunctions .....	23
1.4.2.1 Energy-band diagram and static characteristics .....	23
1.4.2.2 Current Transport .....	24
1.4.3 Solar cell output parameters .....	26
1.4.4 Spectral response.....	28
1.5 Factors influencing efficiency of Solar cells.....	28
1.6 Efficiency Measurement .....	31
1.7 Thin Film Solar cells.....	32
1.8 Scope of present work.....	39



1.9 Conclusion.....	40
References .....	41

## Chapter-1

### SOLAR CELLS: AN INTRODUCTION

#### 1.1 Introduction

Solar electricity, produced by photovoltaic devices, is one of the most promising options whose capabilities and potentials are yet to be identified for sustainably providing the world's future energy requirements. Photovoltaics (PV) involve direct conversion of sunlight into electricity using thin layers of material known as 'semiconductors', which are having electrical properties intermediate between those of metals and insulators. Basic energy supply for a solar cell is photons of the solar spectrum and product is usable electrical energy.

This conversion has the advantage that it introduces no direct contamination to environment. PV cells have an important feature that the voltage of the cell does not depend on its size, and remains fairly constant with changing light intensity. However, the current in a device is almost directly proportional to light intensity and size.

Global annual production of PV devices has about 18-20% growth per year during the last 20 years. This is mainly because of its increasing penetration into remote applications for telecommunications, water pumping, telemetry etc. Worldwide PV shipments show a continuous growth over the last two decades. Assuming an average growth rate of 25%, it is expected that PV production would increase to 65GWp/yr in year 2025 (Fig.1.1) [1].

Ever since the first solar cell was developed, PV was dominated by silicon. However, because of its indirect bandgap and low absorption coefficient, silicon is not the ideal material for PV conversion. In spite of this, crystalline silicon today has a market share of 86%, which is almost equally distributed between single crystal and cast

silicon. Main reason for this dominating position is that silicon technology had already been highly developed and good quality material is being produced in large quantities for the popular semiconductor market, especially consumer electronics and telecommunication.

Manufacturing cost for PV systems is dominated by cost of materials used as well as that of the technology for device fabrication. This favors development of thin-film solar cells on low-cost substrates. While thin film cells achieve lower efficiencies than crystalline cells, production process is considerably less expensive. Moreover, as thin film cells can be extremely light and flexible, they can meet a variety of needs for which crystalline solar cells are too big or too rigid. Also a large number of techniques are available for the deposition of different thin films. The challenge is to develop new or improved thin-film materials with good photovoltaic properties and appropriate band gaps that can be deposited rapidly and uniformly over large areas.

Although the technology in the past has been based on silicon wafers, a transition is in progress to a second generation of a potentially low cost thin film technology.

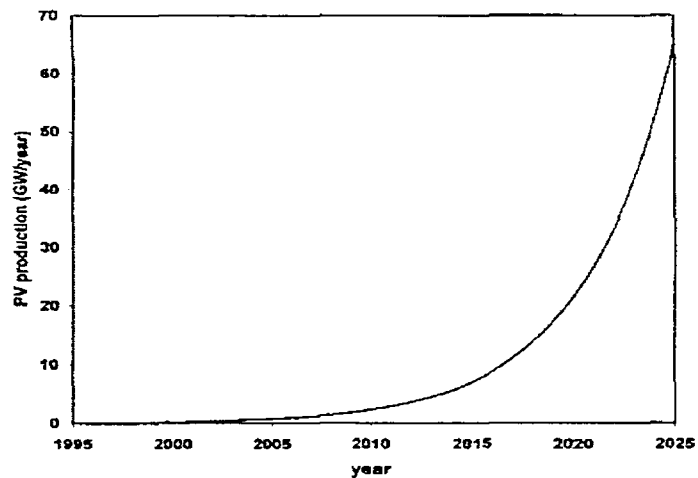


*Fig.1.1 Projected annual PV production assuming 25% growth rate*

### 1.1.1 Brief history of solar cells

Origin of solar cells can be traced back to the discovery of Becquerel in 1839 that a photo voltage resulted from the action of light on an electrode in an electrolyte solution [2]. Later, Adams and Day (1877) observed a similar effect in the solid material selenium shortly after Smith (1873) had demonstrated the phenomenon of photoconductivity in selenium [3]. This was followed by the development of photocells based on both these materials and cuprous oxide. Russel Ohl discovered the first silicon solar cell accidentally in 1940. He was surprised to measure a large electrical voltage from a rod of silicon when he shone a flashlight on it [4]. However, the first efficient silicon solar cell was announced only in 1954 [5].

These cells found application as power sources in space craft as early as 1958. By the early 1960s, design of cells for space application was more or less stabilized [6]. More than thousand satellites using solar cells were launched between 1960 and 1970. However, in the mid 70s efforts were initiated to make solar cells for terrestrial applications and there was a reawakening of interest in terrestrial use of these devices, especially due to oil shortage. In the 1980s, there was a large improvement in technologies resulting in reduction in cost of cells. This opened a new horizon for solar cells in commercial applications [7].

In 1914, solar conversion efficiency of the selenium cell was just 1%. With improved technology, silicon cell efficiency under terrestrial sunlight reached 14% in 1958. Cuprous sulphide/ cadmium sulphide hetero junction was the first all-thin-film photovoltaic system to receive significant attention. First cell of this type, with an efficiency of 6%, was reported in 1954 by Reynolds et al. [8].

At present, a host of new materials are being studied for thin film solar cells and due to the progress of new technologies in material processing and device fabrication, there is considerable improvement in cell efficiency and cost reduction.

## 1.2 Principle of solar cell operation

The most common solar cells are formed by making a junction between n-type and p-type semiconductors and the basic device requirement for photovoltaic energy conversion is an electronic asymmetry in the semiconductor structure. Three major processes are involved in the conversion of sunlight into electrical energy. These are,

- a) Absorption of sun light (photon) in the semiconductor material

Absorption depends on the intensity of the sunlight, the amount of light reflected from the front surface of the solar cell, the semiconductor band gap energy and thickness of the layer.

- b) Generation of electron –hole pairs

When light is absorbed in the semiconductor, a negatively charged electron and a positively charged hole are created.

- c) Separation of charge carriers

Light generated charge carriers are separated by the built-in field existing at the junction. n-type region has large electron densities but low hole densities. Hence, electrons flow readily through such a material while holes find it very difficult. Exactly the same is true for holes in p-type material. The generated electrons flow from p-type region to n-type and hole in the opposite direction. When the illuminated p-n junction is electrically shorted, a current will flow through the short-circuiting lead (Fig.2.2).

## 1.3 Solar Cell Structures

Interfaces between dissimilar materials are important to solar cell devices because they can give rise to built-in fields. Field regions are inherent to solar cell structures and are required for photovoltaic action. There are four principal ways to obtain the internal

field in a semiconducting structure needed to produce photovoltaic behavior: homojunctions, heterojunctions, buried or heteroface junctions, and Schottky barriers. We can classify cells according to the type of inter face structure used to develop the principal field region [9].

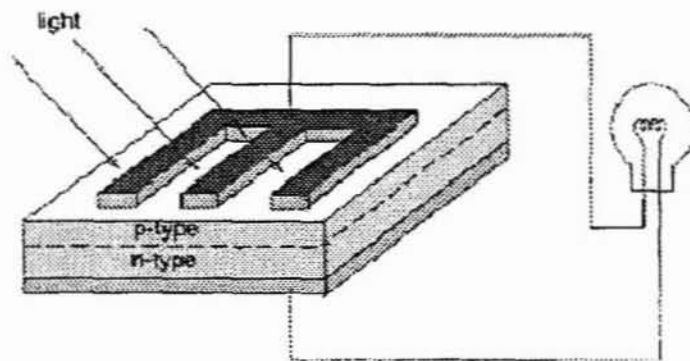


*Fig.2.2 Incoming sunlight is converted to an electrical current flow in a load connected between the cell contacts*

### 1.3.1 Semiconductor- semiconductor homojunctions

A junction between n and p type layers of same semiconductor material is called "homojunction". Usually p-n homojunctions are made by diffusing or implanting one dopant into oppositely doped material. Consequently there are no interface states at the metallurgical junction. Energy band diagram of a p-n abrupt junction is shown in Fig.1.3.

In Semiconductor p-i-n homojunction structure, an intrinsic layer of semiconductor is interjected between two heavily doped regions, which will enhance the built-in electric field, and hence the carrier collection will improve [10].

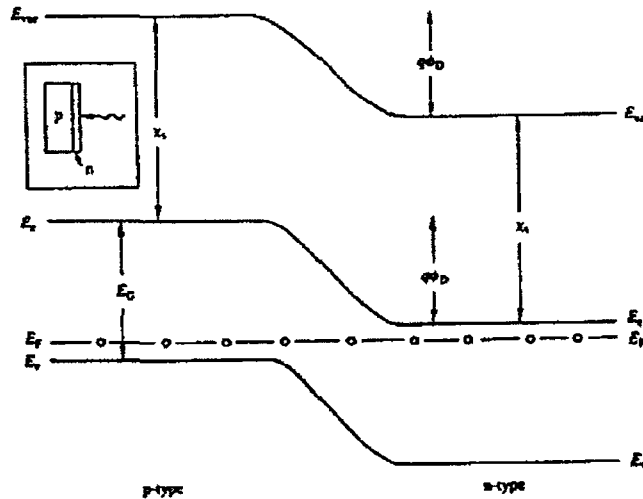


Fig.1.3 Energy band diagram of a p-n homojunction

### 1.3.2 Semiconductor- Semiconductor heterojunctions

A junction formed between a large bandgap (window) material and a low bandgap (absorber) material is known as a “heterojunction”. If conductivity type of these two semiconductors is the same, the junction is called isotype heterojunction and if the conductivity type is different, the junction is called anisotype heterojunction. Energy band diagram of an anisotype heterojunction is represented in Fig.1.4. Brief theory of anisotype heterojunction structure, which is the structure fabricated in the present work, is discussed in the following section.

Main advantages of heterojunction cells are

- i) They allow use of semiconductors, which can only be doped either n-type or p-type
- ii) These have attractive electrical and optical properties and are good from low cost point of view.
- iii) Heterojunctions having window/absorber structure can be formed that protects minority carriers from top surface or bulk recombination sinks.
- iv) These

heterojunction cells are capable of higher efficiencies than homojunction cells due to a better match to the solar spectrum, as there are two band gaps.

However, there are some notable drawbacks and these are listed below. i) If electron affinities and doping levels of the two materials differ very much, these give rise to 'spikes' in the conduction band, which are undesirable for photovoltaic operations. ii) With an ideal case having either small spikes or no spikes at all, the maximum efficiency of a heterojunction cell is limited by the ideal efficiency of the smaller bandgap material. iii) Mismatch between lattice structures of the two materials will give rise to energy levels within forbidden gap, which act as very efficient recombination centers. Hence to produce heterojunctions with nearly ideal properties, it is essential to use semiconductors with nearly identical lattice structures.

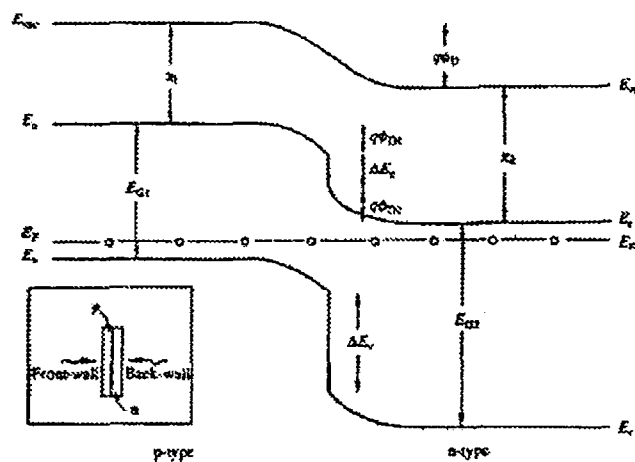


Fig.1.4. Energy band diagram of an anisotype heterojunction

### 1.3.3 Schottky Barriers (Metal- Semiconductor heterojunctions)

When a metal and a semiconductor are brought into contact, because of the differences in the availability of the charge carriers in the metal and semiconductor, all this potential drop occurs on the semiconductor side of the junction. This can give rise



to a depletion region at the interface as in the case of a p-n junction. This type of Schottky diodes has both rectifying and photovoltaic properties. A typical energy band diagram is given in Fig.1.5 [9].

In this type of junctions, it is experimentally observed that since there are a very large number of interface states at the metal-semiconductor interface due to lattice mismatch, the height of the induced barrier at the junction is independent of the work function of the metal. The larger the height of the barrier induced at the junction, the better is the photovoltaic performance of the junction [11].

The main advantage of the Schottky barrier solar cell is that it does not require any high temperature processing and is easy to fabricate. This reduces cost of production considerably. Eventhough dark current in a Schottky barrier diode is of a few orders of magnitude higher than that in the pn junction diode with the same area, open circuit voltage ( $V_{oc}$ ) is low and this reduces the efficiency. However,  $V_{oc}$  can be increased by inserting a thin insulating layer between the metal and the semiconductor, forming metal-insulator-semiconductor (MIS) structure. But when the insulating layer is thick ( $>2\text{nm}$ ), the short circuit current density will be reduced considerably [12].

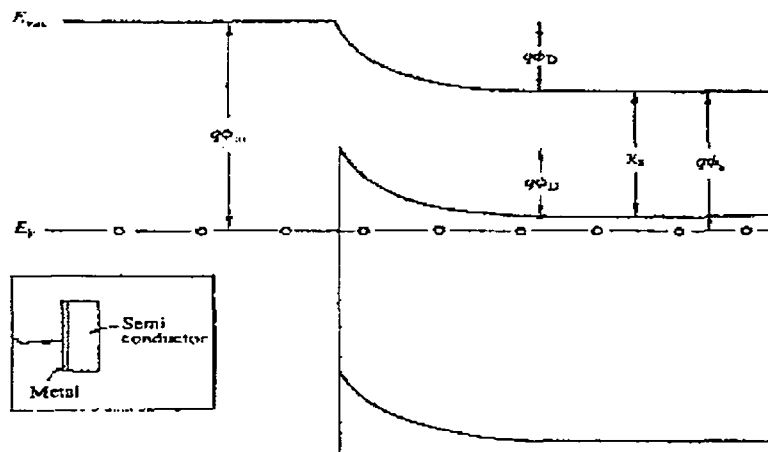


Fig.1.5 Energy band diagram of metal-semiconductor junction

### 1.3.4 Buried or heteroface junctions

Fig1.6 shows a representative energy band diagram for a buried p-n homojunction with a heavily doped  $p^+$ -p heterojunction. The structure is actually that of a  $p^+$ -p-n junction. This structure retains the advantages of a p-n junction while at the same time it provides a different front surface interface for the p-type region of the junction. This will decrease the surface losses.

This device differs from ordinary pn junction in the sense that that here the junction is much deeper and the doping density is moderate on the topside of the junction. A front surface field is used at the top of the device. This approach overcomes limitations imposed on the open circuit voltage by diffused top layer of normal cell structure. Substantial improvement in open circuit voltage was reported using this approach [13]. Carrier collection is not optimum. So current output tends to be less than that of other devices.

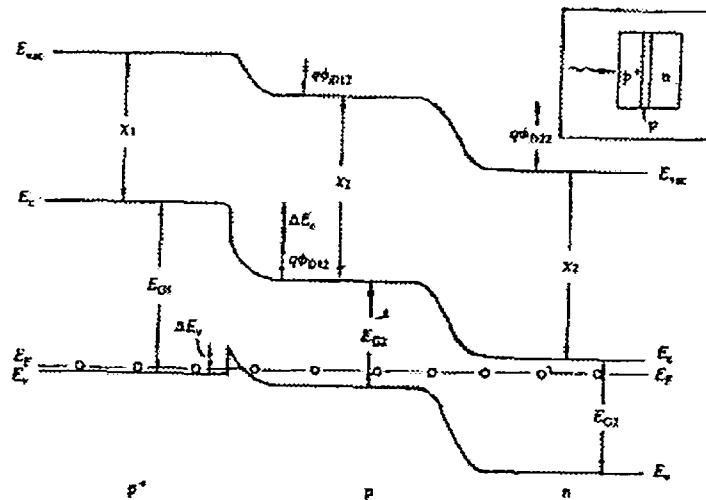


Fig. 1.6. Energy band diagram of a heteroface junction

### 1.3.5 Alternative device structures

There is a wide range of possibilities for photovoltaic possibilities with different structures apart from the above mentioned ones. Some such devices are briefly mentioned below. In addition to these, there are some special approaches specifically made to improve the cell efficiency. These include violet cell, BSF cell, Black cell, Grooved cell, point contact cell, passivated emitter cell, MIS cells and multijunction or tandem cells.

#### *a) Back-Surface Field (BSF) cells*

This type of cell introduced the concept of shielding photo generated minority carriers from high recombination plane of back surface by employing electric field of a low-high junction. A reduced recombination at the back surface can increase short circuit current and hence reduce saturation current, resulting in an overall increase of efficiency [14]. Devices having BSF structure were having efficiencies approaching 19-20% range for silicon single crystal and 21% for GaAs under terrestrial conditions [15].

#### *b) Front surface field cell*

The second one in this list is the 'front surface field cell'. With this approach, it is possible to bring both contacts to the rear of the cell. This eliminates losses due to shadow associated with normal top contact and would make cells easier to inter-connect. This cell has to be thin compared to minority carrier diffusion length to get full current output. However these cells had handling difficulties in the case of large area cells.

#### *c) Vertical Multi Junction cells*

Here junctions are perpendicular to the illuminated surface of the cell. Deep grooves are etched into the cell using anisotropic etch. These vertical junctions ensure that even carriers generated deep in the absorber layer can be collected. In order to make

this effective, distance between the vertical junctions must be of the order of a diffusion length apart.

Heterojunctions formed between liquids and semiconductors also possess interesting photovoltaic properties.

## 1.4 Theory of semiconductor solar cell structures

### 1.4.1 Semiconductor-Semiconductor Homojunctions

#### 1.4.1.1 Electrostatics of p-n junction

When a p-n junction is formed between two semiconductors, at the interface between n-type and p-type, both carrier concentrations have a strong gradient. Electrons diffuse from the n-type to the p-type part where they recombine with holes. At the same time, holes go over from the p to the n-type region and they recombine with electrons. This results in the production of ionized, immobile and uncompensated impurities near the interface, which remains with negative charge in p-type part and positive charges in n-type part. These space charges produce an electric field and thus a potential difference (step) at the p-n junction. Formation of a potential step means that p and n type semiconductors are shifted with respect to one another until their Fermi energies have reached the same value. Constant Fermi level required at thermal equilibrium, results in a unique space charge distribution at the junction. The space charge density  $\rho$  is given by

$$\rho = q(p - n + N_D^+ - N_A^-) \dots\dots\dots(1)$$

where  $p$  and  $n$  are the densities of holes and electrons  $N_D^+$  and  $N_A^-$  are the densities of ionized donors and acceptors. Unique space charge distribution and electrostatic potential  $\psi$  are given by Poisson's equation: [16]

$$\frac{d^2\psi}{dx^2} \equiv -\frac{d\xi}{dx} = -\frac{\rho_s}{\epsilon} = -\frac{q}{\epsilon}(N_D - N_A + p - n) \dots\dots(2)$$

In regions far away from the metallurgical junction, the total charge density is zero. For p-type neutral region, we assume  $N_D = 0$  and  $p \gg n$ . The electrostatic potential of the p-type neutral region with respect to the Fermi level is given by

$$\psi_p = -\frac{kT}{q} \ln \frac{N_A}{n_i} \dots\dots\dots(3)$$

Similarly, electrostatic potential of the n-type neutral region with respect to the Fermi level :

$$\psi_n = \frac{kT}{q} \ln \frac{N_D}{n_i} \dots\dots\dots(4)$$

Total electrostatic potential difference between p-side and n-side neutral regions at thermal equilibrium is called built-in potential ( $V_{bi}$ ):

$$V_{bi} = \psi_n - \psi_p = \frac{kT}{q} \ln \frac{N_A N_D}{n_i^2} \dots\dots\dots(5)$$

An applied voltage  $V_a$  will change the potential difference between the two sides of the diode by  $V_a$ . Hence the potential across the transition region will become ( $V_{bi} - V_a$ ).

In depletion approximation, a solar cell device is divided into two regions: quasi-neutral region where the space charge density is assumed to be zero throughout and a depletion region where the carrier concentration is assumed so small that only space charge from ionized dopants is considered.

Electric field strength can be obtained by integrating the space charge distribution. The maximum field strength in the depletion region can be calculated using the expression [11],

$$\xi_{\max} = \left[ \frac{2q}{\epsilon} (V_{bi} - V_a) \left( \frac{1}{N_A} + \frac{1}{N_D} \right) \right]^{1/2} \dots\dots\dots(6)$$

Width of the depletion region is given by the expression [11],

$$W = l_n + l_p = \left[ \frac{2\epsilon}{q} (V_{bi} - V_a) \left( \frac{1}{N_A} + \frac{1}{N_D} \right) \right]^{1/2} \dots\dots\dots(7)$$

where  $l_n$  and  $l_p$  are the distances up to which the depletion region extends on either side of the junction.

**1.4.1.2 Junction Capacitance**

In the depletion approximation, a change in the applied voltage will cause a change in stored charge right at the edges of the region. This is identical to the situation of a parallel plate capacitor of plate separation  $w$ , where  $w$  is the width of the depletion region. Hence depletion region capacitance  $C$  per unit area is given by

$$C = \frac{\epsilon}{W} \dots\dots\dots(8)$$

where  $\epsilon$  is the dielectric constant

For a two-sided abrupt junction, capacitance per unit area is expressed as [17]

$$C = \left[ \frac{qN_D N_A \epsilon_n \epsilon_p \epsilon_0}{2(\epsilon_n N_D + \epsilon_p N_A)(V_{bi} \pm V)} \right]^{1/2} \dots\dots\dots(9)$$

where  $\epsilon_n$  and  $\epsilon_p$  are dielectric constants on the n and p regions respectively, and  $\epsilon_0$  is the permittivity of free space,  $V$  is the applied reverse bias voltage to the junction, and  $V_{bi}$  is the built in potential.

Under reverse bias, depletion region capacitance dominates the total diode capacitance. Hence measuring  $C$  as a function of reverse bias to the solar cell and plotting  $1/C^2$  vs.  $V$

will allow determining the junction related parameters like depletion layer width and doping profile near junction.

### 1.4.1.3 Current-Voltage characteristics

Current-voltage characteristics of a solar cell help to understand the device function. In the following section, dark and illuminated characteristics of a solar cell are discussed.

#### A. Dark characteristics

It has been found that when a forward voltage is applied to a diode, minority carrier concentration at the edge of the depletion region depends exponentially on the voltage applied to the diode [18]. When quasi-neutral regions are uniformly doped and majority carrier currents small, minority carriers flow primarily by diffusion.

On n-type side of the diode, minority current is given by the expression

$$J_h = -qD_h \frac{dp}{dx} \dots\dots\dots(3)$$

where  $D_h$  is the diffusion coefficient for holes,  $J_h$  is the hole current density and  $dp/dx$  is the hole concentration gradient.

According to continuity equation,

$$\frac{1}{q} \frac{dJ_h}{dx} = -(U-G) \dots\dots\dots(4)$$

where  $G$  is the generation rate and  $U$  is the recombination rate, in n-type region and can be expressed as

$$U = \frac{\Delta p}{\tau_h} \dots\dots\dots(5)$$

Where  $\tau_h$  is the minority carrier life time which can be regarded as constant at least for small disturbances from equilibrium and  $\Delta p$  is the excess concentration of holes.

$$\Delta p = p_n - p_{n0} \dots\dots\dots(6)$$

Where  $p_n$  is the total concentration of holes and  $p_{n0}$  is the equilibrium concentration of holes.

Combining the above equations,

$$D_h \frac{d^2 p_n}{dx^2} = \frac{p_n - p_{n0}}{\tau_h} - G \dots\dots\dots(7)$$

In the dark,  $G = 0$ . Also,

$$\frac{d^2 p_{n0}}{dx^2} = 0, \text{ as } p_{n0} \text{ is equilibrium concentration of holes.}$$

$\therefore$  eqn (7) becomes,

$$D_h \frac{d^2 \Delta p}{dx^2} = \frac{\Delta p}{\tau_h}$$

$$\frac{d^2 \Delta p}{dx^2} = \frac{\Delta p}{L_h^2} \dots\dots\dots(8)$$

where  $L_h = \sqrt{D_h \tau_h}$

$L_h$  has the dimensions of length and is known as diffusion length. This diffusion length is an important parameter in the case of solar cells.

General solution to eqn. (8) is

$$\Delta p = A e^{x/L_h} + B e^{-x/L_h} \dots\dots\dots(9)$$

Constants A and B can be found by applying following boundary conditions.

1. At  $x = 0$ ,  $p_n = p_{n0} e^{qV/kT}$
2.  $P_n$  is finite as  $x \rightarrow \infty$

These boundary conditions lead to the following solution:



$$\left. \begin{aligned} p_n(x) &= p_{n0} + p_{n0}[e^{qV/kT} - 1]e^{-x/L_n} \\ n_p(x') &= n_{p0} + n_{p0}[e^{qV/kT} - 1]e^{-x'/L_n} \end{aligned} \right\} \dots\dots\dots(10)$$

where  $x'$  is defined in Fig.1.7. Semi logarithmic plot of distributions of carriers throughout the p-n junction diode under forward bias is shown in Fig.1.7.

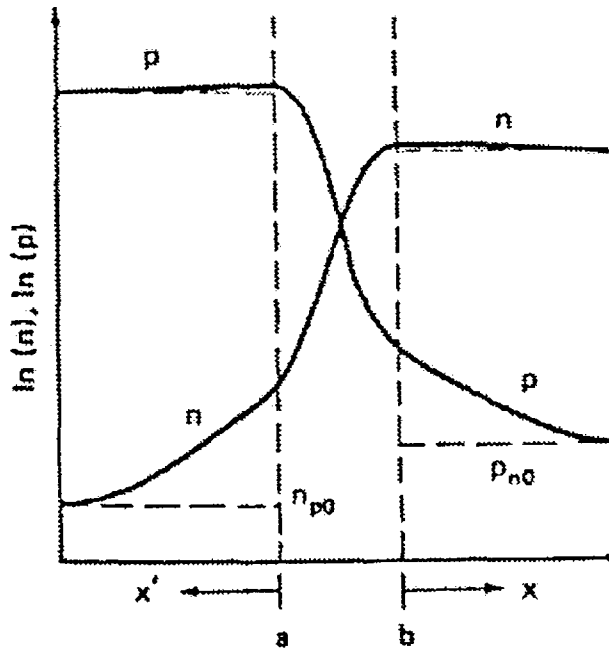


Fig.1.7. Semi logarithmic plot of distributions of carriers throughout the p-n junction diode under forward bias

Once carrier distributions are known, minority current can be calculated by substituting eqn.10 in eqn.3 gives,

$$J_h(x) = \frac{qD_h p_{n0}}{L_h} (e^{qV/kT} - 1)e^{-x/L_h} \dots\dots\dots(11)$$

similarly, in the p-type region,

$$J_e(x') = \frac{qD_e n_{p0}}{L_e} (e^{qV/kT} - 1) e^{-x'/L_e} \dots\dots\dots(12)$$

Considering the total current flow in the depletion region, the continuity equations give

$$\frac{1}{q} \frac{dJ_e}{dx} = U - G = -\frac{1}{q} \frac{dJ_h}{dx} \dots\dots\dots(13)$$

Magnitude of the change in current across depletion region is

$$\delta J_e = |\delta J_h| = q \int_{-w}^0 (U - G) dx \dots\dots\dots(14)$$

Since  $w$  is small, it is reasonable to assume that the integral involved in eqn(14) is negligible. Hence total current is obtained as,

$$\begin{aligned} J_{total} &= J_e|_{x'=0} + J_h|_{x=0} \\ &= \left( \frac{qD_e n_{p0}}{L_e} + \frac{qD_h p_{n0}}{L_h} \right) (e^{qV/kT} - 1) \dots\dots\dots(15) \end{aligned}$$

Eqn.15 can be written as

$$I = I_0 (e^{qV/kT} - 1) \dots\dots\dots(16)$$

where  $I_0$  is the reverse saturation current. Equation (16) is “ideal diode law”. Here,

$$I_0 = A \left( \frac{qD_e n_i^2}{L_e N_A} + \frac{qD_h n_i^2}{L_h N_D} \right)$$

where  $A$  is the cross sectional area of the diode.

### B.Illuminated characteristics

Here for mathematical simplicity, it is assumed that the generation rate of electron-hole pairs due to illumination, is constant throughout the device. This would correspond to a specific physical situation where the cell is illuminated by long wavelength light consisting of photons of energy close to that of the semiconductor

band gap. Current-voltage characteristics of the junction when illuminated can be derived following the same method as the one used to find current-voltage characteristics of the junction kept in darkness.

Since generation rate  $G$  is not zero (but a constant), eqn.8 in the former section, can be rewritten as

$$\frac{d^2 \Delta p}{dx^2} = \frac{\Delta p}{L_h^2} - \frac{G}{D_h} \dots\dots\dots(17)$$

Since  $G/D_h$  is constant, corresponding general solution is obtained as

$$\Delta p = G\tau_h + Ce^{x/L_h} + De^{-x/L_h} \dots\dots\dots(18)$$

Boundary conditions used for analysis of the diode in darkness remain unchanged.

Hence this gives the solution as

$$p_n(x) = p_{n0} + G\tau_h + [p_{n0}(e^{qV/kT} - 1) - G\tau_h]e^{-x/L_h} \dots\dots\dots(19)$$

with a similar expression for  $n_p(x')$

Corresponding current density is given by the following equation,

$$J_h(x) = \frac{qD_h p_{n0}}{L_h} (e^{qV/kT} - 1)e^{-x/L_h} - qGL_h e^{-x/L_h} \dots\dots\dots(20)$$

with a similar expression for  $J_e(x')$ .

Neglecting the effect of recombination in depletion region and including effect of generation in this region, change in the current density across this region can be written as

$$|\delta J_e| = |\delta J_h| = qGw \dots\dots\dots(21)$$

Proceeding as before, we get the following result for current-voltage characteristics:

$$I = I_0 (e^{qV/kT} - 1) - I_L \dots\dots\dots(22)$$

where  $I_L$  is light generated current, and

$$I_L = qAG(L_e + W + L_h) \dots\dots\dots(23)$$

The current-voltage characteristics of a p-n junction in darkness and when illuminated are shown in Fig.1.8. Illuminated characteristics are merely the dark characteristics shifted down by a current  $I_L$ . This gives a region in the fourth quadrant where power can be extracted from the diode.

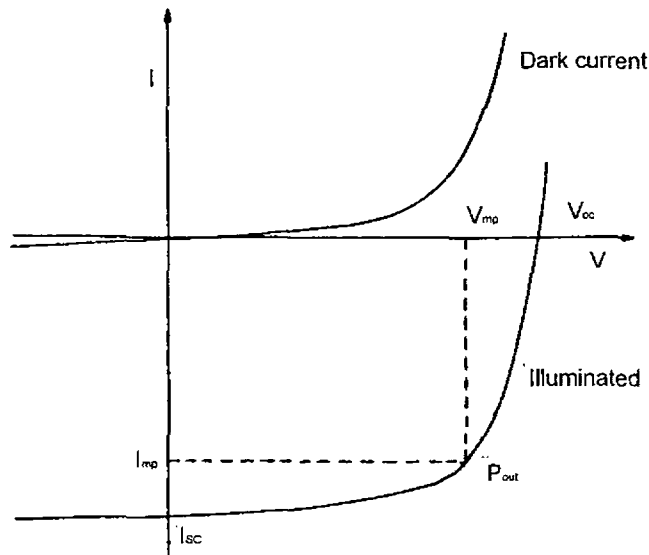


*Fig.1.8 current-voltage characteristics of a p-n junction – with and without illumination*

#### 1.4.1.4 More realistic photovoltaic model

Solar cells generally have a parasitic series and shunt resistance associated with them. There are several physical mechanisms responsible for these resistances. Bulk resistance of semiconductor material of the cell, resistance of the metallic contacts and interconnections and contact resistance between metallic contact and semiconductor are the main contributors to the series resistance ( $R_s$ ). Shunt resistance, ( $R_{sh}$ ) is caused by leakage across the pn junction around the edge of the cell and in nonperipheral regions

in the presence of crystal defects and precipitates of foreign impurities in the junction region.

In a real solar cell, we have to consider effects of non-zero  $R_s$  and non-finite  $R_{sh}$ , voltage depended collection effects that makes the actual light-generated current less than  $I_L$  and the possibility for a change in major parameters  $I_0$ ,  $n$ ,  $R_s$  and  $R_{sh}$  between the dark and light conditions [9].

In general, junction current (in dark) can be expressed as

$$I^d = \gamma^d \{ I_0^d \exp[\alpha^d (V - I^d R_s^d)] + V / R_p^d - I_0^d \} \dots\dots\dots(24)$$

where  $\gamma^d = \frac{1}{(1 + R_s^d / R_p^d)}$  and  $\alpha^d = q / n^d kT$  for transport mechanisms not involving

tunneling. In the light,  $I^l = \gamma^l \{ I_0^l \exp[\alpha^l (V - I^l R_s^l)] + V / R_p^l - I_0^l - H(V)I_L \} \dots(25)$

where  $H(V)$  is a voltage dependent collection function, describing fraction of the light generated carriers that actually contribute to the light generated current.

$H(V) = g(V)h(V)$  where  $g(V)$  describes loss of carriers by recombination in bulk and  $h(V)$  describes loss of carriers by recombination at the junction interface due to interface states. Equivalent circuit of a solar cell indicating series resistance  $R_s$  and Shunt resistance  $R_{sh}$  are shown in Fig.1.9.

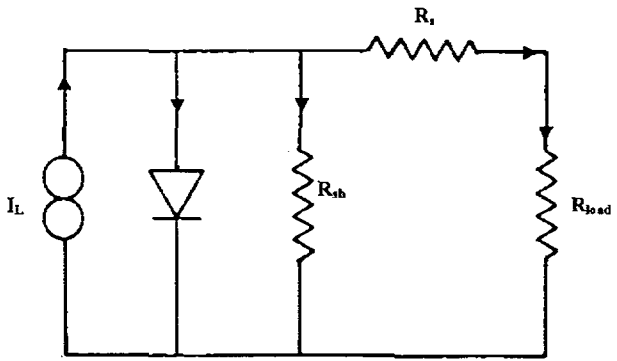


Fig.1.9. Equivalent circuit of a solar cell

## 1.4.2 Theory of Heterojunctions

### 1.4.2.1 Energy-band diagram and static characteristics

Consider two semiconductors 1 and 2 with band gaps  $E_{g1}$  and  $E_{g2}$ , permittivities  $\epsilon_{s1}$  and  $\epsilon_{s2}$ , work functions  $\phi_1$  and  $\phi_2$  and electron affinities  $\chi_1$  and  $\chi_2$ . Let  $\Delta E_c$  be the electron affinity difference and  $\Delta E_v$  be the hole affinity difference. At thermal equilibrium, Fermi level coincides on both sides of the junction. Total built-in potential ( $V_{bi}$ ) is given by

$$\begin{aligned} V_{bi} &= \phi_1 - \phi_2 = V_{d1} + V_{d2} \\ &= E_{g2} - (E_f - E_{v2}) + \chi_2 - \chi_1 - (E_{c1} - E_f) \dots \dots \dots (29) \end{aligned}$$

$$V_{bi} = V_{d2} + \Delta E_c \dots \dots \dots (30)$$

Capacitance and depletion widths can be obtained by solving Poisson's equation, as in the case of homojunction, [19]

$$C = \left[ \frac{qN_{D1}N_{A2}\epsilon_1\epsilon_2\epsilon_0}{2(\epsilon_1N_{D1} + \epsilon_2N_{A2})(V_{bi} \pm V)} \right]^{1/2} \dots \dots \dots (30)$$

$$x_1 = \left[ \frac{2N_{A2}\epsilon_1\epsilon_2\epsilon_0(V_{bi} - V)}{qN_{D1}(\epsilon_1N_{D1} + \epsilon_2N_{A2})} \right]^{1/2} \dots \dots \dots (31)$$

and

$$x_2 = \left[ \frac{2N_{D1}\epsilon_1\epsilon_2\epsilon_0(V_{bi} - V)}{qN_{A2}(\epsilon_1N_{D1} + \epsilon_2N_{A2})} \right]^{1/2} \dots \dots \dots (32)$$

Maximum electric field existing in the interface region is seen to occur at  $x = 0$  and is given by

$$\xi_{\max} = \frac{qN_A x_1}{2\varepsilon_1} \quad \text{or} \quad \xi_{\max} = \frac{qN_D x_2}{2\varepsilon_2} \dots\dots\dots(33)$$

#### 1.4.2.2 Current Transport

Carrier transport properties of heterojunctions are generally dominated by the phenomena in interface region. Several transport mechanisms may be operative at the interface. These include i) ideal diffusion or emission currents for electrons, ii) recombination-generation currents, iii) recombination through interface states, iv) tunneling from band states to localized defect states in the gap, across the interface, and v) band to band tunneling. Several authors have proposed different models based on experimental data as well as theoretical considerations. The model of Anderson forms basis and starting point for most other heterojunction theories [20]. In this section, three main models for abrupt anisotype heterojunctions (viz, i)Anderson's model,ii) tunneling model and iii) interface recombination model) are discussed.

i) Anderson's model:

In this model, effects of dipoles and interface states are neglected. Further it is assumed that, owing to discontinuities in the band edges at the interface, diffusion current consists of only electrons or holes. Current voltage relation, in the absence of generation recombination currents is given by

$$J = A \exp(-qV_{d2} / kT) [\exp(qV_2 / kT) - \exp(-qV_1 / kT)] \dots\dots(37)$$

where

$$A = aqXN_{d2}(D_{n1} / \tau_{n1})^{1/2} \dots\dots\dots(38)$$

X – transmission coefficient for electrons across the interface

A is junction area,  $D_{n1}$  and  $\tau_{n1}$  are diffusion coefficient and lifetime of minority carriers respectively, in the p-type material.

Perlman and Feucht included the effects owing to a spike in the conduction band edges in emission model. Current-voltage relation, neglecting generation and recombination within the space charge region is expressed as [19]

$$I = \frac{I_s [\exp(qV/kT) - 1]}{(I + I_s/I_d)} \dots\dots\dots(39)$$

where  $I_s = aqN_{D1}(D_{n1}/\tau_{n1})^{1/2} \dots\dots\dots(40)$

ii) Tunneling model:

In tunneling model, electrons have to tunnel through potential barrier in the n-type wide bandgap material in order to flow from n-type to p-type or vice versa. If tunneling through the barrier greatly exceeds thermal emission through the barrier, then  $I = I_s(T) \exp(V/V_0)$  where  $V_0$  is a constant and  $I_s(T)$  is a weakly increasing function of temperature.

iii) Interface recombination model:

Current density for interface recombination case, when the smaller bandgap p-type material is degenerate, has the form

$$J = qN_{c2}S_I \exp\left[\frac{-(qV_{d2} + \delta_2)}{kT}\right] \left\{ \exp\left[\frac{q(V - JR_s A_\perp)}{kT}\right] - 1 \right\} \dots\dots\dots(41)$$

where  $N_{c2}$  is effective density of states in n-type wide bandgap semiconductor,  $V_{d2}$  is the diffusion voltage,  $\delta_2$  is equal to  $E_{c2} - E_f$ ,  $R_s$  is series resistance,  $A_\perp$  is normal area of the diode and  $S_I$  is effective interface recombination velocity

$$S_I = v_{th} \sigma N_I^* \dots\dots\dots(42)$$

where  $v_{th}$  is the thermal velocity of electrons,  $\sigma$  is capture cross-section of the interface states, and  $N_I^*$  is density of the empty interface states.



$S_I$  can also be written as

$$S_I = v_{th} \sigma \Delta a / a^3 \dots\dots\dots(43)$$

where  $\Delta a$  is difference in lattice constant between the two materials and  $a$  is average lattice constant in the plane of the junction.

### 1.4.3 Solar cell output parameters

Following parameters are used to characterize performance of a p-n junction solar cell.

- i) Short circuit current ( $I_{sc}$ ) : This is the maximum current that can be extracted from the device by connecting upper and lower electrodes of the cell to an ammeter with negligible internal resistance. Ideally this is equal to the light generated current  $I_L$ . Low energy band gap and high diffusion length of the minority carriers are favorable for high short circuit current.

$$I_{sc} = I_0 [e^{qV_{oc}/nkT} - 1] \dots\dots\dots(44)$$

- ii) Open circuit voltage:- This is the maximum voltage generated by the device while drawing negligible current.

$$V_{oc} = \frac{nkT}{q} \ln\left(\frac{I_L}{I_0} + 1\right) \dots\dots\dots(45) \text{ where } n \text{ is diode quality}$$

factor and its value lies between 1 and 2.

In order to get high open circuit voltage, saturation current of the diode must be as small as possible and for this high band gap is essential. But this is contrary to the requirements for high photocurrent. Maximum conversion efficiency is obtained for semiconductors with an energy band gap between 1.2 and 1.5 eV

- iii). Maximum power output: - Power output of any operating point in the fourth quadrant is equal to area of the rectangle indicated in Fig1.8. One particular operating point ( $V_{mp}$ ,  $I_{mp}$ ) will maximize this power output.

$$P_{mp} = V_{mp} \times I_{mp} \dots\dots\dots(46)$$

iii) Fill factor (FF):- Fill factor is a measure of the flatness of output characteristics. For cells of reasonable efficiency, FF has a value in the range 0.7 to 0.85.

$$FF = \frac{V_{mp} \times I_{mp}}{V_{oc} \times I_{sc}} = \frac{P_m}{V_{oc} \times I_{sc}} \dots\dots\dots(47)$$

Energy conversion efficiency( $\eta$ ) is then given by

$$\eta = \frac{V_{mp} \times I_{mp}}{P_{in}} = \frac{V_{oc} \times I_{sc} \times FF}{P_{in}} \dots\dots\dots(48)$$

where  $P_{in}$  is total power in the light incident on the cell.

$$P_{in} = A \int_0^{\infty} F(\lambda)(hc/\lambda)d\lambda \dots\dots\dots(49)$$

where  $A$  is the total device area,  $F(\lambda)$  is the number of photons per  $\text{cm}^2$  per sec per unit bandwidth incident on the device at wavelength  $\lambda$  and  $(hc/\lambda)$  is the energy carried by each photon [21].

Ideally, FF is a function of the open circuit voltage ( $V_{oc}$ ) alone. Defining normalized voltage  $V_{oc}$  as  $\frac{V_{oc}}{(kT/q)}$ , an empirical expression describing this relationship can be expressed as,

$$FF = \frac{V_{oc} - \ln(V_{oc} + 0.72)}{V_{oc} + 1} \dots\dots\dots(50)$$

Efficiency becomes large when fill factor, short circuit current and open circuit voltage are as high as possible.

### 1.4.4 Spectral response

Photocurrent collected at each wavelength, relative to the number of photons incident on the surface at that wavelength determines “spectral response” of the device. “Internal spectral response” is defined as the number of electron- hole pairs collected at short circuit conditions relative to number of photons entering the material.

$$SR(\lambda) = \frac{J_p(\lambda)}{qF(\lambda)(1-R(\lambda))} + \frac{J_n(\lambda)}{qF(\lambda)(1-R(\lambda))} + \frac{J_{dr}(\lambda)}{qF(\lambda)(1-R(\lambda))} \dots\dots\dots(51)$$

where  $J_p, J_n$  and  $J_{dr}$  are hole diffusion, electron diffusion and drift contributions respectively to the total photocurrent density  $J_L$ .

External response is internal one modified by reflection of light from the surface of the device.

$$SR(\lambda)_{ext} = SR(\lambda)[1 - R(\lambda)] \dots\dots\dots(52)$$

### 1.5 Factors influencing efficiency of Solar cells

A major reason for low efficiency of a solar cell is the fact that each photon irrespective of its high energy, generates one electron- hole pair. The electron and hole quickly relax back to the edges of the respective carrier bands emitting phonons, which has low energy but relatively high momentum than a photon. Energy thus wasted is dissipated as heat. This effect alone limits the maximum available efficiency to about 44% [22].

Excessive recombination of carriers taking place in the bulk of the semiconductor and at the surfaces reduces the efficiency. Only the electron-hole pair generated near the junction contributes to light generated current.

A part of the generated free carriers do not reach the junction because of their low diffusion length or due to recombination at the surface or in the bulk. Loss occurs

due to the reflection of the incident light too. In the case of silicon, about 30% of the light is reflected at the surface. But this loss can be minimized to nearly 0% if an appropriate anti reflection coating is used or the surface is so prepared that the cell appears black [23].

Top electrode of cell reduces active surface area of the semiconductor exposed to sunlight. This blocks 5 to 15 per cent of the incoming light. If the cell is not thick enough, a part of the incident light will not be absorbed, and it passes out at the back.

Short circuit current of solar cells is not strongly temperature-dependent. It tends to increase slightly with increasing temperature. But other cell parameters like open-circuit voltage and the fill factor, both decrease. Power output and efficiency decrease with increasing operating temperature. For silicon, the power output decreases by 0.4 to 0.5% per °C.

Diffusion length is the parameter most directly controlling short circuit current of a cell, and it can also influence open-circuit voltage if the diode current is controlled by the diffusion length of the material [24]. Generally, diffusion length should be as long as possible and certainly equal to the thickness of the absorber layer.

Power loss factor  $L_s$  due to series resistance ( $R_s$ ) is calculated using the following expression

$$L_s = \frac{J_m \times R_s}{V_{oc}} \dots\dots\dots(53)$$

and impact of the shunt resistance ( $R_{sh}$ ) in the power factor is calculated using the expression

$$L_p = \frac{V_m}{J_m \times R_{sh}} \dots\dots\dots(54)$$

Effect of parasitic resistance on the output characteristics of solar cells is indicated in Fig.1.10.

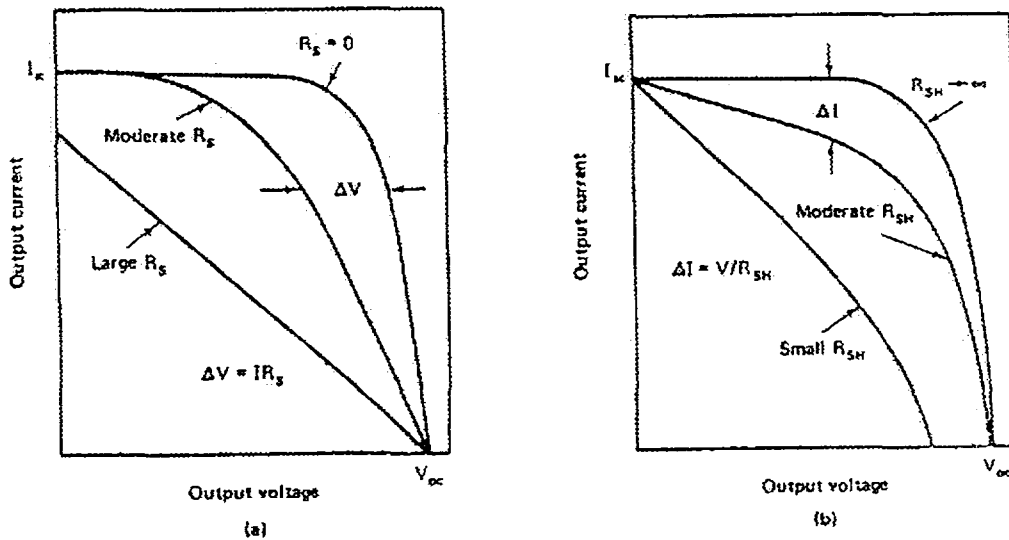


Fig.1.10 Effect of  $R_s$  and  $R_{sh}$  on output characteristics of a solar cell  
 a) Effect of series resistance ( $R_s$ ), b) Effect of Shunt resistance

Magnitude of effect of  $R_s$  and  $R_{sh}$  on fill factor can be found by comparing their values to the characteristic resistance of the solar cell defined as

$$R_{CH} = V_{oc}/I_{sc} \dots\dots\dots(55)$$

If  $R_s$  is a lot less than this quantity, there will be little effect upon the fill factor. An approximate expression for the fill factor in the presence of series resistance can be written as

$$FF = FF_o (1-r_s) \dots\dots\dots(36) \text{ where } r_s = R_s/R_{CH} \text{ and } FF_o \text{ is the ideal } FF \text{ in the}$$

absence of parasitic resistance.

From Fig.1.10, it is also evident that both  $R_s$  and  $R_{sh}$  act to reduce fill factor.

Apart from these, there are certain material and structural characteristics affecting cell performance. They are, stoichiometry, grain size, surface properties, grain boundary properties, bulk lifetime, energy band profiles, impurities, dislocations and interface states. Each of these properties is discussed in detail by L L Kazmerski [24].

## 1.6 Efficiency Measurement

Solar cell efficiency can be measured by measuring power of incident sunlight using a pyranometer and electrical power generated at the maximum power point. However, performance of the cell measured in this way will depend greatly on the precise spectral content of the sunlight, which varies with air mass, water-vapor content, turbidity etc. Hence this approach would make comparison difficult between the performance of devices measured at other than the same time and place. An alternative approach is a method using calibrated reference cells. A central test authority calibrates reference cells under standard illumination conditions. Performance of the cell under test is then measured relative to the reference cell. For this technique to be accurate, reference and test cells must be made from the same semiconductor material using a similar processing technique. Three methods that are approved by NASA – Lewis under the direction of the Department of Energy for the testing of solar cells are summarized in Fig.1.11 [25].

A four point contacting scheme is desirable in which voltage and current leads to the cell under test are kept separate. This eliminates effects due to series resistance of the test leads and associated contact resistances. Cells are mounted on a temperature-controlled block. 25 °C and 28 °C are standard temperature for solar cell measurements. Lamp intensity is adjusted to give desired intensity as measured by a reference cell. By varying load resistances, characteristics of the test cell can be measured.

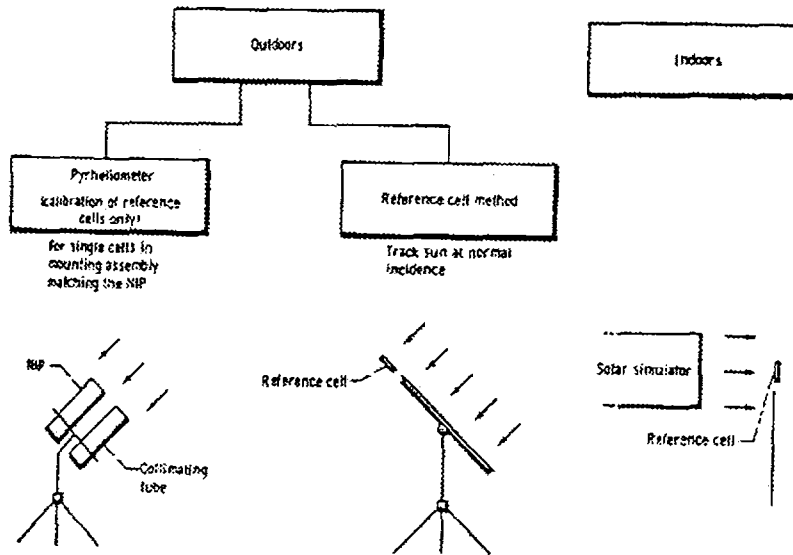


Fig.1.11 DOE/NASA solar cell testing methods

Spectral Response is the output current under short-circuit condition per unit incident power in monochromatic light as a function of wavelength. Measurement of spectral response can provide detailed information about design parameters of any particular solar cell.

Spectral response of a test cell can also be measured by direct comparison with the output of a cell having calibrated spectral response. The simplest technique is to use a steady-state source of monochromatic light from a monochromator.

## 1.7 Thin Film Solar cells

During the energy crisis of early 1970s, both public and private sectors became interested in terrestrial applications of photovoltaic energy generation. Initial efforts focused on lowering the cost of single crystal silicon (sc-Si) solar cell modules. Parallel

efforts were also initiated to find alternative materials that could be processed in thin film form.

Thin film cells are produced by depositing thin layers of semiconductor material onto a supporting substrate such as glass, plastic or stainless steel. Generally speaking, single crystal solar cell is the most efficient in terms of electrical output, but it is also the most expensive. While thin film cells achieve lower efficiencies than crystalline cells, their production cost is considerably less. Moreover thin film cells can be extremely light and flexible, and hence they can meet a variety of needs for which crystalline solar cells are too big or too rigid [26]. Reduced material use is another main advantage. In thin film cells, only one or two micron thickness of semiconductor material is required, which is 100-1000 times less than the thickness of silicon wafer [4]. Because of low consumption of active solar cell material, even rare and expensive elements can be considered here. Further advantage is that such cells have relatively high tolerance for impurities and crystalline imperfections because the diffusion length scales with film thickness [27].

Requirements of ideal solar cell material are: 1) Bandgap between 1.1 and 1.7 eV, 2) Direct band structure, 3) Consisting of readily available, non toxic materials, 4) Easy, reproducible deposition technique, suitable for large area production, 5) Good photovoltaic conversion efficiency and 8) Long-term stability.

Out of a large number of experimentally tested thin film materials, only a handful of materials have emerged as good solar cell absorber layers. One reason is that many chemical, physical and practical conditions have to be fulfilled simultaneously. Most compound semiconductors, when formed in polycrystalline form, have poor electronic properties due to the activity at grain boundaries [28]. Grain boundaries provide recombination surfaces for minority carriers and thus degrade performance of the device. Further it affects device operation by creating shorting paths [29]. However, a few materials maintain good performance in polycrystalline form.



Initially, research was concentrated on thin film solar cells of polycrystalline  $\text{Cu}_2\text{S}/\text{CdS}$ . But due to severe stability problems, this work was discontinued by the early 1980s. Presently, amorphous silicon, copper indium diselenide, and cadmium telluride are the most popular semiconductors in the field of thin film solar cells. All these materials have shown continuous improvement of laboratory efficiency over the years as indicated in Fig.1.13. Each of these technologies has its own strength and weaknesses. Brief descriptions of all these cells are given below.

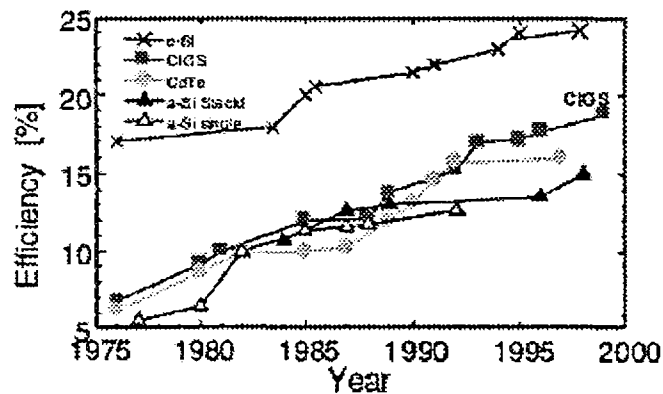


Fig. 1.13 Improvement of efficiency over time for prominent solar cell materials

#### i) Amorphous silicon cell (a-Si:H)

The best known thin film material is amorphous silicon (a-Si), which has been in production for about 15 years [30]. First amorphous silicon cell was produced in 1976 by Carlson [31]. By 1994, its efficiency became 10.2%. Today more than 15% of cells and modules produced worldwide are based on a-Si [4].

This material is actually a-Si-hydrogen alloy, containing 20-30% hydrogen. a-Si is produced by decomposing the silane ( $\text{SiH}_4$ ) gas, at low temperature and it is found that incorporation of hydrogen improves the material quality. It can also be prepared using Glow discharge [32] and chemical vapor deposition techniques [33]. It has high

optical absorption coefficient ( $>10^5 \text{cm}^{-1}$ ) and can be easily doped using boron and phosphorous for p and n-type respectively. Bandgap of a-Si can be tailored from 1.1 eV to 2 eV with addition of carbon or germanium [27].

Major problem of this cell is linked with outdoor usage. Some of the beneficial effects of hydrogen become undone under bright sunshine and the cell performance degrades (Staebler-Wronski effect) and these cells show initially some degradation of efficiency because of this. Stabilized efficiency is only 6-7% for the best commercial modules. However, since the film deposition temperature is low, they can be deposited onto low-temperature substrates such as plastics. This makes them especially suitable for consumer products.

As thinner cells exhibit higher stability, stalked cells have been designed to utilize this effect. Multijunction solar cells have reached 13.7% efficiency and an efficiency of 18.7% has been reported for the hybrid structure a-Si:H/Si [34].

#### ii) *Thin film crystalline silicon solar cells (f-Si)*

Early attempts to develop thin-film solar cells based on the polycrystalline silicon did not give encouraging results since the silicon layers had to be quite thick to absorb most of the available light. However, it is now well recognized that its poor absorption is no longer an issue provided light trapping is introduced whereby the light is confined to regions where the photogenerated carriers have high collection probabilities [35]. Optically a cell can appear about 50 times thicker than its actual thickness if this happens.

Thin-film crystalline silicon (f-Si) covers a broad technological field, which is usually divided in two main routes:

- High-temperature- replacement of thick, expensive, silicon by a thin ( $< 50 \mu\text{m}$ ) silicon film on a low-cost substrate
- Low-temperature- the use of micro crystalline silicon  $< 5 \mu\text{m}$  in an amorphous silicon-like or amorphous silicon-based structure [36].

In low temperature approach, silicon is deposited in amorphous form and then heated for prolonged periods at intermediate temperatures to crystallize it. In another approach, a nanocrystalline phase of silicon is produced by changing the amorphous silicon deposition conditions.

More recently, cell efficiency above 10% has been confirmed with this approach. 19.2% efficiency has been reported for a CVD-epi-Si p<sup>+</sup>/p structure on SIMOX wafer substrate [4]. Tandems are often made with both microcrystalline and amorphous silicon. Presently crystalline thin film technology is being characterized using a wide range of laboratory activities, but considerable work is necessary to put this into production lines. Probably only thin Si-cell concept, which is about to be a commercially available product, is the Silicon Film TM technology developed by Astropower [37].

### *iii) Cadmium Telluride Cells (CdTe)*

CdTe is one of the most promising photovoltaic materials for use as low-cost, high-efficiency thin film solar cells due to the near optimum bandgap (1.5eV at room temperature), high absorption coefficient (around  $5 \times 10^4 \text{cm}^{-1}$ ) and manufacturability. CdTe based solar cells have a theoretical conversion efficiency of the order of 28% [38].

A variety of techniques had been used for the deposition of CdTe thin films. The most widely used techniques are electrodeposition, physical vapor deposition (PVD), close-space sublimation (CSS), screen-printing and spray pyrolysis. Heterojunction devices with n-type cadmium sulfide (CdS) films show very low minority carrier recombination at the absorber grain boundaries and at the metallurgical interface, which results in high quantum efficiencies.

Recently, ~16% efficiency (which is the current world record for CdTe solar cells), was reported by Aramoto et al. [39]. This cell structure is antireflection coat/glass/ITO/CdS/CdTe/Cu-doped carbon/Ag, where CdS and CdTe films were

deposited by chemical vapor deposition (CVD) and close-spaces sublimation (CSS) method respectively. The National Renewable Energy Laboratory [NREL] developed a modified CdTe device structure and fabricated a CdS/CdTe polycrystalline thin film solar cell demonstrating efficiency of 16.4% [40].

Photovoltaic performance of the CdS/CdTe device in the as deposited state is poor. CdCl<sub>2</sub> treatment after CdTe deposition and heat treatment after screen printing of the Cu doped carbon electrode upgrades device performance [41].

One major issue is the high content of cadmium in CdTe solar cells. Cd metal, which is classified as a toxic/ carcinogen is, present both in the window and absorber layers, which gives rise to environmental hazards. Another issue is regarding the electrical contacts.

#### *iv) Copper Indium Diselenide (CuInSe<sub>2</sub>) solar cells*

A promising thin film technology at the moment is the one based on ternary chalcopyrite CuInSe<sub>2</sub> (CIS). Direct bandgap of 1.04 eV is near the optimal value for terrestrial conditions. By substituting Ga for In and S for Se, the bandgap can be modified continuously over a wide range. This material has its absorption coefficient larger than  $5 \times 10^4 \text{ cm}^{-1}$ . CIS forms an ideal heterojunction with CdS, since the lattice mismatch between chalcopyrite CuInSe<sub>2</sub> and hexagonal CdS is only about 1.2%. No interfacial spikes are formed in conduction band, as the electron affinities of the two materials are very close [19].

This compound is often alloyed with copper gallium diselenide (CuGaSe<sub>2</sub>) and copper indium disulphide (CuInS<sub>2</sub>), giving CIGS material with up to five elements involved [42,28]. There are two different approaches for CIGS film deposition. The first is the coevaporation of elements onto a heated substrate and the second process; selenization of stacked layers / metal alloys is more suitable for industrial production.

Conversion efficiencies are now approaching 19% for CIS/CdS/ZnO-based devices [43,44]. In these devices CIS (2 μm) and ZnO (0.5 μm) layers are deposited

using high vacuum physical deposition techniques (coevaporation and sputtering) but the CdS films (20–50 nm) are prepared using chemical bath deposition (CBD) in aqueous solutions [45]. This is a recent and innovative combination between vacuum and solution deposition approaches. The record lab efficiency recently announced by ENREL is an impressive 18.8% for cells. Small modules are having 14% and large modules are having 11-12%. Siemens is now marketing the first products of a pilot line production with efficiencies above 10% [46,47].

Our research group at 'Thin Film Photovoltaic Division' of Cochin University of Science and Technology is also seriously involved in the fabrication of  $\text{CuInSe}_2$  based solar cells. Fabrication of the first  $\text{CuInSe}_2/\text{CdS}$  thin film heterojunction entirely using chemical bath deposition belongs to our credit [48]. Efficiency of the best cell fabricated was 3.1%, with an open circuit voltage 365mV and short circuit current density  $12\text{mA}/\text{cm}^2$ . Thus it was demonstrated for the first time that a simple, low-cost process like CBD could be used for the fabrication of a complete  $\text{CuInSe}_2/\text{CdS}$  solar cell. Details of this work are presented in reference [49].

Also we are successful in preparing  $\text{CuInSe}_2$  films through a new selenization process developed in our lab, which avoids usage of poisonous gases or Se vapor [50]. For this, amorphous selenium films were prepared from an acidified solution of  $\text{Na}_2\text{SeSO}_3$  using CBD at room temperature.  $\text{CuInSe}_2$  films were prepared using two methods: One method is selenization of multilayer having structure In/Cu and the second is thermal diffusion of Cu into  $\text{In}_2\text{Se}_3$  film, prepared using selenization of In film. Research is in progress to fabricate solar cells using these films.

Apart from the use of cadmium, there is another difficulty related due to the limited known resources of indium, often-quoted limitation of this technology viz, 'manufacturability'. It is usually difficult to diagnose problems in production of this material, since the difference between good and bad material is not sufficiently well understood to allow differentiation and control during the various manufacturing steps.

## 1.8 Scope of present work

Although solar cells based on CIGS films have shown good conversion efficiencies, mismatch in the electron affinity and hence band offset at the junction between their absorber layer and the window layer (CdS) is considered to be one of the major limiting factors towards furthering the efficiency value [51]. Use of selenium in synthesizing this material is not favored due to its toxicity. Conventional selenization processes involve usage of selenium vapor or  $H_2Se$  gas which are extremely toxic. In this regard,  $CuInS_2$  films have an edge over the above material since this does not contain any toxic constituent.

$CuInS_2$ , which is the material selected for the present work, possesses several exceptional material properties, which make it potentially well suited for photovoltaic applications. Its direct bandgap of 1.53eV is nearly optimum for solar energy conversion. Absorption coefficient is high. This material can be prepared both in p-type and n-type form so that homojunction is possible. Heterojunction can be fabricated with n-type CdS which is the most commonly used window layer. Its electron affinity is such that there is no spike in conduction band when junction is formed with n-type CdS. Since radiation hardness is high, cells based on this material can also be used for space applications.

Messe et al. predicted theoretical efficiencies between 27% and 32% for the  $CuInS_2$  homojunction and this is the highest figure for any photovoltaic device [52]. Many groups have already reported the possibilities of synthesizing  $CuInS_2$  films leading to the fabrication of solar cells with efficiencies ~12% [53-55]. The best cell efficiencies to date for this ternary material is 12.5% [56]. As the next stage of development, efforts are to be made to produce this absorber layer with simple and cost-effective processes.

In the present work, we developed a new method for the preparation of p-type  $\text{CuInS}_2$  using chemical bath deposited (CBD)  $\text{Cu}_x\text{S}$  thin film. This is a low cost and very convenient process as the preparation of  $\text{Cu}_x\text{S}$  film is carried out using simple and inexpensive CBD technique at room temperature itself. No substantial amount of energy is required in this process. Also we used chemical spray pyrolysis (CSP), which is another low cost deposition technique for preparing device quality films with good photoresponse. We obtained further information about the dependence of film resistivity and photoresponse as a function of composition in the spray solution. This information is useful for designing solar cells using this material. We could fabricate an 'all sprayed'  $\text{CuInS}_2/\text{CdS}$  solar cell with efficiency 1.7% in the present work as a preliminary step. Even though the efficiency is low, we feel that this is the beginning of a challenging work.

## 1.9 Conclusion

After discussing basic theory and principle of solar cell operation, different solar cell structures and factors affecting efficiency of the cells are mentioned. It is obvious that low-cost thin film solar cells fabricated using compound semiconductors are good options. These have potential for developing a highly efficient cell, and they will become important and sustainable resource for our energy needs in the near future. A brief review of the important thin film solar cells is included and the significance of  $\text{CuInS}_2$  thin film as a photovoltaic material is highlighted.

## References

- [1] G.H.Lin and D.E Carlson, *International Journal of Hydrogen Energy*, 25 (2000) 807
- [2] Becquerel.E, C.R. Hebd. Seances Acad. Sci, 9 (1839) p-561
- [3] Alan L. Fahrenbruch and Richard H. Bube, *Fundamentals of solar cells*, Academic press, New York (1983) p- 9
- [4] M.A.Green, *Energy Policy*, 28 (2000) 989
- [5] D. M. Chapin, C. S. Fuller, and G. L. Pearson, *J. Appl. Phys.*, 25 (1954) 676
- [6] M.A.Green, *Solar cells*, Prentice-Hall, Inc, Englewood Cliffs, (1992) p-2
- [7] Rathindra Nath Biswas, *Electronics for You*, Feb (1998) p- 45
- [8] D.C Reynolds, G. Leies, L L Antes, and R.E Marburger, *Phys. Rev.*, 96 (1954) 533
- [9] Richard H Bube, *Photoelectronic properties of semiconductors*, Press Syndicate of the University of Cambridge, New York, USA, 1992
- [10] K.W.Boer, *Survey of semiconductor Physics*, Vol.II, Van Nostrand Reinhold, NewYork (1992) p-820
- [11] M.A.Green, *Solar cells*, Prentice-Hall, Inc, Englewood Cliffs, (1992) p-175
- [12] M. S. Thyagi, *Semiconductor Materials and Devices*, John Wiley & Sons, (1991) p-348
- [13] M.A.Green, *Solar cells*, Prentice-Hall, Inc, Englewood Cliffs, (1992) p-171
- [14] Hans Joachim Moller, *Semiconductors for solar cells*, Artech House, Boston, (1993)p-52
- [15] S.J.Fonash, *Solar Cell Device Physics*, Academic Press, (1981)
- [16] S.M Sze, *Semiconductor devices, Physics and technology*, John Wiley &sons, New York, (1985) p-73



- [17] K L Chopra and S R Das, Thin film solar cells, Plenum press, New York, (1983) p-75
- [18] M.A.Green, Solar cells, Prentice-Hall, Inc, (1992) p-70
- [19] K.L.Chopra and S. R. Das, Thin film solar cells, Plenum press, New York (1983)
- [20] Alan L. Fahrenbruch and Richard H. Bube, Fundamentals of solar cells Academic press, New York (1983) p- 130
- [21] Harold J.Hovel, Semiconductors and semimetals, Vol-II Solar cells, Academic Press, New York, (1975) p-72
- [22] M.A.Green, Solar cells, Prentice-Hall, Inc, Englewood Cliffs, (1992) p- 90
- [23] Krishan Lal (Editor), Synthesis Crystal Growth and characterization, North Holland (1982) p-491
- [24] Lawrence L Kazmerski (Ed) Polycrystalline and Amorphous thin films and devices, Academic press, (1980)
- [25] Alan to Fahrenbruch, R.H.Bube, Fundamentals of solar cells, Academic press New York (1983)p-36
- [26] “An over view of Photovoltaic technology”, Perihelion’s Watts Up article, Winter 2001
- [27] Adolf Goetzberger and Christopher Hebling, *Solar Energy Materials and Solar Cells*; 62 (2000) 1
- [28] Kazmerski L, Photovoltaics: a review of cell and module technologies Renewable and sustainable energy reviews.1 (1997) p-71
- [29] K. L. Chopra and Inderjeet Kaur, Thin Film Device Applications, Plenum Press New York, (1983) p-109
- [30] Nancy B Solomon, AIA article “Architectural Record”- continuing education Series
- [31] D.E.Carlson, C R Wronski, *Appl. Phys. Lett.*28; (1976) 671
- [32] C. Yang Jeffry; *Prog. Photovolt. Res. Appl.*, 6 (1998) 181

- [33] V. M Fthenakis and Moskowitz; *Prog. Photovolt.: Res. Appl*; 3 (1995) 295
- [34] W. H Bloss, F. Pfisterer, Schubert. M and T.Walter; *Prog. Photovolt. Res. Appl*; 3 (1995) 3
- [35] S.R Wenham, MA Green, S Edmiston, P Campbell, L Koschier, C B Honsberg, A.B.Sproul, D.Thorpe, Z.Shi, G.Heiser, *Solar Energy Materials and Solar Cells*; 41/42 (1996) 3
- [36] R.H.Bossert, C.J.J.Tool, J.A.M.van Roosmalen, C.H.M.Wentink, M.J.M. de Vaan, Thin film solar cells-technology Evaluation and Perspectives, May 2000, NOVEM, The Netherlands
- [37] A.M. Barnett, D.H. Ford, J.C. Checchi, J.S. Culik, R.B. Hall, E.L. Jackson, C.L. Kendall, J.A. Rand, Very-large-Area silicon-film TM solar cells, Proceedings of the 14th European Photovoltaic Solar Energy Conference, Barcelona, (1997) p-317
- [38] Robert W. Birkmire and Erten Eser, *Annu. Rev. Mater. Sci*; 27 (1997) 625
- [39] T.Aramoto, S.Kumazawa, H.Higuchi, T.Arita, S.Shibutani, T.Nishio, J.Nakajima, M.Tsuji, A.Hanafusa, T.Hibino, K.Omura, H.Ohyama and M.Murozono, *Jpn.J.Appl.Phys*.36 (1997) 6304]
- [40] [<http://www.ecomall.com/greeshopping/newsolar.htm>].
- [41] Tamotsu Okamoto, Yuichi Matsuzaki, owshad Amin, Akira Yamada and Makoto Konagai, *Jpn.J.Appl.Phys*; 37(1998) 3894
- [42] Brian Pamplin and R.S Feigelson, *Thin Solid Films*, 60 (1979) 141
- [43] J.R. Tuttle, J.S. Ward, A. Duda, T.A. Berens, M.A. Contreras,K.R. Ramanathan, A.L. Tennant, J. Keane, K. Emery,R. Noufi, *Mater. Res. Symp. Proc.* 426 (1996) 123
- [44] Photovoltaic Insider's Report , February,1999, page-2
- [45] M.J. Furlong, M. Froment, M.C. Bernard, R. Cortes, A.N. Tiwari, M. Krejci, H. Zogg, D. Lincot, *Journal of crystal growth*; 193 (1998) 114

- [46] C J Oswald, The PV industry moving into the solar century, Proceedings of the 2<sup>nd</sup> World conference on Photovoltaic solar energy conversion, Vienna, 1998
- [47] H W Shock, A Shah, Proceedings of the 14<sup>th</sup> European PV Solar Energy Conference, Barcelona, 1997, p-2000
- [48] P. K. Vidyadharan Pillai and K. P. Vijayakumar, *Sol. Energy Mat. Sol. Cells*; 51 (1998) 47
- [49] P. K. Vidyadharan Pillai, Ph.D Thesis, Cochin University of Science and Technology, 1997
- [50] K. Bindu, M. Lakshmi, S. Bini, C. Sudha Kartha, K.P. Vijayakumar, T.Abe and Y. Kashiwaba, *Semicon.Sci.technol.*, 17 (2002) 270]
- [51] S.Bandyopadhyaya, S Chaudhuri, A K Pal, *Solar Energy Materials & solar cells* 60 (2000) 323
- [52] J M Meese, J C Manturuthil and D R Locker, *Bull. Am. Phys. Soc*; 20 (1975) 696
- [53] T Walter, R Menner, ch.Koble, H W Shock; Proc.12<sup>th</sup> EC Photovoltaic Solar Energy Conf., Amsterdam,1994,1775
- [54] T Watanabe, M.Matsui, *Jpn. J. Apl. Phys*; 35 (1996) 1681
- [55] D.Braunger, D.Hariskos, T Walter, H W Shock, *Solar Energy Materials & solar cells*; 40 (1996) 97
- [56] Robert W. Birkmire, Compound Polycrystalline Solar Cells: Recent Progress and Y2K perspective, p-4

## Chapter 2

### REVIEW ON COPPER INDIUM SULFIDE FILMS AND CELLS

2.1 Introduction .....	46
2.2 CuInS <sub>2</sub> Thin Films.....	49
2.2.1 Preparation .....	49
2.2.2 Optical Properties.....	55
2.2.3 Electrical properties of CuInS <sub>2</sub> .....	58
2.2.4 Different studies on CuInS <sub>2</sub> thin films .....	59
2.2.5 Study of defects in CuInS <sub>2</sub> .....	64
2.2.6 Effect of incorporation of Na .....	65
2.2.7 Etching of CuInS <sub>2</sub> films using KCN .....	66
2.3 CuInS <sub>2</sub> based solar cells .....	67
2.4 Significance of present study .....	81
2.5 Conclusion.....	82
References .....	83

## Chapter 2

### REVIEW ON COPPER INDIUM SULFIDE FILMS AND CELLS

#### 2.1 Introduction

$\text{CuInS}_2$  belongs to the group of I-III-VI<sub>2</sub> compounds which are probably the most interesting ternary members in the tetrahedral family. These compounds, usually have chalcopyrite structure [1]. In I-III-VI compounds, if I and III atoms are replaced by II atoms, cubic zincblende structure would result. Chalcopyrite structure is the simplest, noncubic ternary analogue of the well-understood binary Zincblende structure, with  $c/a$  ratio approximately equal to 2. Lattice parameters of this compound are given in table-2.1.

All Cu-In-dichalcogenides can have ordered, chalcopyrite structure, with a tetragonal unit cell in which Cu and In atoms sit on distinct lattice sites or the disordered, zincblende structure, with a cubic unit cell in which the Cu and In atoms are distributed randomly on the lattice sites occupied by Zn in cubic ZnS [2].

$\text{CuInS}_2$  has body centered tetragonal structure as represented in Fig.2.1. Chalcopyrite is the most stable phase at 0K. At high temperatures (above 1200 K), the most thermodynamically stable phase is sphalerite, where Cu and In atoms are randomly distributed in the tetragonal cation sub- lattice [3].

Although sphalerite lattice structure is unusual for the bulk material, such lattice structure has been observed in thin films of  $\text{CuInS}_2$  obtained by the method of the sulfurization of CuIn in  $\text{H}_2\text{S}$  at 300 °C [4]. For  $\text{CuInS}_2$  nanocrystals in a glass matrix also, the sphalerite lattice has been observed [5].

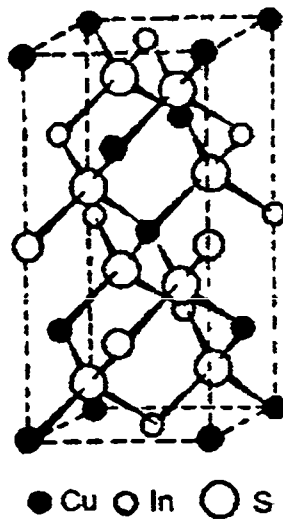


*Fig.1 The tetragonal chalcopyrite structure of CuInS<sub>2</sub>*

Table-1

Chemical Formula:	CuInS <sub>2</sub>
Composition:	Molecular Weight = 242.50gm
	Indium 47.35 % In
	Copper 26.20 % Cu
	Sulfur 26.45 % S
	100.00 %
Empirical Formula:	CuInS <sub>2</sub>
Lattice Parameters:	a = 5.52 Å, c = 11.13 Å
	c/a = 2.01
Melting temperature:	1000-1050 °C [11]
Bandgap	1.55 eV

The optical absorption of  $\text{CuInS}_2$  is very high with optical absorption coefficient nearly  $10^5 \text{cm}^{-1}$  in the visible and near-IR regions [5-6]. A comparison of the absorption length of different semiconducting materials is represented in Fig.2.2

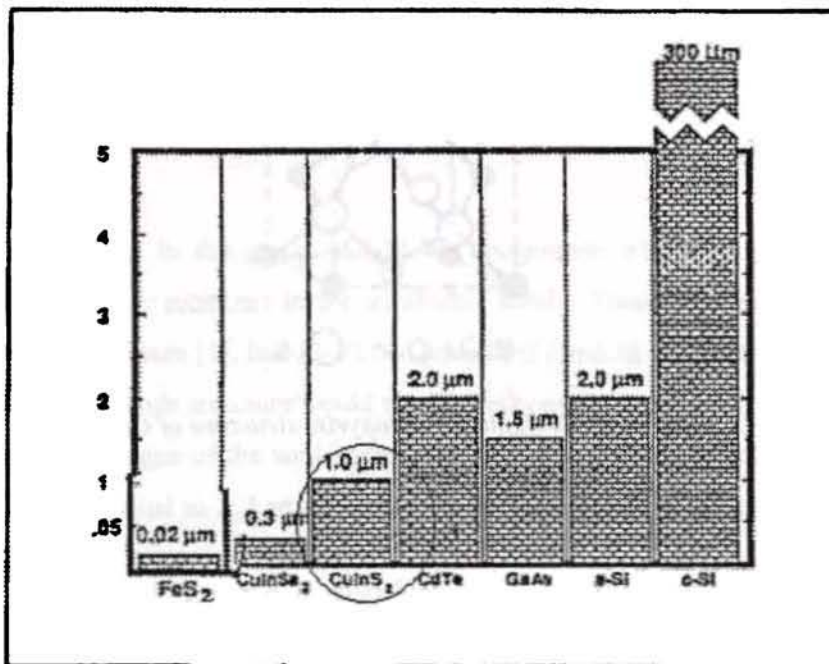


*Fig.2.2 Comparison of the absorption length for different semiconductor materials*

There are four major techniques for the synthesis and subsequent crystal growth of  $\text{CuInS}_2$ . They are, 1) direct synthesis from stoichiometric amounts of the constituent elements, 2) direct synthesis involving binary compounds of the constituent elements, 3) Vapor transport of the constituent elements and 4) solution or flux growth [7]

## 2.2 CuInS<sub>2</sub> Thin Films

### 2.2.1 Preparation

During mid 1970s, the chalcopyrite ternary compounds received considerable attention and attempts were made to prepare these compounds in thin film form. In 1975, two deposition schemes for producing CuInS<sub>2</sub> thin films (viz., single and double source methods), were reported for the first time by Kazmerski et al.[8]. For the single-source method, single-phase CuInS<sub>2</sub> was used as the starting material. The second, and more controllable and reproducible scheme involved a two-source arrangement. First, the single-phase CuInS<sub>2</sub> powder was evaporated from a resistive -heated alumina crucible, and a second sulfur source was utilized to vary the amount of sulfur in the system [8].

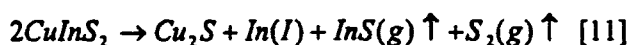
Since then, CuInS<sub>2</sub> thin films have been prepared by a variety of methods, including the three source evaporation [3,6,9] rf sputtering [10,11], close spaced chemical transport [12], chemical deposition [13,14], electrodeposition [15-17], flash evaporation [18,19], painting [20], spray pyrolysis [21-23], stacked elemental layer deposition technique [24] and two-stage process causing chalcogenization of the Cu-In alloy or Cu/In layer with S vapor/H<sub>2</sub>S gas at high temperature [4,25,26]. Among these, the two-stage process was found to be the best method for producing thin films of large area.

However, it has also been found that it is difficult to obtain high-grade single-phase CuInS<sub>2</sub> thin films by using conventionally available two-stage processes, because various impurity phases such as Cu<sub>2-x</sub>S, InS, In<sub>2</sub>S<sub>3</sub>, or CuIn<sub>5</sub>S<sub>8</sub> are inevitably introduced in the sulfurized CuInS<sub>2</sub> film [4]. On the other hand, a single phase CuInS<sub>2</sub> film can be prepared through sulfurization of homogeneous Cu-In thin film. But the preparation of Cu-In thin film by applying a simple annealing on Cu-In alloy or Cu/In layer is nearly



impossible because, an alloy or intermetallic compound containing Cu and In at a ratio of 1:1 does not exist in the Cu-In binary system [27].

Hwang et al. prepared CuInS<sub>2</sub> thin films using flash evaporation [11]. XRD analysis showed that the films prepared at the source temperatures in the range of 1100-1450°C contained In and InS phases. CuInS<sub>2</sub> peaks became more distinct at higher source temperatures. At high temperature range, the incongruent dissociation of CuInS<sub>2</sub> in vacuum could happen like this:



Since CuInS<sub>2</sub> dissociates incongruently, it is very difficult to deposit single phase CuInS<sub>2</sub> thin film by the flash evaporation method. However, Agarwal et al. reported successful preparation of single-phase n-type CuInS<sub>2</sub> thin films in the year 1998 [5]. Influence of substrate temperature on the crystallinity, conductivity activation energy and optical bandgap were investigated. An increase in the conductivity activation energy was observed with increase of substrate temperature, due to the improvement in the crystallite size and crystallinity. Neumann et al. reported optical properties of CuInS<sub>2</sub> thin films prepared using flash evaporation [19].

Hwang et al. used RF sputtering for preparing CuInS<sub>2</sub> films. Stoichiometric CuInS<sub>2</sub> powder was pressed into a 1½" diameter disk under high pressure and this disk was used as the sputtering target and frequency was in the range 12 to 14 MHz [11].

Bhattacharya et al., tried to prepare copper indium sulfide films on Ti substrates using electrodeposition [15]. Plating solution contained 6.2mM InCl<sub>3</sub>, 6.2mM CuCl, 0.125M thiourea, 0.2%(v/v) Triethanolamine and 0.25%(v/v) ammonia in water. pH of the solution was kept at 2 by adding dilute HCl. Plating was carried out using a calomel reference and a platinum auxiliary electrode. As-deposited layers were annealed in Ar. A subsequent heat treatment in H<sub>2</sub>S further improved the photoresponse. Films heated

in S vapor showed some tendency to be p-type. It was found that heating p-type layers in  $H_2$  changed them to n-type [28].

$CuInS_2$  thin films prepared using electrodeposition from aqueous solution of  $Cu^+$  and  $In^{3+}$  ions and thiourea with subsequent annealing in  $H_2S$  atmosphere, were characterized using photo electrochemical measurements in polysulfide electrolyte [16]. Laser scanning of photo current together with microprobe analysis correlated n-and p-type behavior with In rich and Cu rich areas respectively. p-type layers were readily prepared using this method by increasing copper to indium ratio to more than unity. They prepared  $CuInS_2$  layers through electro deposition of a Cu-In alloy and subsequent sulfurization in  $H_2S$ . They also electrodeposited Cu-In alloys from cyanide electrolytes and obtained  $CuInS_2$  after  $H_2S$  treatment [29].

In 1990, there is another report on electrodeposition of Cu-In alloys for preparing  $CuInS_2$  thin films [30]. In this case, Cu-In alloy was prepared using electroplating from less toxic aqueous solution containing low toxicity complexes of copper and indium with citric acid. As-deposited layers were then heated in  $H_2S$ . They noticed that Cu/In ratio in the bath had a great influence on the composition of the film.

Two mechanisms for the formation of  $CuInS_2$  were proposed: one of them is direct formation from reaction between the alloy and  $H_2S$  gas while the other is formation via interdiffusion of the binary sulfides, which can be obtained at low temperatures in  $H_2S$  atmospheres.

Binsma et al. prepared  $CuInS_2$  thin films via a two-stage process, with reproducible results [4]. Double layer consisting of copper covered with indium could be converted into single phase  $CuInS_2$  at  $T > 325$  °C in the presence of liquid sulfur.

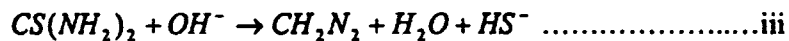
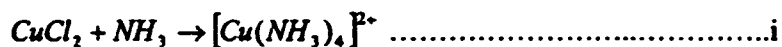
p- $CuInS_2$  films were deposited using spray pyrolysis in 1985 by Tiwari et al. [31]. Vijaya Lakshmi et al. prepared Mn doped p- $CuInS_2$  films using spray pyrolysis and observed an increase in band gap with Mn content in the film [32]. Later, X-ray, kinetic and optical properties of  $CuInS_2$  films prepared using spray pyrolysis were

investigated by Hernandez et al. [33]. Evolution of properties of spray-deposited CuInS<sub>2</sub> films with post-annealing treatment was reported very recently [34].

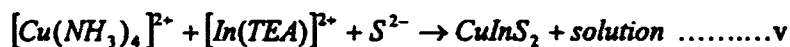
Samaan et al. prepared CuInS<sub>2</sub> thin films using rf sputtering in argon atmosphere ( $3 \times 10^{-2}$  Torr) with a frequency of 13.56 MHz supplied from a crystal-controlled generator via a matching unit [10]. The loose powder sputter target was prepared from p-type polycrystalline material. Rutherford Back Scattering (RBS) analysis indicated that films had an overall sulfur deficiency. They found that this deficiency was a function of dc bias voltage induced on the target surface and increasing the dc bias could increase the S content of the films. CuInS<sub>2</sub> samples prepared on water-cooled substrates showed presence of Ar impurities, which had been trapped during the sputter deposition process.

In 1986, Padam et al. reported for the first time, chemical deposition of CuInS<sub>2</sub> thin films from a bath containing 10ml CuCl<sub>2</sub>.21/2H<sub>2</sub>O (0.5M), 5.5ml InCl<sub>3</sub> (0.5M), 40ml thiourea (0.5M), 6ml triethanolamine (0.5M) and 20 ml ammonia (13.4M). They studied the effect of deposition parameters on the structural and electrical properties of these films [13].

Chemical bath deposition is based on slow reaction between the slowly released Cu<sup>+</sup>, In<sup>+</sup> and S<sup>-</sup> ions from their complexes, according to the following steps: [14]



The overall reaction is represented in the following equation,



Surface topography of the films was studied using scanning electron microscope. On increasing the film thickness, grain size increased and grain boundary became better and an increase in the grain size was observed.

Tembhurkar et al. prepared  $\text{CuInS}_2$  thin films using aqueous solutions of cupric chloride, indium tri chloride and thiourea [35]. Molarity of each solution was 0.003 M and were mixed in the ratio 1:1:3.2 by volume. Lattice parameters of films were calculated from X-ray diffraction measurements and the values obtained are  $a = 0.5524$  nm,  $c = 1.1105$  nm. The tetragonal distortion  $\Delta (=2-c/a)$  was -0.01031.

Polycrystalline  $\text{CuInS}_2$  thin films were prepared through sulfurization of Cu-In-O films deposited from a sintered  $\text{Cu}_2\text{In}_2\text{O}_5$  target by using a pulsed laser deposition (PLD) method [36]. Subsequent annealing in  $\text{H}_2\text{S}$  gas atmosphere produced  $\text{CuInS}_2$  films. Films with chalcopyrite structure were obtained when Cu-In-O films were sulfurized at a temperature higher than  $400^\circ\text{C}$ .

Takahiro et al. reported a two-stage process in which Cu-In-O films are prepared from a  $\text{Cu}_2\text{In}_2\text{O}_5$  target by pulsed laser deposition, during the first process. In the second process, these Cu-In-O films were transformed into  $\text{CuInS}_2$  by annealing in  $\text{H}_2\text{S}$  atmosphere [27]

Polycrystalline thin films of single phase  $\text{CuInS}_2$  were prepared from copper/indium/ sulfide stacked layer through various heat-treatments in the nitrogen atmosphere [24]. Stacked layers were converted to single phase  $\text{CuInS}_2$  at optimum heat-treatment temperature of  $500^\circ\text{C}$ . Post deposition heat treatments were carried out to investigate how the as-deposited films were affected by heat treatment.

Yamamoto et al. prepared  $\text{CuInS}_2$  thin films using RF sputtering from binary compounds  $\text{Cu}_2\text{S}$  and  $\text{In}_2\text{S}_3$  [37].

One-step electrodeposition of Cu-In-S thin films using  $\text{Na}_2\text{S}_2\text{O}_3$  as sulfur source was carried out for the preparation of  $\text{CuInS}_2$  films [17]. Sulfur content in the film was sufficient compared with the films deposited using  $\text{CS}(\text{NH}_2)_2$ . These films did not show

a 'waste thread 'like morphology which is characteristic of electrodeposited Cu-In precursors.

Yukawa et al reported electrodeposited  $\text{Cu}_2\text{S}$  thin films as first step for the preparation of  $\text{CuInS}_2$  films by two-stage electrodeposition [17].

$\text{CuInS}_2$  thin films were also grown through a two-step process without  $\text{H}_2\text{S}$ . Here they used elemental sulfur for sulfurization of sequentially evaporated Cu/In stalks [38].

Another method for the preparation of  $\text{CuInS}_2$  absorber layers was developed by J.Penndorf et al. in 1998 [39]. This technique is called "CIS on copper tape" or "CISCuT". In a continuous roll-to-roll process, a copper tape is first electrochemically plated with In layer. This tape undergoes rapid sulfurization process in the second step at  $600^\circ\text{C}$  in atmospheric pressure. Different analyses reveal that in this high-speed and highly productive process, photoactive  $\text{CuInS}_2$  is formed.

Miles et al. prepared Polycrystalline thin films of  $\text{CuInS}_2$  using a two-step process [25]. Magnetron sputtering of alternate ultra thin layers of Cu and In resulted in the formation of  $\text{Cu}_{1.1}\text{In}_9$  precursor layer. This was converted into chalcopyrite  $\text{CuInS}_2$  by annealing in a closed graphite box containing elemental sulfur, at temperature around  $350^\circ\text{C}$ .  $\text{CuInS}_2$  thin films were grown using close-spaced vapor transport in a vertical reactor closed under vacuum. Solid iodine was used to act as the reagent. Electrical, optical and structural characterizations of the films were done. Samples grown at the low temperatures ( $360^\circ\text{C}$  &  $370^\circ\text{C}$ ) showed very high Hall mobilities that could be due to CuI, which is present in these films [12].

In 2001, there is another report on the electrical properties of Cu-In-S absorber prepared by CISCuT technique [40]. When sulfurized under special transient conditions, an internal structure with at least four different semiconducting layers was found, and this structure has a rectifying I-V characteristic without any buffer layer. Electron beam induced current (EBIC) investigation and thermo power measurement revealed pnp

structure with the n-type layer being the In-rich one. The lower part of the film contained a short-circuited p-n junction, switched in series in the opposite direction.

In the same year, another new technique, ion-layer gas reaction (ILGAR) for the deposition of  $\text{CuInS}_2$  was developed by Moller et al. [41]. This technique involved chemical bath deposition of Cu(I) and In(I) salts by dipping porous substrates in appropriate precursor solutions. In a subsequent gas phase reaction with pre-heated  $\text{H}_2\text{S}$  vapor, deposited ion salts were converted into  $\text{CuInS}_2$ . Typical layer thickness after a single ILGAR cycle was 10-20 Å, and thicker layers were obtained by repeating the process.

$\text{CuInS}_2$  and  $\text{CuIn}_{(1-x)}\text{Al}_x\text{S}_2$  thin films were prepared on various substrates using the chemical spray pyrolysis technique (CSP) [42]. It was found that the nature of the substrate and the presence of Al atoms in the material noticeably affect growth and structure of the film. Annealing of  $\text{CuInS}_2$  film deposited on  $\text{SnO}_2$  resulted in best composition.

In order to get information on work function ( $\Phi$ ) of the film (deposited over pyrex), Kelvin method was used, which allows to determine contact potential difference  $(\Phi_1 - \Phi_2)/q$  between the surface of these samples. Work function difference ( $\Phi_{\text{material}} - \Phi_{\text{probe}}$ ) for  $\text{CuInS}_2$  was -350 meV. But by introducing Al atoms in the film, this was increased to -400 meV.

### 2.2.2 Optical Properties

Optical properties of  $\text{CuInS}_2$  near fundamental edge were studied using measurements of absorption, reflectivity, electroreflectance, photorefectance, wavelength-derivative reflectance, photovoltage and photoconductivity.

Sun et al. measured absorption coefficient of vacuum-deposited  $\text{CuInS}_2$  thin films at room temperature [43]. Absorption edge corresponding to direct bandgap transition ( $1.54 \pm 0.02$  eV) is observed in the  $\alpha$  vs.  $h\nu$  graph. In p-type  $\text{CuInS}_2$  thin films,

another edge is evident at lower energies (1.41-1.42eV) and is attributed to transition from a copper vacancy level to the conduction band.

Annealing a vacuum deposited p-type CuInS<sub>2</sub> film in H<sub>2</sub>S/Ar, results in increase of magnitude of  $\alpha$  for  $h\nu > 1.54\text{eV}$  and sharpening of the absorption edge. In addition, the structure associated with the Cu-vacancy band diminishes. Improvement in absorption characteristics is attributed to the grain growth, resulting from the annealing procedure and reduction of copper vacancies in the film. This is probably due to two mechanisms. First is migration of copper interstitials to the lattice sites and the second is filling of sites with excess sulfur during annealing [43].

Neumann et al. studied optical absorption of flash evaporated CuInS<sub>2</sub> thin films in the photon energy range from 0.5- 4.2 eV [19]. Band gap was found to be  $1.524 \pm 0.005$  eV at room temperature. Ground state energy of exciton was found to be  $8 \pm 2\text{meV}$ . An indirect allowed transition was observed at  $1.565 \pm 0.005$  eV and was ascribed to an optical transition from the valence band maxima at the boundary of the Brillouin zone to the lowest conduction band minimum at the zone center. Three further transitions (which were probably due to the copper d states in the valence band) were found at energies well above the fundamental edge.

CuInS<sub>2</sub> has positive temperature coefficient of energy gap below 120 K, which has been explained as the result of thermal expansion, whereas, the negative temperature coefficient above 120 K is considered to be the result of electron- phonon interaction. Contribution of electron-phonon interaction to energy gap in CuInS<sub>2</sub> was studied using photocurrents of Schottky barrier diode in the temperature range 10 to 300K [44]. Experiments done by Hsu et al. show that electron- phonon interaction for the band transition is dominated by the highest energy phonons. Wada et al. observed an increase in the bandgap of the films with annealing temperature [27].

Optical properties of sprayed CuInS<sub>2</sub> thin films in fundamental absorption region was studied by Ghafor et al. [45].

Evaporated films demonstrated two optical direct transitions of 1.5 eV and 1.72eV [14]. It was concluded that the higher gap might be due to optical transitions from the copper d states in the valance band to the lowest conduction band minimum, which disappeared due to heating. This result was confirmed by Neumann et al. [19].

### 2.2.2.1 Luminescence studies of CuInS<sub>2</sub>

First observation of homojunction electroluminescence in CuInS<sub>2</sub> was reported by P M Bridenbaugh et al. [46]. Two peaks at 1.48 and 1.40eV were present in the 300K spectrum, whereas a deep emission at 1.42eV dominates the 77K electroluminescence spectrum.

In low temperature photoluminescence spectrum of CuInS<sub>2</sub>, Emission peak at 8075Å is attributed to radiative recombination of free excitons associated with the lowest direct energy gap and is based on the observation of exciton reflection anomalies at approximately the same wavelength.

A number of investigators detected emissions at 1.446eV and 1.406eV and attributed these to the transitions between donor ( $V_s$ , In<sub>i</sub>) and acceptor ( $V_{cu}$ ) levels [47]. Characteristic emission near 1.44 eV , could be particularly promoted by sulfur annealing. Wu et al. found that 1.425eV emission was only observed in sulfur-rich thin film samples (p-type) [9].

In the case of nanoparticles of CuInS<sub>2</sub> in a glass matrix, luminescence signal was observed in the region of 700-1100 nm, corresponding to long-wavelength tail of the optical absorption [5]. Investigation of the photoluminescence at liquid nitrogen temperature revealed two maxima in the region of 870nm (1.43eV) and 960nm (1.29eV). Since ratio of their intensities is not constant, Gurinovich et al. suggested a possibility of two different channels of luminescence.



### 2.2.3 Electrical properties of $\text{CuInS}_2$

It is observed that electrical properties of I-III-VI compounds containing S or Se can readily be controlled by suitable annealing conditions [48]. Electrical characteristics of  $\text{CuInS}_2$ , which has been annealed under maximum or minimum sulfur pressures, is given in table-2. Significant changes in resistivity and mobility can be obtained by annealing at different temperatures.

Table-2

Room temperature electrical properties of annealed  $\text{CuInS}_2$

Sample specifications	Type	$\rho(\Omega\text{-cm})$	Carrier density ( $\text{cm}^{-3}$ )	$\mu$ ( $\text{cm}^2/\text{V-s}$ )	References
Crystals, Annealed under maximum S pressure	P	5	$1 \times 10^{17}$	15	[Ref.1, 188]
Annealed under minimum S pressure	N	1	$3 \times 10^{16}$	200	[Ref.1, 188]
$\text{CuInS}_2$ thin films prepared using two-source evaporation	P	0.8-400	$10^{13}$ - $10^{16}$	0.2, 3.2 <sup>c</sup>	[(8)]
$\text{CuInS}_2$ thin films prepared using two-source evaporation	N	0.1-800	$10^{14}$ - $10^{19}$	1-10, 28 <sup>c</sup>	[(8)]

<sup>c</sup>Recrystallized in  $\text{H}_2\text{S}$ , initially n type.

$\text{CuInS}_2$  is readily made p-type by annealing at temperatures in the range 600-800°C for 24hr under maximum S pressure, and quenching to room temperature. On the other hand, annealing under minimum S pressure at a temperature of 650 °C for a time as short as 15 minutes results in n-type conductivity [49].

Electrical resistivity was reduced in the case of RF sputtered films by annealing the samples in argon atmosphere ( $10^{-2}$  torr) for 10 minutes at 410 °C [10]. Similar behaviour was observed by Pamplin et al. for films annealed in air at 500 °C [21].

Electrical conductivity of n-type  $\text{CuInS}_2$  is governed by sulfur vacancies, copper vacancies and indium interstitials while that of p-type is controlled by interaction of sulfur and copper vacancies. Masse et al. attributed n-type conduction to the creation of sulfur vacancies and the p-type conduction to the creation of copper vacancies [50]. Wu et al further reported the existence of indium interstitials as donors in undoped  $\text{CuInS}_2$  [9].

#### 2.2.4 Different studies on $\text{CuInS}_2$ thin films

Scheer et al. studied microstructure and phase chemistry of  $\text{CuInS}_2$  thin films prepared using coevaporation [6]. They found that morphology of evaporated single-layer  $\text{CuInS}_2$  films depends on stoichiometry, mainly the Cu/In ratio. In- rich films had gray-black shiny region while Cu-rich regions had gray-blue and dull appearance.

Compositional relations in the ternary phase diagram of Cu-In-S can be expressed by the parameters “molecularity deviation ( $\Delta m$ )” and “stoichiometric deviation ( $\Delta s$ )”.

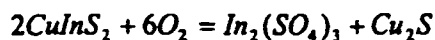
$$\Delta m = \frac{[\text{Cu}]}{[\text{In}]} - 1, \text{ and } \Delta s = \frac{2[\text{S}]}{[\text{Cu}] + 3[\text{In}]} - 1$$

Formation of Cu chalcogenide secondary phases in films prepared using three different preparation techniques with positive non-molecularity ( $\Delta m > 1$ ) was studied by Scheer et al.[46] Using X-ray diffraction and electron spectroscopy, they found that the films prepared by coevaporation and sulphurization has a CuS overlayer at the front surface. Segregation of CuS is not found in films prepared using spray pyrolysis [51].

Migge et al. performed a thermochemical analysis in Cu-In-S system at 298 K to estimate free energies of the compounds  $\text{In}_6\text{S}_7$ ,  $\text{In}_{2.8}\text{S}_4$ ,  $\text{CuInS}_2$ ,  $\text{CuIn}_5\text{S}_8$  and the recently discovered  $\text{CuIn}_2$ . They reported that free energy of  $\text{CuInS}_2$  is  $-315 \pm 54$  kJ/mol [52].

Influence of post deposition annealing of coevaporated  $\text{CuInS}_2$  films in hydrogen and oxygen atmosphere is studied using photoluminescence (PL) and nuclear reaction analysis (NRA) techniques [53]. Intensity of the PL peak at 1.445 eV can be drastically influenced by post-deposition treatments. This transition is ascribed to the donor-acceptor pair recombination between a sulfur vacancy and a copper vacancy. They found that sulfur vacancy can be activated by hydrogen annealing and passivated by oxygen annealing.

Grzanna et al. studied chemical stability of  $\text{CuInS}_2$  in oxygen at 298 K [54] by performing thermochemical analysis in the quaternary system Cu-In-S-O. They found 12 quaternary two-phase equilibria for Cu-In-S-O system. From the predominance area diagram of Cu-In-S-O for different partial pressures of oxygen, they found that the area of existence of  $\text{CuInS}_2$  become smaller and those of  $\text{In}_2\text{O}_3$  and  $\text{In}_2(\text{SO}_4)_3$  larger with increasing oxygen pressure. The field of  $\text{CuInS}_2$  just vanishes if the oxygen pressure becomes -51.5 Pascal. This pressure corresponds to the equilibrium,



Thus for oxygen pressures larger than this value,  $\text{CuInS}_2$  is unstable and will be transformed into  $\text{Cu}_2\text{S}$  and  $\text{In}_2(\text{SO}_4)_3$ .

C.Dzionk et al. investigated reactive annealing of Cu-In precursors in  $\text{H}_2$  atmosphere for preparing  $\text{CuInS}_2$  thin films [26]. They used a combination of XRD and complementary Perturbed Angular Correlation (PAC) measurements. It is found that  $\text{CuInS}_2$  films having chalcopyrite structure can be obtained at 400 °C and 500 °C. At higher temperature, a significant loss of indium due to the formation of the volatile  $\text{In}_2\text{S}_3$  compound occurs resulting in copper sulfide precipitation.

Based on these measurements they derived a model for the phase formation during reactive annealing process. In the first step, Cu-In precursors undergo a phase transformation. In the second step, In contained in the stoichiometric or In-rich precursors, is transformed into  $\text{In}_2\text{S}_3$ . Then remaining Cu-In phase reacts to form  $\text{CuInS}_2$  and CuS. The binary sulfides in the third step react to form  $\text{CuInS}_2$ . Later reaction is incomplete in the case of In rich precursors. So  $\text{In}_2\text{S}_3$  remains and slowly combines with  $\text{CuInS}_2$  to form  $\text{CuIn}_5\text{S}_8$ . In Cu-rich samples, there is no  $\text{In}_2\text{S}_3$ . Hence the third reaction does not apply and CuS remains as the minor phase.

Hydrogen diffusion in  $\text{CuInS}_2$  thin films was studied by measuring the spreading of implantation profiles upon annealing [55]. Hydrogen diffusion observed was too slow and was attributed to the intrinsic diffusion of hydrogen in these materials. It is found that in poly crystalline  $\text{CuInS}_2$  films, hydrogen leaves the samples through pores between grains.

Interaction of atomic hydrogen with the surface of Cu-III-VI<sub>2</sub> chalcopyrite semiconductors was studied by Lippold et al.[56]. Technique of low energy broad beam ion implantation into heated targets was used to introduce atomic hydrogen. They found that for temperatures above 150 °C, surface layer becomes rich in indium. Based on the results of micro Raman analysis and EDAX, they proposed a model for this effect: copper in-diffusion, caused by the filling of Cu vacancies and possible substitution of Cu by hydrogen. They also suggested that incorporation of atomic hydrogen at elevated temperatures could be a tool for controlled post growth stoichiometry variation of Cu chalcopyrite surfaces

Otte et al. implanted  $\text{H}^{3+}$  at 300eV into Cu-chalcopyrite semiconductors at temperatures between 50 °C and 300°C [57]. They found an increase of radiative recombination, which has been attributed to defect passivation due to hydrogen incorporation.

Ordering of Cu and In atoms in near stoichiometric  $\text{CuInS}_2$  epitaxial films was studied using transmission electron microscopy by Su et al. Nonchalcopyrite ordering of metal atoms was observed, which was identified as CuAu-type ordering. It was found that the CuAu-ordered structure coexists with chalcopyrite ordered structure [58].

Matsushita et al investigated formation process of  $\text{CuInS}_2$  phase from both  $\text{Cu+In+2S}$  and  $\text{CuIn+2S}$  mixtures using Differential Thermal Analysis (DTA) and powder x-ray diffraction measurement [59]. In the chemical reaction process of former mixture, an explosive endothermic reaction occurs at 640 °C, which is ascribed to formation of In-S materials. In the latter case, an explosive sulfurization reaction occurs at about 700°C, leading to the complete formation of the  $\text{CuInS}_2$  phase.

Electronic switching in thin films received much attention due to its potential applications in electronic industry. Recently, Kanzari et al. observed current controlled electronic switching effect in amorphous p- $\text{CuInS}_2$  thin films, when sandwiched between gold and copper electrodes [60].

In solar cells made of amorphous silicon or Indium phosphide, hydrogen is either an essential part of the system or is used to improve the performance of the cells. Effect of hydrogen in the chalcopyrite materials is now beginning to receive attention. Gil et al. performed muon spin rotation ( $\mu\text{SR}$ ) experiments on  $\text{CuInS}_2$  to study the effect and behavior of hydrogen in the material [61]. Muon spin rotation can provide information on the local structure and electronic configuration of isolated hydrogen because; muon can be regarded as a proton analogue or 'light isotope' of hydrogen.

Recently, there was a report on microstructure and secondary phases in coevaporated  $\text{CuInS}_2$  films on Mo coated glass and soda lime glass, using Raman scattering, Auger electron spectroscopy (AES), transmission electron microscopy, and x-ray diffraction techniques. Using combination of micro-Raman and AES techniques they identified that major secondary phases in Cu rich films are  $\text{CuS}$  at the surface of the as-grown layers and  $\text{MoS}_2$  at  $\text{CuInS}_2/\text{Mo}$  interface. Raman spectrum of  $\text{CuInS}_2$  is

characterized by the presence of dominant  $A_1$  mode, at about  $290\text{cm}^{-1}$ . This corresponds to vibrations of S anions in X-Y crystallographic directions of the tetragonal cell. Position and width of this peak are very sensitive to structural features [3].

Effect of post-deposition thermal treatments on properties of sprayed  $\text{CuInS}_2$  was reported by Krunk et al. [62] They found that vacuum annealing at  $500\text{ }^\circ\text{C}$  and hydrogen treatment at  $400\text{-}500\text{ }^\circ\text{C}$  purify the films from secondary phases, reduced chlorine content and improved crystallinity. Vacuum annealing resulted in n-type films due to the formation of  $\text{In}_2\text{O}_3$  phase while treatment in hydrogen reduced oxygen-containing residues resulting in p-type  $\text{CuInS}_2$  films with resistivity close to  $10\Omega\text{-cm}$ .

Removal of a deleterious CuS phase in  $\text{CuInS}_2$  through KCN etching is considered to be problematic. Aggour et al. developed a novel electrochemical treatment for  $\text{CuInS}_2$  films, to remove the segregated CuS phase [63]. Electrochemical treatments were carried out in a glass cell having three electrode potentiostatic arrangement with a Pt counter and a saturated calomel electrode as the reference. They were able to remove CuS phase and photo effect observed using this method was as good as that obtained after the KCN etch.

Electric and magnetic properties of Mn and Fe doped  $\text{CuInS}_2$  compounds were studied by Tsujii et al. [64]. Electrical conductivity changes drastically with increasing Mn concentration, indicating an increase of carrier density. It is found that susceptibility is reduced due to increase in Mn concentration, which indicates enhancement of antiferromagnetic interaction. However, magnetic ordering is not observed in these systems. For Mn doped samples, magnetization shows a step like increase around the field  $B_{\text{step}} = 25\text{ T}$ . This phenomenon was well explained by assuming the presence of Mn-Mn pairs or clusters, within which antiferromagnetic exchange interaction couples Mn ions. In the case of samples doped with Fe, magnetization increases monotonically

without any step, as antiferromagnetic interaction of Fe ions is weak since Fe-Fe distance is much larger than that of Mn-Mn.

Non-stoichiometric  $\text{CuInS}_2$  is a novel material for thin film solar cells. Electrical energy loss spectrometry analysis revealed that there are considerable lateral inhomogeneities on a scale of less than 100nm [65]. It is yet unknown whether Cu or In surplus comes in nano precipitates irregularly distributed in the otherwise stoichiometric matrix, or forms super cells where particular atoms are replaced by their complements

### 2.2.5 Study of defects in $\text{CuInS}_2$

Sulfur deficient  $\text{CuInS}_2$  thin films prepared using rf sputtering exhibited p-type conductivity. This behavior in thin films is not well understood. Two different models to identify the electrically active intrinsic defects in ternary compounds, free of a secondary phase, were proposed.

According to Neumann, one should use covalent bonding model instead of ionic model to assign electrical nature of cation and anion vacancies and interstitials [66]. Based on this model, group VI vacancies should act as acceptors, contrary to the assumption of ionic model, which predicts donor behavior for group VI vacancies. This was observed in both  $\text{CuInS}_2$  and  $\text{CuInSe}_2$  samples, which have overall anion deficiency and p-type conductivity. However, this model fails to be totally consistent, since by decreasing the anion deficiency, one should observe a decrease in the net hole concentration and not an increase as observed by Samaan et al. [10].

Noufi et al. suggest that p-type conductivity in selenium deficient  $\text{CuInS}_2$  is accounted for, if one assigns to In a valence charge state of  $\text{In}^{2+}$  and/or  $\text{In}^+$  instead of  $\text{In}^{3+}$ . This could also result in the creation of acceptor states. However, there is no direct experimental evidence on the different charge states of In in  $\text{CuInS}_2$  or  $\text{CuInSe}_2$  (or  $\text{CuInTe}_2$ ) single crystals. Hence it seems that origin of p-type conductivity in sulfur deficient  $\text{CuInS}_2$  is still an open question. Sulfur vacancies for bulk single crystal  $\text{CuInS}_2$  can

form a shallow acceptor level ( $\Delta E_A = 0.15$  eV) that disappears after annealing in sulfur vapor [5].

### 2.2.6 Effect of incorporation of Na

Sodium incorporation into  $\text{CuInS}_2$  is of great interest because controlled incorporation of Na into this material has improved cell performance remarkably. In 1997, Watanabe et al. investigated characteristics of Na-incorporated  $\text{CuInS}_2$  films by intentional addition and diffusion from a soda-lime glass [67]. They observed a striking difference in the film morphology between the Na containing and Na-free  $\text{CuInS}_2$  films in the size and shape of the grains. SEM micrographs revealed that Na-free  $\text{CuInS}_2$  films had needle like grains on the surface. However, with sodium, grains changed significantly to large and coarse. Also the full width at half maximum (FWHM) of the (112) peak for sodium containing  $\text{CuInS}_2$  films was much narrower than that of sodium free films. Enhancements in conductivity, crystallite quality and device performance is also reported in controlled Na- incorporated  $\text{CuInS}_2$ .

In 1998, they investigated effects of intentional Na incorporation on electrical conductivity of Cu-poor  $\text{CuInS}_2$  thin films [68]. These films were deposited through sulfurization of In-S/Cu/Na<sub>2</sub>S/In precursors. Sodium incorporation resulted in a remarkable increase in conductivity and cell efficiency of  $\text{CuInS}_2$ -based solar cells. Photoluminescence measurements revealed that enhancements were due to annihilation of donor states, (most likely In interstitials) by sodium incorporation.

Changes in the electronic structure of  $\text{CuInS}_2$  thin films due to Na incorporation were studied by Fukuzaki et al. [69]. XPS spectra were recorded for Na free Cu deficient  $\text{CuInS}_2$  and Na incorporated films. Peaks corresponding to Cu 2p, In 4d and S 2p of  $\text{CuInS}_2$  films were shifted by  $-0.5$  eV, due to Na incorporation. They suggested formation of a new (Na,Cu)InS<sub>2</sub> phase on the film surface. Electron density of states increased by Na incorporation and increments were larger for films with larger Cu



deficiency. They propose that the electrons were delivered from  $Na_{Cu}$  into the valent band of the Cu-deficient p-CuInS<sub>2</sub>.

Yamamoto et al. investigated electronic structures of Na-incorporated In-rich CuInS<sub>2</sub>, based on *ab initio* electronic band structure calculations. They found the formation of ionic  $Na_{Cu}$ -S bond decreases Madelung energy, resulting in a shift in energy levels of S 3p orbitals, in the vicinity of Na atoms, towards lower energy regions [70]. Mobile Na will act as a passivator of donor states such as  $In_{Cu}$  and interstitial In.

### 2.2.7 Etching of CuInS<sub>2</sub> films using KCN

Dissolution of metal chalcogenides in cyanide solutions is established since long before and was applied in surface treatment of solar cells. KCN is known to dissolve copper selenides and copper sulfides and was used successfully to prepare CuGaSe<sub>2</sub> based solar cells from very Cu-rich material [71]. Post deposition stoichiometric adjustment can be done using chemical etching step, using KCN. Complexing of copper by cyanide results in soluble species allowing to remove a variety of electronically deleterious copper chalcogenides [51].

In order to remove quasi-metallic CuS layer, which predominantly precipitates at the front surface of the Cu-rich films, Scheer et al. chemically treated the samples in KCN solution with X = Na, K [72].

Ogawa et al. have also applied KCN treatment on the CuInS<sub>2</sub> film [73]. For this CuInS<sub>2</sub> film was dipped in aqueous solution of 10% KCN for 3 minutes at room temperature and rinsed in deionized water. They found that after KCN treatment, Cu/In ratio was lowered to ~1 and is almost independent of the ratio existing before treatment. Resistivity increased by a factor of ~100, mainly due to a reduction of excess carrier concentration.

Hashimoto et al. found that KCN treatment adjusted the conduction band offsets from  $-0.7\text{eV}$  to  $-0.05\text{eV}$ . It also changed the interface Cu/ In ratio at the interface. KCN treatment removed  $\text{Cu}_x\text{S}$  phase or corrected structurally poor interface and made the band offsets close to the theoretical estimation [74].

### 2.3 $\text{CuInS}_2$ based solar cells

For economical reasons as well as because of the possibility of large-scale production, thin-film photovoltaic technology had been identified as an effective method, during the 1970s itself. But if the thin-film device is to be cost effective, substantial increase in device efficiency must be attained.

In 1977, Kazmerski et al. reported fabrication and characterization of vacuum deposited thin-film heterojunctions of several ternary compounds, including  $\text{CuInS}_2$  [75].  $\text{CuInS}_2$  films were grown by dual source deposition technique and CdS window layer was evaporated from a Ta- baffled source. Substrates were polished alumina with a Zn-Au-metallization for back contact. Efficiency of the  $\text{CuInS}_2/\text{CdS}$  cell was 2.55%.

First ternary thin film homojunction device (n-p  $\text{CuInS}_2$ ) solar cell was also reported in the same year by Kazmerski et al.[76]. Here also,  $\text{CuInS}_2$  films were grown using dual source deposition technique, employing a resistive-heated quartz crucible for single-phase ternary powder and a Ta boat for sulfur. Purpose of second chalcogen source was to alter S content in the film during the growth and hence, to control carrier type. Device with efficiency  $\eta = 3.33\%$  was reported and the best efficiency obtained was 3.62%.

In 1979, Gorska et al. reported an attempt to prepare solar cells using spray pyrolysed  $\text{CuInS}_2$  thin films [77]. They prepared heterojunction by spraying  $\text{CuInS}_2$  onto heated CdS single crystals. However, photoactivity was very poor. They also

prepared an all-thin-film heterojunction device, by spraying CdS over the CuInS<sub>2</sub> layer. In this case also, voltage and current values obtained were very low. ( $V_{oc} \approx 0.25V$  and  $I_{sc} \approx 0.004mA/cm^2$  respectively).

Totally sprayed CuInS<sub>2</sub>/Cd(Zn)S cell with an efficiency of 2.66% was reported by Ram et al., in 1985 [78].

Heterojunctions of hydrogenated a-Si films prepared by R.F.sputtering, with spray pyrolysed CuInS<sub>2</sub> films have been reported by Kumar et al., in 1986 [79]. Capacitance-voltage measurements showed the formation of a abrupt heterojunction exhibiting photovoltaic behavior with  $V_{oc} = 220mV$  and  $I_{sc} = 0.20mA/cm^2$ .

In 1992, Walter et al. investigated heterojunctions formed with coevaporated CuInS<sub>2</sub> and CuIn(Se,S)<sub>2</sub>, an alloy of CuInS<sub>2</sub> with CuInSe<sub>2</sub> [71]. During spectral response measurements, he observed reversal of photocurrent for certain wavelength range even at zero bias condition. This was attributed to the presence of quasi-metallic CuS phase, because the reversed photocurrent could not be observed in samples etched using KCN. They could get efficiency of 6.1% for a (Zn,Cd)S / CuInS<sub>2</sub> solar cell and an efficiency of 10.1% ZnO / CdS/ CuIn(Se,S)<sub>2</sub> structure.

In 1993, Scheer et al. prepared heterojunctions having structure glass/ Mo/p-CuInS<sub>2</sub>/ n-CdS/ n<sup>+</sup>-ZnO/ Al with an efficiency of 10.2% [72]. Absorber layer was deposited using the technique of coevaporation of the elements and over this, CdS layer was deposited from a chemical bath. Sputtered ZnO:Al layers served as transparent conductive window layer. Although they attempted to fabricate a configuration of CuInS<sub>2</sub> / ZnO also, without the bath-deposited CdS, those cells exhibited much lower photovoltages than in the previous case. Mitchell et al. reported 7.3% efficiency for ZnO/ CdS/ CuInS<sub>2</sub> thin-film cell [80].

In 1994, an efficient thin-film photovoltaic cell was fabricated using the heterostructure consisting of CuInS<sub>2</sub> film obtained by sulfurization of a metallic precursor, a chemical bath deposited CdS layer and an atom-beam-sputtered In<sub>2</sub>O<sub>3</sub> film

[73]. A preceding KCN treatment of the Cu-rich  $\text{CuInS}_2$  film lowered the Cu/In ratio and raised the resistivity. Conversion efficiency obtained was 9.7%.

In the same year, 3.1% efficient solar cell was reported by Uenishi et al [81]. This heterojunction had atom beam sputtered ZnO film, chemical bath deposited CdS layer, and  $\text{CuInS}_2$  film prepared using sulfurization of metallic precursor. Cells prepared with Cu/In ratio 1.68 had an efficiency of 1.2%, while cells having Cu/In ratio 1.85 exhibited an efficiency of 2.75%. But an efficiency of 3.15% was obtained for a film with Cu/In ratio 1.21 after annealing in vacuum at  $150^\circ\text{C}$  for 30 minutes.

According to Hovel, for a heterojunction solar cell, the best photovoltaic output will be obtained, when conduction band offset ( $\Delta E_c$ ) is small [82]. If  $\Delta E_c$  is positive, a notch is found in the absorber. But if  $\Delta E_c$  is negative, open circuit voltage is limited by the built in potential, which is smaller than the bandgap of the absorber layer material by  $-\Delta E_c$ .

In 1995, Hashimoto et al. reported the band offsets at the  $\text{CuInS}_2/\text{CdS}$  interface, determined by XPS [74]. In order to accurately calculate the band offsets, they measured  $\text{Cd}4d$  and  $\text{In}4d$  core levels as well as the valence band maximum (VBM). Then the band offsets are given by

$$\Delta E_v = E_{v-\text{In}4d} - E_{v-\text{Cd}4d} - \Delta E_{CL} , \text{ and}$$

$$\Delta E_c = -\Delta E_v - E_g(\text{CuInS}_2) + E_g(\text{CdS})$$

$\Delta E_{CL}$  is the energy difference between  $\text{Cd}4d$  and  $\text{In}4d$  levels of  $\text{CdS}/\text{CuInS}_2$  heterojunction and the values were,  $\Delta E_v = 1.8 \pm 0.3\text{eV}$  and  $\Delta E_c = -0.7 \pm 0.4\text{eV}$

After KCN treatment for removing degeneracy in carrier concentration, band offset changed to  $\Delta E_v = 1.08 \pm 0.1\text{eV}$  and  $\Delta E_c = -0.05 \pm 0.15\text{eV}$ . KCN treatment not only reduced carrier concentration of the  $\text{CuInS}_2$  film, but also improved the interface to establish alignment of conduction band minima.

In 1996, Braunger et al. showed that in  $\text{CuInS}_2$  based heterojunctions, CdS can be replaced by  $\text{In}_x(\text{OH,S})_y$ , which is Cd free buffer layer [83]. For the fabrication of this,  $\text{CuInS}_2$  thin layer was formed using thermal coevaporation of the three elements and the secondary CuS phase was removed by KCN etching. Cd-free buffer layer was deposited from aqueous solution of thioacetamide ( $\text{CH}_3\text{CSNH}_2$ ) and  $\text{InCl}_3$  at room temperature as well as temperature up to  $70^\circ\text{C}$ . The highest efficiency of this Cd-free, Se-free thin film chalcopyrite cell was 11.4%.

In almost all solar cells made from Cu-rich  $\text{CuInS}_2$  films, KCN treatment was essential to remove the secondary CuS phase, and to improve efficiency of the cell. Watanabe et al. tried to prepare high efficiency  $\text{CuInS}_2$  solar cell without using poisonous KCN treatment [84]. For this,  $\text{CuInS}_2$  films were prepared using a two-stage process in which Cu-In-S precursors were sputtered in  $\text{H}_2\text{S}/\text{Ar}$  and then annealed in  $\text{H}_2\text{S}$  atmosphere. They felt that reduction of secondary phases in In-rich samples is very important to obtain high efficiency without using poisonous KCN. They achieved an efficiency of 6.3% for the ITO/ CdS/  $\text{CuInS}_2$  structure, without KCN treatment.

CdS has been successfully used as buffer layer for Cu-III-VI<sub>2</sub> thin film absorbers for a long time. However from the point of view of environmental safety, the development of a Cd-free material is highly desirable. Finding out an alternative for CdS to produce Cd-free solar cells has been one of the most important intentions of several research groups working in this field. Several new n-type layers have been used to fabricate heterojunction with  $\text{CuInS}_2$  films.

Crystalline silicon (c-Si) is one such material. Lattice mismatch of 2% between c-Si and  $\text{CuInS}_2$  is quite moderate. First epitaxial Si /  $\text{CuInS}_2$  heterojunction device was reported in the year 1997 by Metzner et al [85]. They deposited slightly Cu-rich  $\text{CuInS}_2$  epilayers on sulfur terminated Si-(111) surfaces of n-type wafer. The heterojunction was completed by the deposition of indium tin oxide (ITO) layer and Ga

metallic back contacts. However, photoactivity of the device was very low. AM 1.5 illumination yielded a photocurrent of only 1.2mA.

Ennaoui et al. used ZnO, a material having band gap higher than that of CdS, as buffer layer for CuInS<sub>2</sub> solar cells [86]. ZnO films were prepared using chemical bath deposition or successive ionic layer adsorption and reaction (SILAR) method. Due to the large bandgap of the ZnO buffer layer, an enhanced response in the short wavelength of the spectrum was observed. However, the cells had lower efficiency (~3.8%).

Solar cells were fabricated using CuInS<sub>2</sub> thin-films prepared through sulfurization of Cu-In-O precursors in H<sub>2</sub>S gas in H<sub>2</sub> atmosphere [87]. The cell having structure ITO/ ZnO/ CdS/ CuInS<sub>2</sub>/ Mo/ glass, was fabricated after KCN treatment. Performance of these cells was studied as a function of the H<sub>2</sub> gas pressure during sulfurization and found that open-circuit voltage, short circuit current and fill factor increased with increasing the H<sub>2</sub> gas pressure. Conversion efficiency of the cell was strongly affected by the reduction of Cu-In-O precursors and the best cell had an efficiency of 7.5%.

Cells were also fabricated using CuInS<sub>2</sub> thin films through sulfurization of sequentially deposited Cu/In stacks with elemental sulfur. The window layer CdS/ZnO was deposited after removal of CuS secondary phase segregated at the surface by KCN etch and could get an efficiency of 10.4% [38]

In 1997, there was an interesting report by Scheer et al. They found that annealing of Cu-poor coevaporated films in S atmosphere during an extended cool-down period enhanced the lateral conductivity at room temperature [88]. They also observed an improvement of solar cell parameters of the CuInS<sub>2</sub>/ CdS/ ZnO cells fabricated using films subjected to the cool-down process. This influence was explained by the saturation of S vacancies during the cool-down period. By reducing the cooling

rate from 10K/min to 2K/min, efficiency increased from 3% to 8.3%, under AM 1.5 simulations.

Without toxic KCN treatment, conversion efficiencies of over 6% was achieved by using  $\text{CuInS}_2$  films prepared by sulfurization of precursors containing Na, while the cells using Na-free absorber layers showed poor cell performance of about 1%. Na incorporation was carried out deliberately by adding layer of a sodium compound between the precursor and the Mo electrode. The enhancement of  $V_{oc}$  (from 0.235V to 0.665V) and FF (from 0.270 to 0.526) is striking compared with  $J_{sc}$ . However, high concentrations of Na reduced cell efficiency [67]. They speculate that this must be due to the formation of  $\text{NaInS}_2$  phase, which is highly resistive.

Nature of substrates has very much influence on the properties of the film deposited over it. In the case of  $\text{CuInS}_2$  films prepared by sulfurization of metallic precursors deposited on Mo coated soda lime glass, it was observed that Cu-rich film often peeled off from the substrate. Film's adhesion to the substrate was significantly improved by introducing a very thin Ga layer between the Mo surface and the stacked Cu/In precursor layer [89]. An efficiency of 10.5% was obtained using this adherent thin film. Comparable efficiency was obtained for cells prepared on Pt substrates.

An 8.25% efficient  $\text{CuInS}_2$  solar cell having a four-layer structure (low  $\rho$ - $\text{CuInS}_2$ / high  $\rho$ - $\text{CuInS}_2$ / high  $\rho$ - $\text{CdS}$ / low  $\rho$ - $\text{CdS}$ ) was fabricated by Park et al.[90]. They found that lattice mismatch between  $\text{CuInS}_2$ /  $\text{CdS}$  has reduced to 2.8%.

The highest efficiency reported so far for  $\text{CuInS}_2$  based solar cells is 11.1% (total area efficiency) or 12.5% (active area efficiency) for a  $\text{CuInS}_2$ /  $\text{CdS}$ /  $\text{ZnO}$  structure with  $\text{MgF}_2$  antireflection coating [91]. In this work, they used a sequential process; at first the metal layers were deposited using DC magnetron sputtering and later this was sulfurized using elemental sulfur vapor. Heterojunctions were then prepared using chemical bath deposited  $\text{CdS}$  and a sputtered transparent conducting

ZnO window layer. The best cell with lowest defects was made from copper rich precursor layer having Cu/In ratio 1.8.

Gal et al. electrodeposited films of size quantized CdS as buffer layer on the CuInS<sub>2</sub> [92]. The resulting CuInS<sub>2</sub>/CdS thin film solar cells exhibited higher photocurrents and conversion efficiency (11.4%) than those made with conventional non-quantized CdS films. This was mainly due to the increased band gap of quantized CdS, allowing more light to reach the active CuInS<sub>2</sub> layer.

CuInS<sub>2</sub> thin films prepared through the new 'CISCuT' technique mentioned earlier [39] was also been used for preparing solar cells. Attempts to prepare conventional p-CuInS<sub>2</sub>/ n-CdS heterojunction failed all the time. Surprisingly, only a structure of CuInS<sub>2</sub>/ p-type semiconductor leads to a diode characteristic. ZnTe, Cu<sub>2</sub>O, Cu<sub>2-x</sub>S and Cu(S,O) have successfully been used to form such devices. First solar cell made from this material {CuInS<sub>2</sub>/ Cu(S,O)} had an efficiency of 6.1%.

As incorporation of Na increases conductivity of CuInS<sub>2</sub>, Watanabe et al. prepared solar cells using Na incorporated CuInS<sub>2</sub> [68]. These films were prepared through sulfurization of In-S/ Cu/ Na<sub>2</sub>S/ In precursors. The cell structure was ITO/ CdS/ CuInS<sub>2</sub>/ Mo/ SiO<sub>2</sub>/ SLG, and efficiency was 8.8%.

In order to have further improvement in efficiency of the cells fabricated using Na-incorporated CuInS<sub>2</sub> thin films, it was felt that there should be an increase in the open circuit voltage and hence the band gap has to be increased. Gallium (Ga) is commonly used as isovalent substitute for In, in order to increase the band gap. Watanabe et al. could attain higher open circuit voltage (exceeding 0.80V) by adding Ga to Na-incorporated CuInS<sub>2</sub> thin films [93]. Cu(In,Ga)S<sub>2</sub> films were prepared through the sulfurization of Na-containing Cu-In-Ga precursors in H<sub>2</sub>S atmosphere. The cell structure was ITO/ ZnO/ CdS/ Cu(In,Ga)S<sub>2</sub>/ Mo/ Ti/ SiO<sub>2</sub>/ SLG and the efficiency was 11.2% which is the highest efficiency reported for CuInS<sub>2</sub> solar cells fabricated without KCN treatment



Until recently, there have been a few studies to elucidate conversion losses, which limit performance of the thin film  $\text{CuInS}_2$  solar cells. Device or material parameters involved in its performance remain still unknown. Kneisel et al. applied thermal admittance spectroscopy to characterize trap properties of high efficiency  $\text{CuInS}_2/\text{CdS}/\text{ZnO}$  thin film solar cells. Defect spectra revealed that there is no dependence on the buffer layer. Two pronounced trap levels were found at 0.3 eV and 0.5 eV [94]. Both were identified as majority carrier traps in bulk p- $\text{CuInS}_2$  space charge region. The trap at 0.5 eV is correlated with a decrease in open circuit voltage of the cell.

Hashimoto et al. analyzed  $\text{CdS}/\text{CuInS}_2$  heterostructure using XPS [74]. Band offsets at  $\text{CdS}/\text{CuInS}_2$  interfaces formed on untreated  $\text{CuInS}_2$  as well as those formed on KCN treated  $\text{CuInS}_2$  were precisely determined by measuring core-level binding energies. They found that KCN treatment reduced conduction band offset ( $\Delta E_c$ ) from  $\sim 0.7$  eV to a very small value of 0.05 eV and correspondingly, cell efficiency increased from 3.01% to 9.67%.

Performance of  $\text{CuInS}_2$  solar cell, consisting of a transparent conductive oxide/ $\text{CdS}/\text{CuInS}_2$  heterostructure have been analyzed by Ito et al. [95]. A theoretical model, in which a very thin n-type  $\text{CuInS}_2$  layer is assumed to exist at the interface between the p-type  $\text{CuInS}_2$  and the n-type  $\text{CdS}$  buffer layer, was developed to explain the characteristics. In this case, an n-n heterojunction was formed between n-type  $\text{CdS}$  buffer layer and n-type  $\text{CuInS}_2$  layer. Two types of junctions (an abrupt junction and a graded junction) were theoretically discussed.

$\text{CuInS}_2$  solar cells were prepared by "rapid thermal process (RTP)" using a sequential preparation in which metallic layers of Cu and In are rapidly heated in presence of elemental sulfur vapor [96]. It is found that RTP improved crystal growth at

detrimental phases can be avoided by passing intermediate temperatures rapidly. Cells prepared from these films could reach 11.4% (total area) efficiency.

Recently, Klaer et al reported development of CuInS<sub>2</sub> based mini-module on 5x5 cm<sup>2</sup> glass substrate with 9.2% efficiency [97]. It consisted of 7 integrated series connected cells, with a total area of 16.2cm<sup>2</sup>. Absorber layer was grown using a sequential process, consisting of deposition of metallic films using sputtering followed by sulfurization in elemental sulfur vapor. Layer structure of the complete module was Mo/ CuInS<sub>2</sub>/ CdS/ ZnO.

It is well known that for polycrystalline cells, grain size must be large compared with the absorbing layer thickness, if an appreciable fraction of short circuit current potentially available is to be realized in practice. Onama et al. developed a process to fabricate higher efficiency solar cells using large grain CuInS<sub>2</sub> thin film synthesized from sulfur precursor [98]. They could prepare films with a maximum thickness of 9μm, having very large grains. To prevent peeling from substrate, a very thin Pt or Pd layer was deposited between the Mo and CuInS<sub>2</sub>. They characterized CuInS<sub>2</sub> absorbers having different film thicknesses varying from 2-9μm and related this to the performance of the photovoltaic device. The higher limit of film thickness for high efficiency device was found to be about 4 μm. Devices using thick films (>4 μm) gradually showed low efficiency and low stability in spite of high quality of the film. It is worth noting that device with very thick absorber layer (9 μm) showed a low efficiency. However, when the layer was thinned by chemical etching process, the cells showed an efficiency of ≈ 12%.

For CISCuT cells, commonly used p-type buffer layer is Cu(O,S), with a band gap of 2.6 eV. To increase the cell performance, CuI buffer layer with a higher band gap of 3.1 eV has been used. This lead to an improvement in performance of CISCuT cell from 3.89% to 5.2% [99].

Luck et al. investigated influence of different Na concentrations on  $\text{CuInS}_2$  film and corresponding  $\text{CuInS}_2/\text{CdS}/\text{ZnO}$  thin-film solar cells [100]. While morphology of the absorbers seemed to be not affected by this variation, corresponding PL spectra differed significantly. Properties of the cells, however, showed no dependence on Na concentration. This implies that even though the defect chemistry of  $\text{CuInS}_2$  is changed by the presence of Na, this influence has no impact on properties of corresponding solar cells.

Preliminary results of a new cell designed using an extremely thin  $\text{CuInS}_2$  absorber (eta-solar cell) has been reported recently [101]. Absorber is embedded in a porous and transparent structure in order to increase effective path length of light in absorbing material and to attain high absorption. For this, nano-porous /micro-porous  $\text{TiO}_2$  films were deposited over  $\text{SnO}_2/\text{glass}$  substrates using screen-printing /sol-gel pyrolysis and  $\text{CuInS}_2$  layer was deposited using ion layer gas reaction (ILGA). Heterojunction was completed with electrodeposited p-type  $\text{CuSCN}$  layer. Multiple scattering within porous structure and effective separation of charge carriers within depletion layer were obtained using an absorber layer of thickness 540nm.

Solar cell parameters, structure, and preparation methods of some of the reported cells are tabulated in Table-2.3

Table-2.3

Cell structure	Method of fabrication of different layers	Solar cell parameters					Reference
		Voc mV	Jsc/Isc mA/cm <sup>2</sup>	FF	$\eta$ %	Cell area(c m <sup>2</sup> )	
CuInS <sub>2</sub> / CdS	CIS- Dual source evaporation CdS - CBD	—	—	—	5.42	—	Kazmerski et al., 1977, [75]
n-CuInS <sub>2</sub> /p-CuInS <sub>2</sub>	CIS- dual source evaporation CdS- CBD	410	2.34m A	0.43	3.33	0.124	Kazmerski et al., 1977, [76]
CuInS <sub>2</sub> /Cd(Zn)S	CIS & Cd(Zn)S - Spray pyrolysis	440	8.25	0.27	2.66	—	Raja Ram et al., 1985, [78]
Al/p-CuInS <sub>2</sub> /a-Si:H/SnO <sub>2</sub> /F/glass	—	220	0.20	—	—	—	Kumar et al., 1986, [79]
(Zn,Cd)S/CuInS <sub>2</sub>	Three source evaporation	549	19.82	0.56	6.1	—	Walter et al., 1992, [71]
ZnO/CdS/CuIn(Se,S) <sub>2</sub>	—	492	31.2	0.66	10.1	—	Walter et al., 1992, [71]
Mo/CuInS <sub>2</sub> /CdS/ZnO	Cis-three source evaporation, CdS-CBD, ZnO-	697	21.5	0.69	10.2	0.4	Scheer et al., 1993,[72]
In <sub>2</sub> O <sub>3</sub> /CdS/CuInS <sub>2</sub>	CIS- sulfurization of metallic precursors, CdS-CBD, In <sub>2</sub> O <sub>3</sub> -	717	22.1	0.61	9.7	—	Ogawa et al., 1994,[73]

Cell structure	Method of fabrication of different layers	Solar cell parameters					Reference
		Voc	Jsc/Is <sub>c</sub>	FF	η %	Cell area(cm <sup>2</sup> )	
ZnO/CdS/CuInS <sub>2</sub>	CIS-sulfurization of metallic precursors, CdS-CBD, ZnO-sputtering	570	13.4	0.41	3.1	—	Uenishi et al., 1994,[81]
ZnO/In(OH,S)/CuInS <sub>2</sub>	CIS-thermal coevaporation, ZnO-	735	23.2	0.67	11.4	0.38	Braunger et al.,
ITO/CdS/CuInS <sub>2</sub>	CIS-reactive sputtering with H <sub>2</sub> S gas, CdS-CBD, ITO-magnetron	547	22.5	0.51	6.32	0.08	Watanabe et al., 1996,[84]
Ga/n-Si/p-CuInS <sub>2</sub> / ITO	Cis-epitaxial deposition, Csi-wafers, Ga-metallic alloying,	—	1.2	—	—	—	Metzner et al., 1997,[85]
ITO/ZnO/CdS/CuInS <sub>2</sub> /Mo/glass	CIS-sulfurization of Cu-In-O, CdS-CBD,	702	16.2	0.65	7.50	—	Negami et al.,
CuInS <sub>2</sub> /CdS/ZnO	CIS-coevaporation, CdS-CBD, ZnO-sputtering	596	23.4	0.61	8.3	—	Scheer et al., 1997,[88]
CuInS <sub>2</sub> /CdS/ZnO	CIS-sulfurization of Cu/In stacks, CdS-CBD, ZnO-sputtering	714	22.9	0.64	10.4	—	Klenk et al., 1997,[38]

Cell structure	Method of fabrication of different layers	Solar cell parameters					Reference
		Voc	Jsc/Is <sub>c</sub>	FF	η %	Cell area(c m <sup>2</sup> )	
SLG/Mo/CuInS <sub>2</sub> /CdS/ZnO:Al	CIS-reactive sputtering, CdS-CBD, ZnO:PF	665	18.9	0.52	6.61	.06	Watanabe et al., 1997,[91]
In <sub>2</sub> O <sub>3</sub> /CdS/CuInS <sub>2</sub>	CIS-sulfurization of Cu-In precursors, CdS-CBD,	700	24	0.63	10.5	—	Nakabayashi et al., 1997,[89]
Low ρ CuInS <sub>2</sub> /high ρ CuInS <sub>2</sub> /high ρ CdS/low ρ CdS	Electron beam evaporation	580	30.6	0.697	8.25	—	Park et al., 1997,[90]
ZnO/CuInS <sub>2</sub>	ZnO-CBD	360	19.4	0.55	3.8	—	Ennaoui et al., 1998,[86]
CuInS <sub>2</sub> /CdS/ZnO/MgF <sub>2</sub>	CIS-sulfurization of Cu/In,	728	21.4	0.71	11.1	—	Klaer et al., 1998,[91]
CuInS <sub>2</sub> /CdS/ZnO:Al	CIS-coevaporation, CdS-	745	21.6	.71	11.4	0.5	Gal et al., 1998,[92]
n-CuInS <sub>2</sub> /Cu(S,O)	CIS-CISCuT, Cu(S,O)-thermal deposition	653	16.1	0.57	6.1	3	Penndorf et al., 1998, [39]

Cell structure	Method of fabrication of different layers	Solar cell parameters					Reference
		Voc	Jsc/Isc mA/cm <sup>2</sup>	FF	η %	Cell area (cm <sup>2</sup> )	
SLG/SiO <sub>2</sub> /Mo/CuInS <sub>2</sub> /ITO	CdS-CIS-sulfurization of In-S/Cu/Na <sub>2</sub> S/In, CdS-CBD, ITO-RF sputtering	715	20.5	0.59	8.8	—	Watanabe et al., 1998, [68]
ITO/ZnO/CdS/Cu(In,Ga)S <sub>2</sub>	CIGS-sulfurization of Cu-In-Ga, CdS-CBD, Mo/Ti & ZnO- sputtering	802	20.9	0.66	11.2	—	Watanabe et al., 1999, [93]
Mo/ CuInS <sub>2</sub> / CdS/ZnO/ MgF <sub>2</sub>	CIS- rapid thermal process, CdS-CBD, ZnO-sputtering	729.4 mV	21.83	0.71	11.4	0.511	Siemer et al., 2001,[96]
Mo/CuInS <sub>2</sub> /CdS/ZnO (mini module)	CIS- sequential deposition, CdS-CBD, ZnO-sputtering	5.09V(727mV/cell)	19.1	0.65	9.2	16.2	Klaer et al., 2001, [97]

## 2.4 Significance of present study

We developed two new methods for the preparation of  $\text{CuInS}_2$  thin films. The first one is starting from CBD  $\text{Cu}_x\text{S}$ . In this method,  $\text{CuInS}_2$  film was prepared by evaporating indium over CBD  $\text{Cu}_x\text{S}$  and subsequently annealing the bilayer in vacuum. In the second method, we prepared  $\text{CuInS}_2$  using  $\text{Cu}_x\text{S}$  film prepared from CBD CdS (using Clevite process). Attempts were made to fabricate  $\text{CuInS}_2/\text{CdS}$  solar cells using  $\text{CuInS}_2$  films prepared by these two techniques. However, photoactivity was observed only for the cell fabricated using  $\text{CuInS}_2$  films prepared starting from CBD CdS. Although open circuit voltage of the junction was quite measurable, current was very feeble.

Also we made attempts to fabricate 'all-sprayed'  $\text{SnO}_2:\text{F}/\text{CuInS}_2/\text{CdS}$  solar cell. For this purpose, we characterized CSP  $\text{CuInS}_2$  films using XRD, Absorption and transmission studies. In addition, we used XPS analysis to investigate atomic concentration percentage of each element present in the film, from surface up to the substrate. Also photosensitivity was measured by irradiating the sample under illumination (intensity  $40 \text{ mW}/\text{cm}^2$ ) and the sample with best photosensitivity was used for fabricating solar cell.

We could fabricate an 'all-sprayed cell' with an efficiency 1.3% ( $\sim 1.9\%$  when corrected for transmission losses at the  $\text{SnO}_2:\text{F}$  layer). When low resistive CdS film was used as the window layer, there was slight increase in efficiency to 1.7% ( $\sim 2.4\%$  after correction). In most of the efficient solar cells, usually a thin layer of ZnO is deposited over CdS layer. An improvement in efficiency may be obtained using all sprayed  $\text{CuInS}_2/\text{CdS}/\text{ZnO}$  structure. In our lab, efforts are being made in this direction. Also, since there is a great interest in replacing CdS by a Cd-free buffer layer,  $\text{CuInS}_2/\text{In}_2\text{S}_3$  solar cells can be fabricated with chemical spray pyrolysed  $\text{In}_2\text{S}_3$ .



## 2.5 Conclusion

A review of  $\text{CuInS}_2$  thin films is made and its preparation, optical properties, and electrical properties are arranged separately. Results of etching of  $\text{CuInS}_2$  using KCN, effect of incorporation of sodium, results of defect studies and different other studies are also discussed. A review on solar cells based on  $\text{CuInS}_2$  thin films is made and some of the reported devices are tabulated.

## References

- [1] J.L Shay and J.H.Wernick, Ternary Chalcopyrite Semiconductors: Growth, Electronic properties and Applications, Pergamon Press, Oxford,(1975) p-4
- [2] David Cahen, *Solar Energy Materials*, 15 (1987) 225
- [3] J Alvarez-Garcia, A Perez-Rodriguez, A Romano-Rodrigues, J R Morante, L Calvo-Barrio, R. Scheer and R Klenk, *J. Vac. Sci. Technol. A*, 19 (2001) 232
- [4] J. J M Binsma, and H a Van Der Linden, *Thin Solid Films*, 97 (1982) 237
- [5] L I Gurinovich, V S Gurin, V A Ivanov, I V Bodnar, A P Molochko and N P Solovei, *Phys. Stat. sol.(b)*, 208 (1998) 533
- [6] R.Scheer, K.Diesner, H.-J.Lewerenz, *Thin Solid Films*, 268 (1994) 130
- [7] J.L Shay and J.H.Wernick, Ternary Chalcopyrite Semiconductors: Growth, Electronic properties and Applications, Pergamon Press, Oxford, (1975) p-50
- [8] L L Kazmerski, M S Ayyagari, and G A Sanborn, *J. Appl. Phys*, 46 (1975) 4865
- [9] Y.L.Wu, H.Y.Lin, C.Y.Sun, M.H.Yang, and H.L.Hwang, *Thin Solid Films*, 168 (1989) 113
- [10] A N Y Samaan, S M Wasim, A E Hill, D G Armour and R D Tomlinson, *Phys. Stat. Sol.(a)*, 96 (1986) 317
- [11] H L Hwang, C Y sun, C Y Leu, C L Cheng and C C Tu, *Revue De Physique Appliquee*, 13 (1978) 745
- [12] K. Djessas, G. Masse, and M. Ibannaim, *J.Electro. Chem. Soc.*, 147 (2000) 1235
- [13] G K Padam and S U M Rao, *Solar Energy Materials*, 13 (1986) 297
- [14] Siham Mahmoud and Abdel-Hamid Eid, *Fizika A*, 6 (1997)171
- [15] R N Bhattacharya, David Cahen and Gary Hodes, *Solar Energy materials*, 10 (1984) 41

- [16] Gary Hodes, Tina Engelhard, David Cahen, L.L.Kazmerski and Charles R Herrington, *Thin Solid Films*, 128 (1985) 93
- [17] Sigeeyuki Nakamura and Akio Yamamoto, *Sol. Energy Mat. Sol. Cells*, 49 (1997) 415
- [18] M K Agarwal, P D Patel, Sunil H Chaki and D Lakshminarayana, *Bull. Mater. Sci.*, 21 (1998) 291
- [19] H.Neumann, W Horig, V.Savelev, J.Lagzdonis, B. Schumann, and G.Kuhn, *Thin Solid Films*, 79 (1981) 167
- [20] G.Hodes, D.Cahen, J. manassen, and M.David, *J. Electrochem. Soc.*, 127 (1980) 2252
- [21] B. Pamplin and R.S.Feigelson, *Thin Solid Films*, 60 (1979) 141
- [22] P.Rajaram,R. Thangaraj, A.K.Sharma, A.Raza and O.P. Agnihotri, *Thin Solid Films*, 100 (1983) 111
- [23] A.N. Tiwari, D.K. Pandya, and K.L.Chopra, *Thin Solid Films*, 130 (1985) 217
- [24] S.K.Kim, W.J.Jeong, G.C.Park, Y.G.Back, Y.G.Jeong, and Y.T.Yoo, *Synthetic Metals*, 71 (1995) 1747
- [25] R W Miles, K T Ramakrishna Reddy, I Forbes, *J. Crystal Growth*, 198/199 (1999) 316
- [26] C. Dzionk, H.Metzner, S.Hessler, H.-E. Mahnke, *Thin Solid Films*, 299 (1997) 38
- [27] Takahiro Wada, Takayuki Negami, and Mikihiko Nishitani, *Appl. Phys. Lett.*, 62 (1993) 1943
- [28] J J M Binsma, L.J. Giling and J.Bloem, *J. Luminescence*, 27 (1982) 35
- [29] G Hodes and D Cahen, *Sol. Cells*, 16 (1986) 245
- [30] J Herrero, and J Ortega, *Solar Energy Materials*, 20 (1990) 53
- [31] A. N. Tiwari, D.K. Pandya, and K. L. Chopra, *Thin Solid Films*, 129-131 (1985) 217

- [32] R.P. Vijaya Lakshmi, R. Venugopal, D. Raja Reddy and B. K. Reddy, *Solid State Communications*, 82 (1992) 997
- [33] J. Gonzalez-Hernandez, P.M Gorley, P. P. Horley, O. M. Vartsabyuk, and Yu.V. Vorobiev, *Thin Solid Films*, 403/404 (2002) 471
- [34] S. Marsillac, M.C. Zouaghi, J.C. Bernede, T. Ben Nasrallah, and S. Belgacem, *Sol. Energy Mat. Sol. Cells*, [Article in press]
- [35] Y D Tembhurkar and J P Hirde, *Bull. Mater. Sci.*, (1992) 143
- [36] Takahiro Wada, Takayuki Negami, and Mikihiko Nishitani, *J. Mater.Res.*, 8 (1992) 545
- [37] Y. Yamamoto , T. Yamaguchi, T. Tanaka, N. Tanahashi, and A. Yoshida, *Sol. Energy Mater. Sol.Cells*, 49 (1997) 399
- [38] R. Klenk, U. Blieske, V. Dieterle, K. Ellmer, S. Fiechter, I. Hengel, A. Jager-Waldau, T. Kampschulte, Ch. Kaufmann, J. Klaer, M.Ch. Lux-Steiner, D. Braunger, D. Hariskos, M. Ruckh, H.W.Schock, *Sol.Energy Mat. Sol. Cells*, 49 (1997) 349
- [39] J. Penndorf, M. Winkler, O. Tober, D. Roser, K. Jacobs, *Sol. Energy Mater. Sol. Cells*, 53 (1998) 285
- [40] 40[(44) I. Konovalov, O. Tober, M. Winkler, and K. Otte, *Sol. Energy Mater. Sol. Cells*, 67 (2001) 49
- [41] J. Moller, Ch.-H. Fischer, H. J. Muffler, R. Konenkamp, I. Keiser, C. Kelch, and M.Ch. Lux-Steiner, *Thin Solid Films*, 361/362 (2000) 113
- [42] N. Kamoun, N. Jebbari, S. Belgacem, R. Bennaceur, J. Bonnet, F. Touhari, and L. Lassabatere, *J. Appl. Phys.*, 91 (2002) 1952
- [43] L Y Sun, L L Kazmerski, A.H Clark, P J Ireland and D W Morton, *J. Vac. Sci. Technol.*, 15 (1978) 265
- [44] T.M.Hsu, *Physics Letters A*, 133 (1988) 79

- [45] W A S Abdul Ghafor, N. A. Awad , and N.S.Othman, *Indian J. Pure & Appl. Phys.*, 31 (1993) 123
- [46] P M Bridenbaugh and P Migliorato, *Appl. Phys. Lett.*, 26 (1975) 459
- [47] A.W.Verheijen, L.J.Giling, and J. Bloem, *Mater. Res. Bull.*, 14 (1979) 237,
- [48] B.Tell, J.L Shay and H M Kasper, *J.Appl.Phys.*,43(1972) 2469
- [49] J.L Shay and J.H.Wernick, Ternary Chalcopyrite Semiconductors: Growth, Electronic properties and Applications, Pergamon Press, Oxford,(1975) p-188
- [50] G.Masse, N. Lahou, and C.Butti, *J. Phys. Chem. Solids*, 42 (1981) 449
- [51] R.Scheer, I. Luck, H. Sehnert, and H.J. Lewrenz, *Sol. Energy Mater. Sol. Cells*, 41/42 (1996) 261
- [52] H. Migge, *J. Mater. Res.*, 6 (1991) 2381
- [53] K.Topper, J. Krauser, J. Bruns, R. Scheer, A. Weidinger, and D. Brauning, *Sol. Energy Mater. Sol. Cells*, 49 (1997) 383
- [54] J. Grzanna and H. Migge, *J. Mater. Res.*, 12 (1997) 355
- [55] A.Weidinger, J.Krauser, TH.Riedle, R.Klenk, M.CH.Lux-Steiner, and M.V.Yakushev, *Mat. Res. Soc. Symp. Proc.*, 513 (1998) 177
- [56] Gerd Lippold, Karsten Otte, Hermann Schlemm, and Wolfgang Grill, *Mat. Res. Soc. Symp. Proc.*, 513 (1998) 269
- [57] K Otte, G.Lippold, D.grambole, F.Hermann, H.Schlemm, A.Schindler, and F.Bigl, *Mat. Res. Soc. Symp. Proc.*, 513 (1998) 275
- [58] D S Su, W Neumann, R Hunger, P Schubert-Bischoff, M Giersig, H J Lewerenz, R.Scheer and E. Zeitler, *Appl. Phys. Lett.*, 73 (1998) 785
- [59] Hiroaki Matsushita, Tomohiro Mihira, Takeo Takizawa, *J.Crystal Growth*, 197 (1999)169
- [60] M Kanzari, B Rezig, *J.Mat.Sci: Materials in Electronics*, 10 (1999)151

- [61] J.M. Gil, P.J.Mendes, L.P.Ferreira, H.V. Alberto, R.C. Vilao, N. Ayres de Campos, A. weidinger, Y. Tomm, Ch.Niedermayer, M.V. Yakushev, R.D. Tomlinson, S.P. Cottrell, and S.F.J.Cox, *Physical Review B*, 1999; 59(3), 1912
- [62] M. Krunk, O. Bijakina, V. Mikli, H. Rebane, T. Varema, M. Altosaar, and E. Mellikov, *Sol. Energy Mater. Sol. Cells*, 69 (2001) 93
- [63] M.Aggour, U.Storkel, C.Murrell, S.A.Campbell, H.Jungblut, P.Hoffmann, R.Mikalo, D.Schmeiber, and H,J.Lewrenz, *Thin Solid Films*, 403-404 (2002) 57
- [64] N.Tsujii, H.kitazawa, and G.Kido, *Phys. Stat. Sol.(a)*, 189 (2002) 951
- [65] Dipl.Ing. Michael Stöger - June 2002 -
- [66] H.Neumann, *Cryst. Res. Technol.*, 18 (1983) 483
- [67] Takayuki Watanabe, Hidenobu Nakazawa, Masahiro Matsui, Hiroki Ohbo, and Tokio Nakada, *Sol. Energy Mater. Sol. Cells*, 49 (1997) 357
- [68] Takayuki Watanabe, Hidenobu Nakazawa, and Masahiro Matsui, *Jpn. J. Appl. Phys.*, 37(11B) (1998) L1370
- [69] Koichi Fukuzaki, Shigemi Kohiki, Hideki Yoshikawa, Sei Fukushima, Takayuki Watanabe, and Isao Kojima, *Appl. Phys. Lett.*, 73 (1998) 1385
- [70] Tetsuya Yamamoto, *Jpn. J. Appl. Phys.*, 37 (1998) L1478
- [71] T. Walter, A. Content, K. O. Velthaus, and H. W. Schock, *Sol. Energy Mater. Sol. Cells*, 26 (1992) 357
- [72] R. Scheer, T. Walter, H.W. Schock, M. L. Fearheiley, and H. J. Lewrenz, *Appl.Phys.Lett.*,63 (1993) 3294
- [73] Yoshitaka Ogawa, Arnulf Jager-Waldau, Yoshio Hashimoto, and Kentaro Ito, *Jpn. J. Appl. Phys.*, 33(12B) (1994) 1775
- [74] Yoshio Hashimoto, Kazuhiro Takeuchi, and Kentaro Ito, *Appl. Phys. Lett.*, 67 (1995) 980
- [75] L L Kazmerski, F. R. White, M. S. Ayyagari, Y. J. Juang, and R. P. Patterson, *J. Vac. Sci. Technol.*, 14 (1977) 65

- [76] L. L. Kazmerski and G. A. Sanborn, *J. Appl. Phys.*, **48** (1977) 3178
- [77] M. Gorska, R. Beaulieu, J. J. Loferski, and B. Roessler, *Solar Energy Materials*, **1** (1997) 313
- [78] Poola Raja Ram, R. Thangaraj, A. K. Sharma, and O. P. Agnihotri, *Solar Cells*, **14** (1985) 123
- [79] Satyendra Kumar, A. N. Tiwari, O. S. Sastry, D. K. Pandya, and K. L. Chopra, *Bull. Mater. Sci.*, **8** (1986) 285
- [80] Proc. 20<sup>th</sup> IEEE Photovoltaic Specialist conference, New York, 1988
- [81] S. Uenishi, K. Tohyama, and K. Ito, *Sol. Energy Mater. Sol. Cells*, **35** (1994) 231
- [82] Harold J. Hovel, 'Semiconductors and Semimetals', Vol. II-Solar cells, Academic Press, New York, 1975, p-132
- [83] D. Braunger, D. Hariskos, T. Walter, H. W. Schock, *Sol. Energy Mater. Sol. Cells*, **40** (1996) 97
- [84] Takayuki Watanabe and Masahiro Matsui, *Jpn. J. Appl. Phys.*, **35** (1996) 1681
- [85] H. Metzner, Th. Hann, Chr. Schmiga, J. H. Bremer, D. Borchert, W. R. Fahrner, and M. Seibt, *Sol. Energy Mater. Sol. Cells*, **49** (1997) 337
- [86] A. Ennaoui, M. Weber, R. Scheer, and H. J. Lewerence, *Sol. Energy Mater. Sol. Cells*, **54** (1998) 277
- [87] Takayuki Negami, Yasuhiro Hashimoto, Mikihiko Nishitani, and Takahiro Wada, *Sol. Energy Mater. Sol. Cells*, **49** (1997) 343
- [88] R. Scheer, M. Alt, I. Luck, and H. J. Lewerenz, *Sol. Energy Mater. Sol. Cells*, **49** (1997) 423
- [89] T. Nakabayashi, T. Miyazawa, Y. Hashimoto, and K. Ito, *Sol. Energy Mater. Sol. Cells*, **49** (1997) 375
- [90] Gye-Choon Park, Hae-Duck Chung, Chang-Dae Kim, Hyuk-Ryeol Park, Woo-Jo Jeong, Jong-Uk Kim, Hal-Bon Gu, and Ki-Sik Lee, *Sol. Energy Mater. Sol. Cells*, **49** (1997) 365

- [91] J. Klaer, J. Bruns, R. Henninger, K. Seimer, R. Klenk, K. Ellmer, and D. Braunig, *Semicond. Sci. Technol.*, 13 (1998) 1456
- [92] Dori Gal, Gary Hodes, Dimitri Hariskos, Deiter Braunger, and Hans-Werner Shock, *Appl. Phys. Lett.*, 73 (1998) 3135
- [93] Takayuki Watanabe, and Masahiro Matsui, *Jpn. J. Appl. Phys.*, 38 (12A), (1999) L1379
- [94] Joachim Kneisel, Kai Seimer, Ilka Luck, and Dieter Braunig, *J. Appl. Phys.*, 88 (2000) 5474
- [95] Kentaro Ito, Naoki Matsumoto, Tsuyoshi Horiuchi, Katsuhiko Ichino, Hiroshi Shimoyama, Tsuyoshi Ohashi, Yoshio Hashimoto, Imke Hengel, Jutta Beier, Reiner Klenk, Arnulf Jager-Waldau and Martha Ch. Lux-Steiner, *Jpn. J. Appl. Phys.*, 39 (2000) 126
- [96] Kai Siemer, Jo Klaer, Ilka Luck, Jurgen Bruns, Reiner Klenk and Dieter Braunig, *Sol. Energy Mater. Sol. Cells*, 67 (2001) 159
- [97] Jo Klaer, Kai Siemer, Ilka Luck, and Dieter Braunig, *Thin Solid Films*, 387 (2001) 169
- [98] Yoshio Onuma, Kenji Takeuchi, Sumihiro Ichikawa, Mina Harada, Hiroko Tanaka, Ayumi Koizumi, and Yumi Miyajima, *Sol. Energy Mater. Sol. Cells*, 69 (2001) 261
- [99] J. Wienke, V. Groen-Smit, M. Burgelman, S. Degraeve, and J. Penndorf, *Thin Solid Films*, 387 (2001) 165
- [100] I. Luck, J. Kneisel, K. Siemer, J. Bruns, R. Scheer, R. Klenk, N. Janke, D. Braunig, *Sol. Energy Mater. Sol. Cells*, 67 (2001) 151
- [101] I. Keiser, K. Ernst, Ch.-H. Fischer, R. Konenkamp, C. Rost, I. Sieber, M.Ch. Lux-Steiner, *Sol. Energy Mater. Sol. Cells*, 67 (2001) 89



## Chapter 3

### PREPARATION OF $\text{CuInS}_2$ THIN FILMS STARTING FROM CBD $\text{Cu}_x\text{S}$ AND CBD $\text{CdS}$

3.1 Introduction .....	92
3.2 Deposition techniques .....	93
3.2.1 Chemical bath deposition (CBD) .....	93
3.2.1.1 Chemical aspects of CBD .....	94
3.2.2 Vacuum Evaporation.....	95
3.3 Experimental Details.....	96
3.3.1 Brief review of $\text{Cu}_x\text{S}$ films.....	96
3.3.2 Preparation of $\text{Cu}_x\text{S}$ films using CBD.....	97
3.3.3 Evaporation of indium.....	98
3.3.4 Annealing of the bilayer film .....	98
3.4 Results and Discussion.....	99
3.4.1 XRD Analysis .....	99
3.4.2 Optical Absorption Studies .....	103
3.4.3 Electrical properties .....	105
3.4.3.1 Sheet resistance .....	105
3.4.3.2 Hall measurement.....	106
3.3.4 Energy Dispersive X-ray analysis (EDAX) .....	107
3.3.5 Scanning Electron Micrograph (SEM).....	107
3.3.6 Electron Spectroscopy for Chemical analysis (ESCA).....	109
3.5 Sulfurization of $\text{CuInS}_2$ films.....	117
3.6 Experimental Details.....	117

<b>3.7 Results and Discussions .....</b>	<b>118</b>
3.7.1 XRD .....	118
3.7.2 Electrical properties .....	119
3.7.3 Optical Properties.....	121
3.7.4 Photosensitivity measurements .....	124
3.7.5 XPS analysis.....	124
<b>3.8 Conclusion.....</b>	<b>127</b>
<b>3.9 Experimental Details .....</b>	<b>128</b>
<b>3.11 Results and Discussions .....</b>	<b>131</b>
3.11.1 XRD Analysis .....	131
3.11.2 XPS Analysis .....	134
<b>3.12 Trial for the fabrication of CuInS<sub>2</sub>/ CdS solar cell.....</b>	<b>136</b>
<b>References .....</b>	<b>138</b>

## Chapter 3

### PREPARATION OF $\text{CuInS}_2$ THIN FILMS STARTING FROM CBD $\text{Cu}_x\text{S}$ AND CBD $\text{CdS}$

#### 3.1 Introduction

It is well known that a major reason that limits popular usage of PV devices today is high cost. Apart from material cost, cost of production is very decisive factor determining the cost of solar cells. As far as thin film solar cells are concerned, material consumption is very low. Hence for lowering the cost, adoption of low cost thin film deposition techniques is inevitable. Also the technique adopted should be simple, reproducible, suitable for large area deposition and should not create any environmental or health problems.

Recently, there has been considerable interest in developing  $\text{CuInS}_2$  thin films using various techniques. This chapter describes preparation and characterization of  $\text{CuInS}_2$  thin films prepared using two new techniques developed in our lab.

Although CBD is one of the prominent techniques for the preparation of binary compounds, when we prepare ternary films using this method, it is very difficult to control various parameters and produce films with good stoichiometry. In our lab, we tried to prepare  $\text{CuInS}_2$  films using CBD technique. We were able to prepare uniform, adherent films. However, XPS and ICP analysis indicated that In content in the film is very low, and hence we concluded that the film was most probably the binary compound  $\text{Cu}_x\text{S}$ , with traces of indium.

Hence we selected another route to prepare  $\text{CuInS}_2$  thin films and reported the preliminary results of our attempt [1]. For this,  $\text{Cu}_x\text{S}$  films were prepared using CBD technique and In was introduced into this film by thermal diffusion. For this, 99.999% pure In was evaporated onto the  $\text{Cu}_x\text{S}$  film and was subsequently annealed in vacuum. This is quite new technique and is simple and low cost as the binary film  $\text{Cu}_x\text{S}$  is prepared using the low-cost CBD technique at room temperature itself. Moreover, there is no requirement of vacuum for  $\text{Cu}_x\text{S}$  deposition. Earlier, Yukawa et al have reported electrodeposited  $\text{Cu}_2\text{S}$  thin films as the first step for the preparation of  $\text{CuInS}_2$  films by two-stage electrodeposition and to the best of our knowledge, this is the only technique similar to ours' and reported earlier [2].

Brief description of CBD and vacuum evaporation techniques used in the present work is given below.

## 3.2 Deposition techniques

### 3.2.1 Chemical bath deposition (CBD)

Although CBD has been used as a technique for preparing films since 1910, utilization of this technique to deposit thin films of semiconductors in photovoltaic devices started very recently. Later CBD became a useful method for the deposition of thin films of compound semiconductor materials, which are sulfides and selenides of some metals. Many of these compound semiconductors were identified as good candidates for PV device fabrication. Many groups started working in this area as this technique involves only low-tech process and is suitable for deposition of large area films.

### 3.2.1.1 Chemical aspects of CBD

Like any other thin film deposition process, CBD involves three main steps: 1) production of appropriate atomic, molecular or ionic species, 2) their transport to substrate through a medium and, 3) condensation on substrate, either directly or via a chemical reaction, to form a solid deposit. Formation of a thin film takes place via nucleation and growth process [3].

According to solubility product principle, in a saturated solution of a weakly soluble compound, ionic product is a constant at a given temperature. If the ionic product exceeds the solubility product, precipitation occurs. It is necessary to eliminate spontaneous precipitation in order to form a thin film by a controlled ion-by-ion reaction. Concentration of the ions in the solution can be controlled by adding appropriate complexing agents and by adjusting the temperature and pH of the solution. When precipitation is controlled, the compound gets deposited on the substrates, kept immersed in the reaction bath. Growth kinetics depend on concentration of ions, their velocities, as well as nucleation and growth processes on the immersed surfaces. Effect of these parameters on film deposition process is discussed in detail in references [4] & [5].

CBD process has several advantages over other methods of thin film deposition, which can be listed as follows. 1) the technique is simple and requires very low capital investment, 2) the process may be easily adapted to large area processing at low fabrication cost, 3) in many cases, films may be deposited at room temperature itself upon a variety of substrates, 4) thickness of the deposited layers may be readily controlled by variation of deposition time 5) does not require vacuum, 6) does not require high purity materials for film deposition, 7) can be operated by a technician for large scale production 8) no reaction involving gas or vapor.

### 3.2.2 Vacuum Evaporation

This is probably the most popular technique used for thin film deposition. There are several review articles / books giving detailed descriptions of this technique [6-9].

In this process, material is heated to a high temperature in a vacuum chamber so that large number of atoms or molecules leaves the surface of the material and gets deposited on the substrate. Because of low pressure in the chamber, most evaporated molecules suffer no collisions with residual gas molecules and travel in straight lines to the substrate. Small amounts of active residual gases can cause contamination and can change significantly the properties of the evaporated film. Rate of free evaporation of vapor molecules from clean surface of unit area in vacuum is given by

$$N_e = 3.513 \times 10^{22} p_e \sqrt{\frac{1}{MT}} \text{ molecules}/(\text{cm}^2)(\text{sec}) \dots\dots\dots(3.1)$$

where  $p_e$  is the equilibrium vapor pressure ( in Torr) of the evaporant under saturated-vapor conditions at a temperature T, and M is the molecular weight of the vapor species. Rate of deposition of vapor on substrate also depends on source geometry, its position relative to substrate and condensation coefficient.

Thermal evaporation can be achieved directly or indirectly (via a support) by a variety of physical methods such as resistive heating, flash evaporation, arc evaporation, exploding-wire technique, laser evaporation, RF heating, and electron bombardment heating. In the present work, we used resistive heating method for the evaporation of indium.

This method consists of heating the material using resistively heated filament or boat, generally made of refractory metals such as W, Mo, Ta and Nb, with or without ceramic coatings. Choice of supporting material is primarily determined by

evaporation temperature and resistance to alloying and/or chemical reaction with evaporant. Vapor sources of various types, geometries and size can easily be constructed or obtained commercially. Details of dependence of growth, structure and adhesion of evaporated films etc with different deposition parameters are described in many references [7-9].

## Part-1 CuInS<sub>2</sub> thin films from CBD Cu<sub>x</sub>S

### 3.3 Experimental Details

#### 3.3.1 Brief review of Cu<sub>x</sub>S films

Cu<sub>x</sub>S ( $x = 1-2$ ) thin films have recently received considerable attention due to numerous technological applications in the area of PV devices. At room temperature, Cu<sub>x</sub>S in bulk form, is known to exist in five stable phases: chalcocite (Cu<sub>2</sub>S), djurleite (Cu<sub>1.95</sub>S), digenite (Cu<sub>1.8</sub>S), anilite (Cu<sub>1.75</sub>S), and covellite (CuS). Mixed phases are also known in the intermediate compositions [10] This material (especially Cu<sub>2</sub>S) possesses extremely favorable properties which make it suitable for large-scale photovoltaic applications, particularly in combination with CdS. Low production cost and material availability make this cell suitable for large scale PV applications. Cu<sub>x</sub>S/CdS thin film solar cell has been the most extensively investigated thin film photovoltaic system. Main problem regarding this cell is degradation in presence of moisture. Interestingly, Partain et al., observed that degraded Cu<sub>x</sub>S/CdS solar cells could be recovered by annealing in presence of H<sub>2</sub> and air [11].

Kimihiko et al. studied electrical conductivity and phase transition of copper sulfide [12]. Various techniques such as vacuum evaporation [13], spray pyrolysis [10], sputtering [14], and chemical bath deposition [15,16], were

employed to prepare  $\text{Cu}_x\text{S}$  thin films. Fatas et al. prepared  $\text{Cu}_x\text{S}$  from a bath containing 1M  $\text{CuSO}_4$ , 1M sodium acetate, 1M thiourea and 7.4 M TEA. A. J. Varkey reported deposition from bath containing  $\text{CuCl}$ ,  $\text{NaCl}$  and hydroxylamine hydrochloride solutions, using EDTA as a complexing agent. Rezig et al. prepared  $\text{Cu}_x\text{S}$  films by conversion of spray deposited  $\text{CdS}$  by ion exchange [17].

### 3.3.2 Preparation of $\text{Cu}_x\text{S}$ films using CBD

In the present work,  $\text{Cu}_x\text{S}$  films were prepared using CBD technique. Bath used for this contained 1M Cupric Chloride (10 ml), 2M Thiourea (10 ml) and 5ml Ammonia solution (25%). Here triethanolamine (TEA) was used as complexing agent. pH of final solution was maintained at 9.8. Microscope glass slides (75mm  $\times$  25mm  $\times$  1.25mm) were used as the substrate. These slides were washed thoroughly first using soap solution and then using chromic acid. Microscopic impurities were removed using ultrasonic cleaning. These cleaned glass slides were dipped vertically in the bath. Four slides were dipped at a time and time of deposition was 15 minutes at room temperature. No stirring was given during deposition. Films obtained were uniform and golden in colour. Multiple dip films were prepared for the present work. Thickness of the double-dip sample, measured using Stylus method, was found to be 0.1 micron.

It is reported that annealing in hydrogen and other reducing atmospheres causes an increase in stoichiometry of  $\text{Cu}_x\text{S}$  layers where as exposure to or annealing in air always causes oxidation, with a deterioration in the stoichiometry and a decrease in the resistivity [13]. Hence, prepared  $\text{Cu}_x\text{S}$  samples were dried and were immediately transferred to vacuum chamber of the coating unit to deposit thin films of indium.



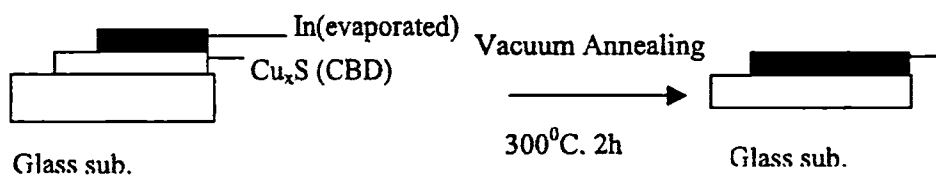
### 3.3.3 Evaporation of indium

The  $\text{Cu}_x\text{S}$  samples were masked 5mm from the four edges using teflon-tape (were having an area  $\sim 25\text{mm} \times 15\text{mm}$ ) and were loaded in the vacuum chamber. Required amount of 99.999% pure indium was weighed accurately using a microbalance and was placed in the Mo boat which was at a distance of 14cm from the substrates. Chamber was evacuated to a pressure of  $<10^{-5}$  torr. The boat was resistively heated until whole In was evaporated and deposited on surface of  $\text{Cu}_x\text{S}$  film. In this case, thickness of the In layer was varied as 200Å, 400Å, and 600Å and for this, 20 mg, 40 mg and 60 mg of indium were used respectively.

### 3.3.4 Annealing of the bilayer film

The In/ $\text{Cu}_x\text{S}$  bilayer film was then annealed in vacuum at 300 °C for 2 hours. Annealing chamber was made of a glass tube over which nichrome wire was wound uniformly along the entire length. This tube was heated by passing a current through the nichrome wire. Temperature was controlled by adjusting current using a variac. Two samples were placed well inside the tube, at a time to ensure uniform heating. The tube was then placed in the vacuum chamber and was evacuated to a pressure of  $<10^{-5}$  torr. Temperature on the sample surface was measured using chromel-alumel thermocouple, kept in contact with the samples. In all the cases, heating and cooling rate was 3°C/minute.

After annealing, it was found that entire indium diffused into  $\text{Cu}_x\text{S}$  film, forming a uniform film with a dark brown appearance. No indium layer was left behind at the surface after annealing. New preparation method developed for  $\text{CuInS}_2$  thin films can be summarized as follows



**I Step: Preparation of  $Cu_xS$** 

1M  $CuCl_2$  (10 ml) + 2M  $CS(NH_2)_2$  (10 ml) + 5drops TEA  
 + 5ml  $NH_3$  solution (25%) at pH 9.8, time of deposition- 15mts at  
 room temp

II step : deposition of indium over  $Cu_xS$  film by vacuum evaporation

III Step: annealing bilayer  $Cu_xS/In$  for 120mts., in vacuum

**3.4 Results and Discussion****3.4.1 XRD Analysis**

XRD is one of the most powerful methods for exploring structure of materials. It can be used to determine phase content in many minerals and materials. It requires no elaborate sample preparation and is essentially non-destructive. Generally, it gives a whole range of information about crystal structure, orientation, crystallite size, composition (with the help of standards), defects and stresses in thin films. Experimentally obtained diffraction pattern of sample is compared with Joint Council Powder Diffraction (JCPDS) data for standards. This gives information of different crystallographic phases, relative abundance and preferred orientations. From width of the diffraction peak, average grain size in the film can also be estimated.

Interplanar spacing  $d$  was calculated from X-ray diffraction profiles using the formula,

$$2d \sin \theta = n\lambda \dots\dots\dots(3.2)$$

where  $\theta$  is the Bragg angle and  $n$  is order of the spectrum,  $\lambda$  is the wavelength of X-rays. Using  $d$ - values the set of lattice planes ( $h k l$ ) were identified from standard data and lattice parameters are calculated using following relations.

For the tetragonal systems,

$$\frac{1}{d^2} = \frac{(h^2 + k^2)}{a^2} + \frac{l^2}{c^2} \dots\dots\dots (3.3)$$

and for hexagonal systems,

$$\frac{1}{d^2} = \frac{4(h^2 + hk + k^2)}{3a^2} + \frac{l^2}{c^2} \dots\dots\dots (3.4)$$

where  $a$  and  $c$  are lattice parameters. Grain size ( $L$ ) can be evaluated using Scherrer's formula,

$$L = \frac{k\lambda}{\beta \cos \theta} \dots\dots\dots (3.5)$$

where  $k$  is a constant, which is nearly equal to one and  $\beta$  is "full width at half maximum (FWHM)", usually measured in radians.

In the present study, XRD analysis was done using Rigaku (D.Max.C) X-Ray Diffractometer, with  $\text{Cu K}\alpha$  ( $\lambda = 1.5405 \text{ \AA}$ ) radiation and a Ni filter operated at 30kV and 20mA. XRD studies of as-prepared  $\text{Cu}_x\text{S}$  sample revealed that films were not crystalline. So these samples were annealed at different temperatures 200°C and 300°C for two hours in rotary vacuum. Even after annealing, there was no improvement in the crystallinity as revealed by the XRD analysis (Fig.3.1a, b & c)

$\text{CuInS}_2$  films obtained after diffusing indium layer thickness of 200Å, 400 Å and 600 Å are named CIII(2), CIII(4) and CIII(6) respectively. All these films were annealed at 300 °C for 120 minutes in order to diffuse indium. Fig.3.2 shows XRD pattern obtained for films after diffusing indium into  $\text{Cu}_x\text{S}$  film. When indium film

of thickness 200Å was diffused into  $\text{Cu}_x\text{S}$  layer [sample CIII(2)], 100% intensity peak (112) of  $\text{CuInS}_2$  appeared in the spectrum (Fig.3.2a). Second peak corresponding to (220) of  $\text{CuInS}_2$  at  $2\theta = 46^\circ$  has also become visible. But when thickness of the indium layer was increased to 400Å [Sample CIII(4)], peaks became more prominent as evident from Fig.2b. This clearly indicated that annealing  $\text{Cu}_x\text{S}$  samples after giving a thin layer of indium over the surface improved the crystallinity and lead to formation of  $\text{CuInS}_2$  phase in the film. On further increasing the indium layer thickness to 600 Å [sample CIII(6)], there is no appreciable change in the XRD pattern (Fig.3.2c). Hence for latter studies, thickness of the indium layer was fixed at 400 Å, annealing temperature at 300°C and annealing time at 120 minutes. Calculated 'd' values are listed in Table-1. One can see that predominant plane of the  $\text{CuInS}_2$  is (112)

Table-3.1

X-ray data of  $\text{CuInS}_2$  thin film

$2\theta$	D Å	hkl	Standard 'd' Value( Å)	Variation ( $\Delta d$ )
27.8	3.2	112	3.19	+0.01
32.66	2.74	200	2.74	0
46.00	1.97	220	1.95	+0.02

Grain size of the film was calculated from peak at  $2\theta = 27.8^\circ$  using Scherrer's formula  $D = 0.9\lambda / \beta \cos\theta$  where D is diameter of the crystallites forming the film,  $\lambda$  is the wavelength of the  $\text{CuK}_\alpha$  line,  $\beta$  is FWHM and  $\theta$  is the Bragg angle. Grain size value obtained is 32 nm.

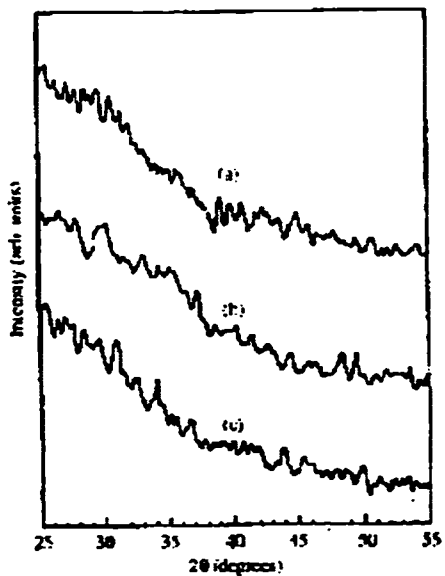


Fig. 3.1 XRD pattern of  $\text{Cu}_x\text{S}$  films: a) as-prepared  $\text{Cu}_x\text{S}$ ; b) annealed at  $200^\circ\text{C}$ ; c) annealed at  $300^\circ\text{C}$

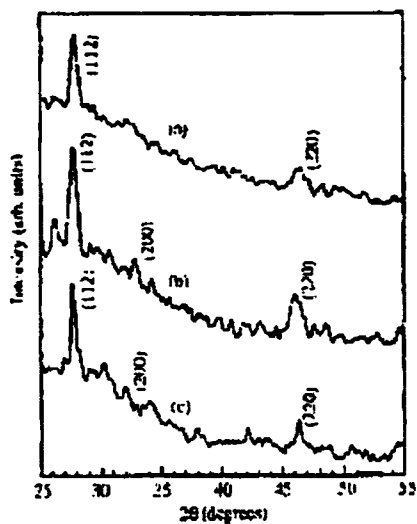


Fig.3.2 XRD pattern obtained after diffusing indium into the  $\text{Cu}_x\text{S}$  film: a)  $\text{CIII}(2)$ ; b)  $\text{CIII}(4)$ ; c)  $\text{CIII}(6)$

### 3.4.2 Optical Absorption Studies

The most direct and the simplest method for probing the band structure of semiconductors is to get optical absorption spectrum. Absorption is expressed in terms of a coefficient  $\alpha(h\nu)$  which is defined as relative rate of decrease in light energy  $L(h\nu)$  along its propagation path: [18]

$$\alpha = \frac{1}{L(h\nu)} \frac{d[L(h\nu)]}{dx} \dots\dots\dots(3.6)$$

absorption coefficient  $\alpha$  is related to the energy gap  $E_g$  according to the equation

$$\alpha h\nu = A(h\nu - E_g)^n \dots\dots\dots(3.7)$$

where  $A$  is a constant,  $h$  is Planck's constant,  $\nu$  the frequency of incident beam and  $n$  is equal to  $\frac{1}{2}$  for a direct gap and 2 for an indirect gap.

Absorption spectra of samples were recorded using UV-VIS-NIR spectrophotometer (Hitachi 3410) model. Fig.3.3a and 3.3b show variation of the absorption coefficient with photon energy ( $h\nu$ ) of incident light for samples  $\text{Cu}_x\text{S}$  and CIII(4). From the plot of  $(\alpha h\nu)^2$  against photon energy ( $h\nu$ ) (Fig.3.4a), a direct band gap of 1.86 eV was obtained for the  $\text{Cu}_x\text{S}$  film which compares well with published data [19]. But due to the sensitivity of optical properties to the exact structure and composition of layers, there is a wide variation in the reported results regarding the bandgap in  $\text{Cu}_x\text{S}$  films.

$(\alpha h\nu)^2$  Vs  $h\nu$  plot of the sample CIII(4) ( Fig3.4b) shows a direct band gap of 1.41 eV which can be attributed to p-type  $\text{CuInS}_2$  films [20]. This is lower than band gap value reported for crystals of  $\text{CuInS}_2$  [21]. Such lower band gap has been reported earlier for  $\text{CuInS}_2$  thin films [22-23]

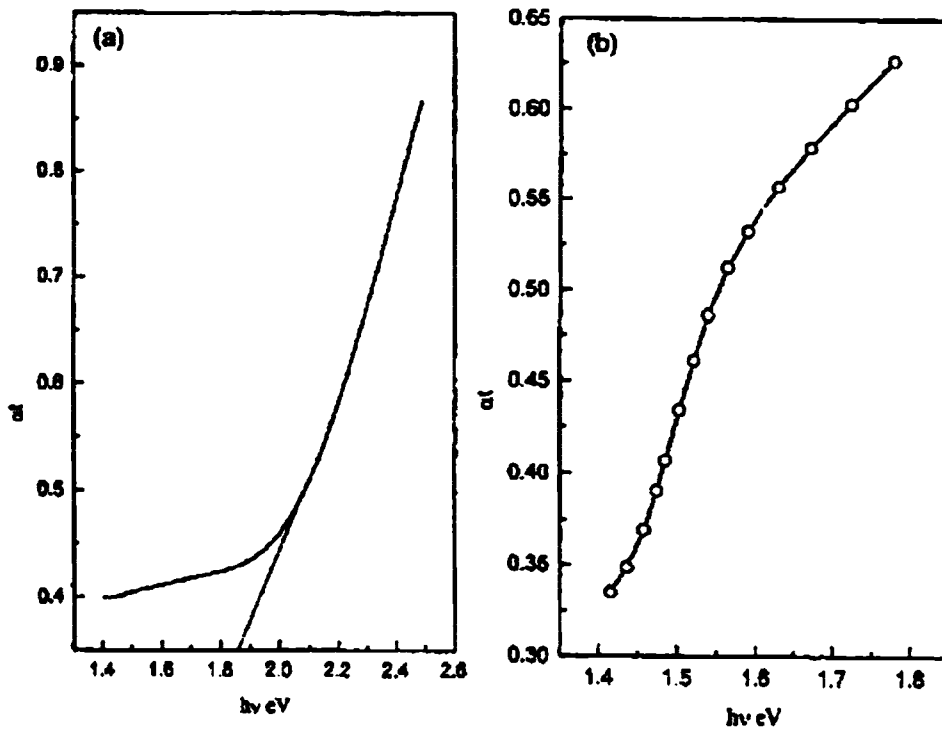


Fig.3.3. Variation of  $\alpha$  with photon energy ( $h\nu$ ): a)  $\text{Cu}_x\text{S}$ ; b)  $\text{CIII}(4)$

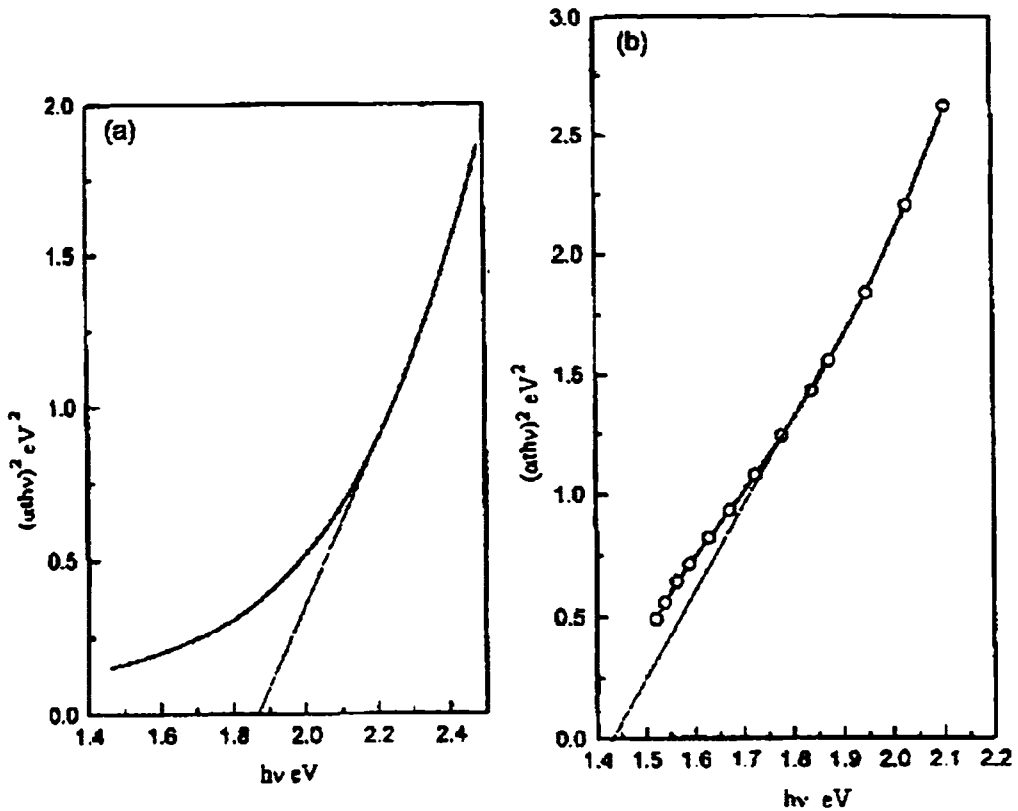


Fig.3.4.  $(\alpha hv)^2$  vs.  $(hv)$  plot for samples : a)  $Cu_xS$ ; b)  $CIII(4)$

### 3.4.3 Electrical properties

#### 3.4.3.1 Sheet resistance

Sheet resistance of  $Cu_xS$  and  $CIII(4)$  was measured at room temperature using Keithley I-V measurement system. Silver electrodes were painted on top surface of the film keeping a distance of 5mm between the electrodes. Sheet resistance of as-prepared  $Cu_xS$  (sample A) was  $1.267 \text{ k}\Omega/\square$ . After indium diffusion,



sheet resistance decreased to 119.5  $\Omega/\square$ . Using hot probe technique, it was observed that both  $\text{Cu}_x\text{S}$  and  $\text{CuInS}_2$  samples were p-type.

### 3.4.3.2 Hall measurement

Conductivity type, mobility and density of charge carriers of samples were investigated at room temperature using Hall measurement set up made by MMR Technologies Inc. having MP350 power supply to vary magnetic field and K50 temperature controller. These parameters were evaluated using Vander Pauw method by four-probe measurement technique [24].

Resistivity, mobility, and carrier concentration of  $\text{Cu}_x\text{S}$  and  $\text{CuInS}_2$  films are given in table-3.2. Resistivity of  $\text{Cu}_x\text{S}$  is 19.5  $\Omega\text{-cm}$  and this decreases as amount of In in the film increases. When 400 Å of indium was introduced by thermal diffusion, mobility and carrier concentration became 5.10  $\text{cm}^2/\text{V-s}$  and  $4.77 \times 10^{20} \text{cm}^{-3}$  respectively. On increasing the In layer thickness to 600 Å, slightly increased carrier mobility, with no significant change in carrier concentration, was observed ( $6.84 \times 10^{20} \text{cm}^{-3}$  and 7.47  $\text{cm}^2/\text{V-s}$  respectively). Mobility values obtained are greater than the values reported earlier for p-type  $\text{CuInS}_2$  films, prepared using two source evaporation, (0.2  $\text{cm}^2/\text{V-s}$  and 3.2  $\text{cm}^2/\text{V-s}$ ) [25], but is less than the mobility value reported for p-type crystals (15  $\text{cm}^2/\text{V-s}$ ) [26]. Type of carriers in all these films was found to be holes.

*Table-3.2*

*Hall measurement results of different samples*

Sample	Resistivity ( $\rho$ ) $\Omega\text{-cm}$	Mobility ( $\mu$ ) $\text{cm}^2/\text{Vs}$	Carrier density ( $\text{cm}^{-3}$ )	Hall coeff. $\text{cm}^3/\text{C}$	Type of carriers
$\text{Cu}_x\text{S}$	19.5	0.152	$2.11 \times 10^{18}$	2.96	holes
CI(4)	$2.56 \times 10^{-3}$	5.10	$4.77 \times 10^{20}$	0.0137	holes
CI(6)	$1.22 \times 10^{-3}$	7.47	$6.85 \times 10^{20}$	$9.11 \times 10^{-3}$	holes

### 3.3.4 Energy Dispersive X-ray analysis (EDAX)

Here the sample is irradiated by electron beam and emitted x-rays is directly measured using energy dispersive X-ray spectrometer, producing a spectrum of counts versus energy. As each x-ray photon enters the detector, it produces photoelectrons, whose total number is linearly proportional to the energy of the entering X-rays. Charge collected from detector is very small since only a few hundreds or thousands of electrons are produced by each X-ray photon. Hence it is amplified by a pre-amplifier whose output voltage is proportional to the X-ray energy [27].

In the present work, we used this technique to confirm presence of indium in the  $\text{CuInS}_2$  samples. EDAX spectrum of CIII(2) and CIII(4) samples showed presence of Cu, In and S in the samples and is shown in Fig.3.5 and Fig.3.6 respectively. For CIII(4) sample, indium peak intensity is high, showing a higher concentration of indium in the film. Concentration of sulfur is also higher in this film than that for CIII(2) sample. There is one peak corresponding to Si, which is from the glass substrate used for the preparation of the films.

### 3.3.5 Scanning Electron Micrograph (SEM)

SEM is the most widely used instrument for obtaining microstructural and surface features of thin films. A finely focused electron beam is scattered over the surface of the specimen and secondary electrons emanating from the specimen are used for imaging the surface. Since secondary electrons come from the surface layer, picture obtained is a faithful reproduction of surface features. Secondary electron imaging can provide high-resolution imaging of fine surface morphology. Quantitative and qualitative chemical analysis information can also be obtained using Energy Dispersive X-ray spectrometer (EDS) with the SEM [28].

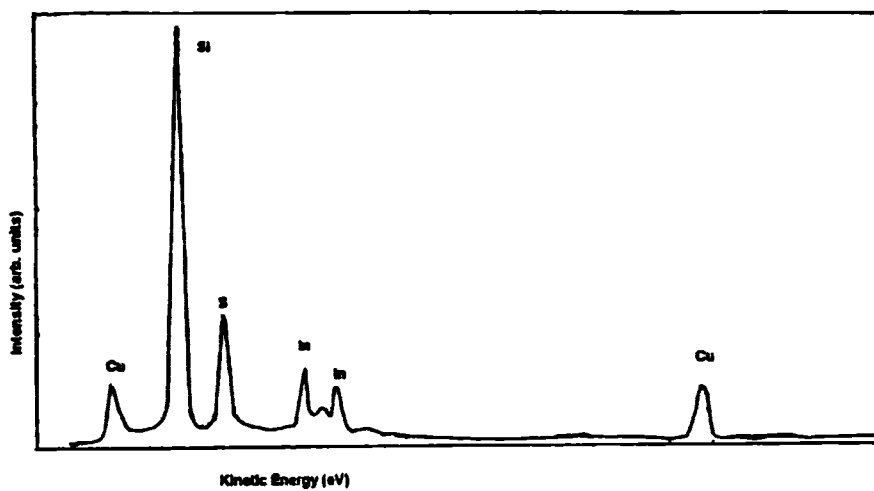


Fig.3.5 EDAX spectrum of CIII(2)

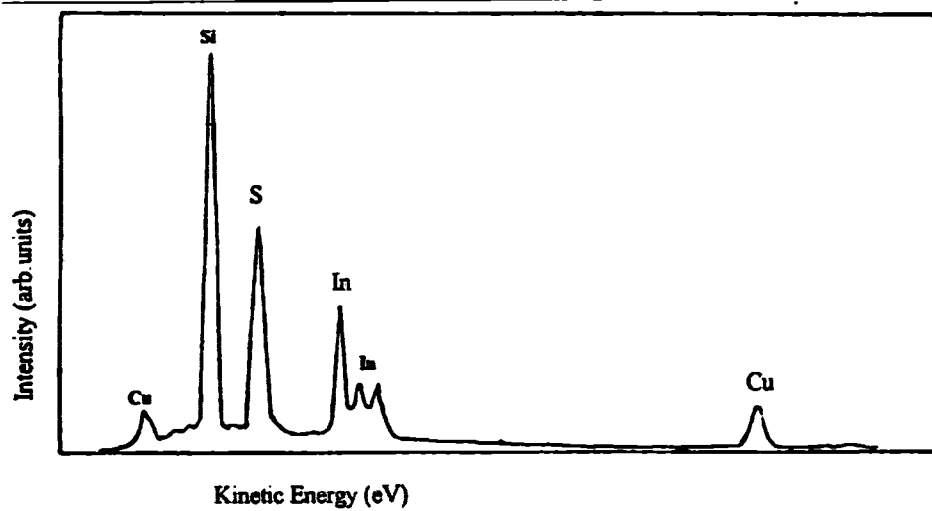


Fig.3.6 EDAX spectrum of CIII(4)

SEM was used to find out uniformity of  $\text{CuInS}_2$  films prepared. Fig.3.7 gives the SEM micrograph of the same area of CIII(4) sample with two different magnifications. Films are uniform over a large area with defined grains and no pinholes or cracks are found. There are some agglomerated areas in this film, which may be due to segregated  $\text{Cu}_x\text{S}$  impurity phase. A similar feature was obtained for Cu-rich sprayed samples [29].

### 3.3.6 Electron Spectroscopy for Chemical analysis (ESCA)

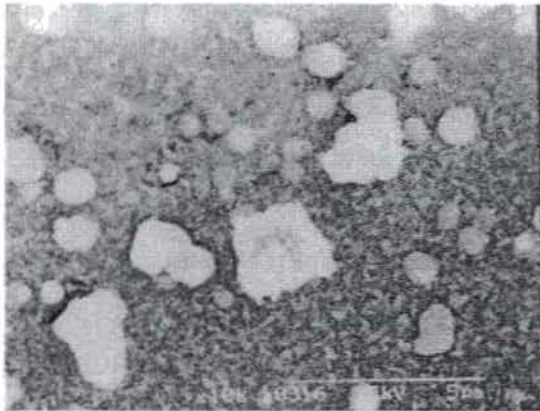
ESCA is one of the major techniques for studying thin films. It provides information on the elemental composition of a sample as well as on the chemical state of the observed atoms.

In this technique, sample is irradiated using electromagnetic radiation of energy  $h\nu$ . Due to photoelectric effect, electrons are emitted with kinetic energy

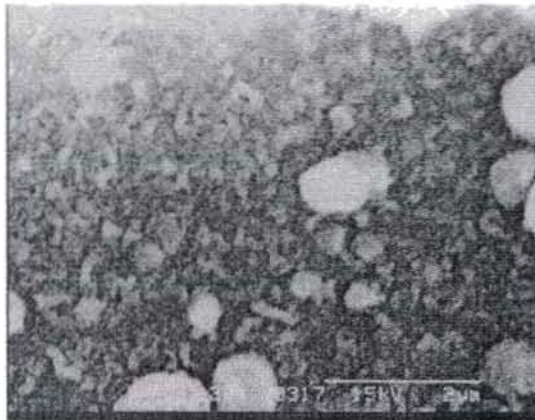
$$E_{kin} = h\nu - E_B - \phi \dots\dots\dots(3.8)$$

where  $E_B$  is binding energy of a particular electron shell and  $\phi$  is the sample work function. Photoelectrons are energy-analyzed in the spectrometer and, since photon energy is known, one can determine characteristic binding energies of valence electrons coming from different elements present in the sample. Depending on the energy of incident radiation, this technique is called either "Ultra Violet Photoelectron Spectroscopy (UPS)" for lower photon energies ( $\leq 50\text{eV}$ ) or "X-ray Photoelectron Spectroscopy (XPS)" for higher photon energies ( $\geq 1\text{k eV}$ ) [30].

Chemical composition of film was evaluated using XPS technique in the present work. XPS spectra of samples were recorded using an ULVAC-PHI unit (model: ESCA 5600 CIM) employing argon ion sputtering (Voltage = 3 kV, Raster size =  $3 \times 3 \text{ mm}^2$ , pressure  $10^{-8}$  mbar) Al  $K\alpha$  X-ray (1486.6eV) with a beam diameter of 0.8mm and power of 400W was used as the incident beam.



(a)



(b)

*Fig.3.7 SEM of CIII(4) sample at magnifications: (a) 10K ; (b)20K*

XPS technique gives information about chemical state of elements present in surface layer only (of thickness few hundred angstroms). In order to know variation in stoichiometry as well as chemical state all along the thickness of the samples, we performed XPS depth profile of all these samples. Here the presence of the elements Cu, In, S, O, & Si was checked along the sample thickness. For this, measurements on sample surface was taken first and then the sample was etched slowly using Ar ion sputtering for 3 minutes to remove approximately 100Å thickness of the film. Again the sample was checked for these elements (this is called one cycle). This process was repeated till substrate surface was reached.

In this fashion, sample was etched for about 100 cycles and the depth wise presence of the elements plotted together for sample CIII(4) is shown in Fig.3.8. Binding energies of the elements are represented along the X-axis. The spectra were calibrated against shifts due to machine errors, using the C 1s line (of the hydrocarbon contamination in the films) as the standard. (Binding energy of C 1s is 284.5 eV). After 40 cycles, peaks corresponding to O, and Si could be seen, which indicates the beginning of the glass substrate ( $\text{SiO}_2$ ). So the film is present up to this, after which the glass substrate starts. Hence from this cycle, only peaks corresponding to O and Si were obtained.

From (Fig.3.8), it is obvious that indium diffused uniformly throughout the depth of the sample and is present up to the glass substrate. At the surface, there is one peak at binding energy value 531.7 eV corresponding to O, which is due to surface contamination. Its atomic concentration decreases along depth of the sample as evident from Fig.3.9b. It can also be seen that all these elements have diffused slightly into the glass substrate, probably during the annealing of the films at 300°C for 2 hours. Binding energy values obtained are 952.5 eV & 932.5 eV for Cu  $2p_{3/2}$

& Cu  $2p_{1/2}$ ; 452.5 eV & 444.6 eV for In  $3d_{3/2}$  & In  $3d_{5/2}$ ; and 162 eV for S  $2p$ , which are in agreement with reported values of  $\text{CuInS}_2$  [23,31,32]. Similar binding energy values were obtained for Cu levels in  $\text{CuInS}_2$  [33] and they also noticed no significant shift in binding energy for Cu levels from metallic state.

Fig.3.9 shows depth profile of atomic concentrations of Cu, In & S for samples CIII (2), CIII(4) & CIII(6). For sample CIII(2), Cu and In are not uniformly present throughout the depth of the sample (Fig.3.9a). Concentration of In is maximum at surface and gradually decreases to very small value (7.5%) near the substrate. After applying Ar ion sputtering for 10 minutes, it was found that Cu/In ratio in the film is equal to 1 (28.4% each). At the same time in the depth, the ratio increases to 5.58. Although S was uniformly present throughout the depth of the sample, its atomic percentage was only around 10%. So it becomes clear that indium layer of thickness  $200\text{\AA}$  is not sufficient to produce films of uniform composition.

Fig.3.9b shows depth profile of atomic concentration of sample CIII(4). From the figure, it is clear that Cu, In and S are present almost uniformly from the surface to the substrate. Cu/In ratio in the film is 1.29 Here also sample exhibits a deficiency of sulfur. Atomic concentration of sulfur is almost half the value expected for stoichiometric  $\text{CuInS}_2$ . This may be probably due to the preferred sputtering of group VI elements such as sulfur and selenium. Also sensitivity factors of Cu and S are very different. Similar problem was observed in the case of  $\text{Cu}_{2-x}\text{Se}$  films prepared in our lab. In that case, for applying correction, Cu/Se ratio was measured with a standard sample of CuSe powder and the correction factor was found to be 2 [4,5].

Percentage atomic concentration of sample CIII(6) is shown in Fig.3.9c. Here again the concentration of Cu & In is not uniform throughout depth of the

sample. Cu/In in that film is 1.5 after etching for 20 minutes. Percentage of sulfur is lower than that of CIII(4).

In the case of sample CIII(4), there is slight decrease in atomic concentration of S at the surface and in the bulk. This is may be due to the fact that S has a high vapor pressure and hence during deposition process, mainly at the stage of indium diffusion, some S may escape from the surface of the film.

From Fig.3.9a,b&c, it is evident that all above samples contain a good percentage of oxygen. This is due to the fact that after coating indium, all samples were annealed at 300°C for 2 hours in rotary vacuum. To reduce the oxygen content in the films, for later preparations, all the samples were annealed in high vacuum ( $\sim 10^{-5}$  torr). XPS spectra of such samples showed nearly zero percentage concentration of oxygen throughout the depth of the sample (Fig3.16b).



ESCA PROFILE 11/8/98 START=1, END=102, NFB=1  
FILE: C1859 CIII(4)

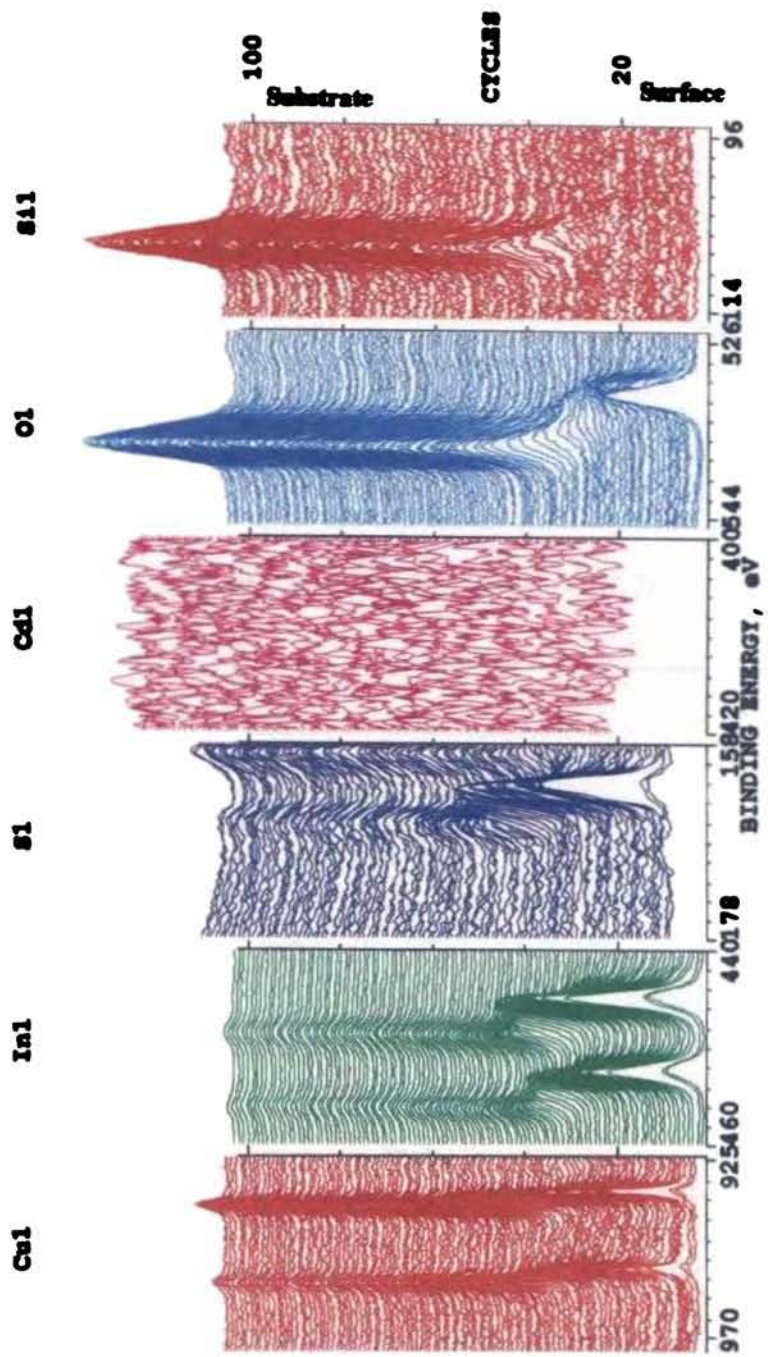
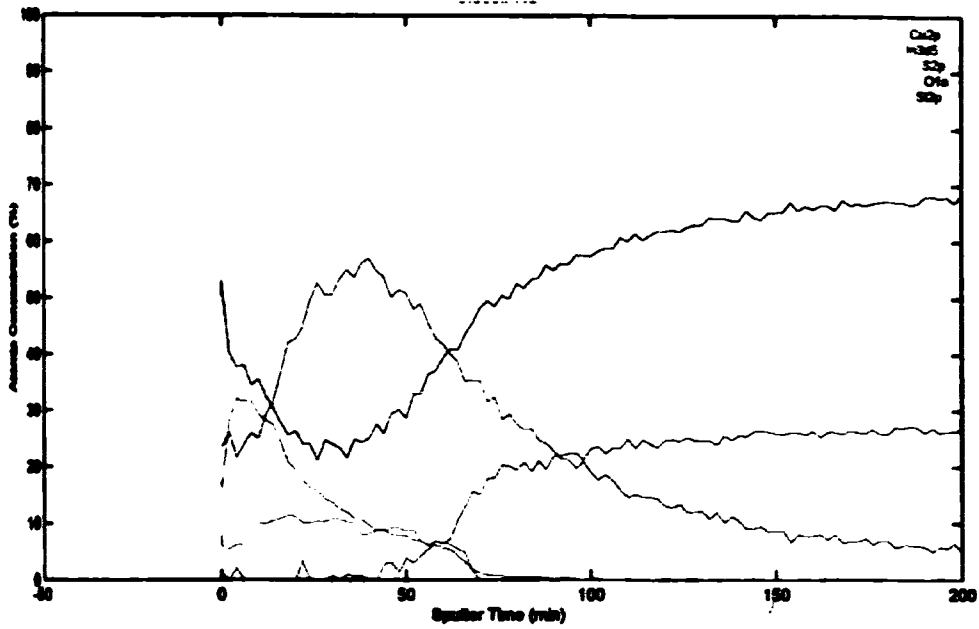
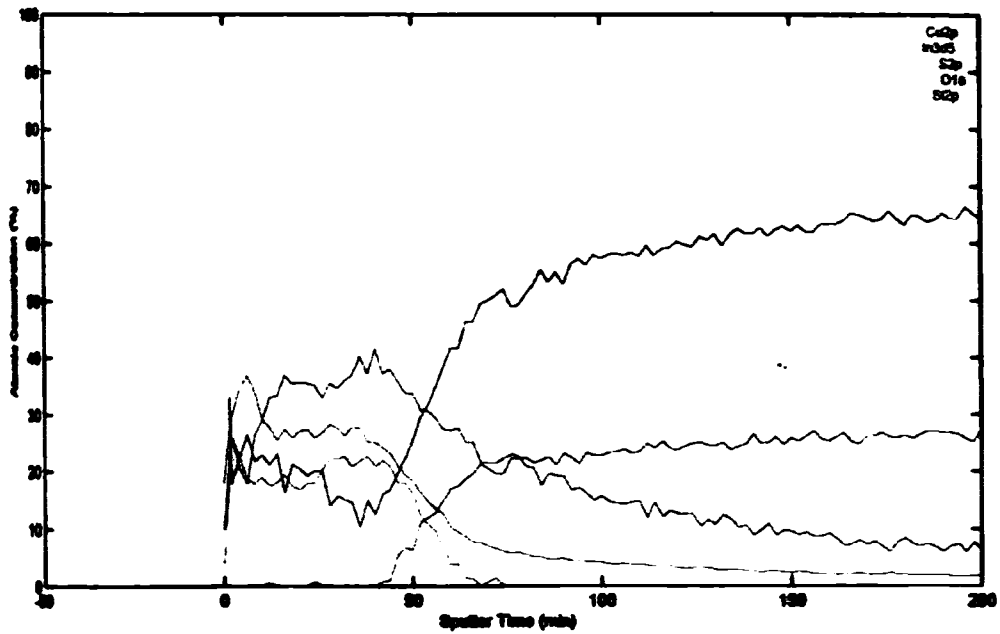


Fig. 3.8. XPS depth profile of sample CIII(4)



*Fig.3.9a, At.conc.% vs sputter time graph of sample CIII(2)*



*Fig.3.9b, At.conc.% vs sputter time graph of sample CIII(4)*

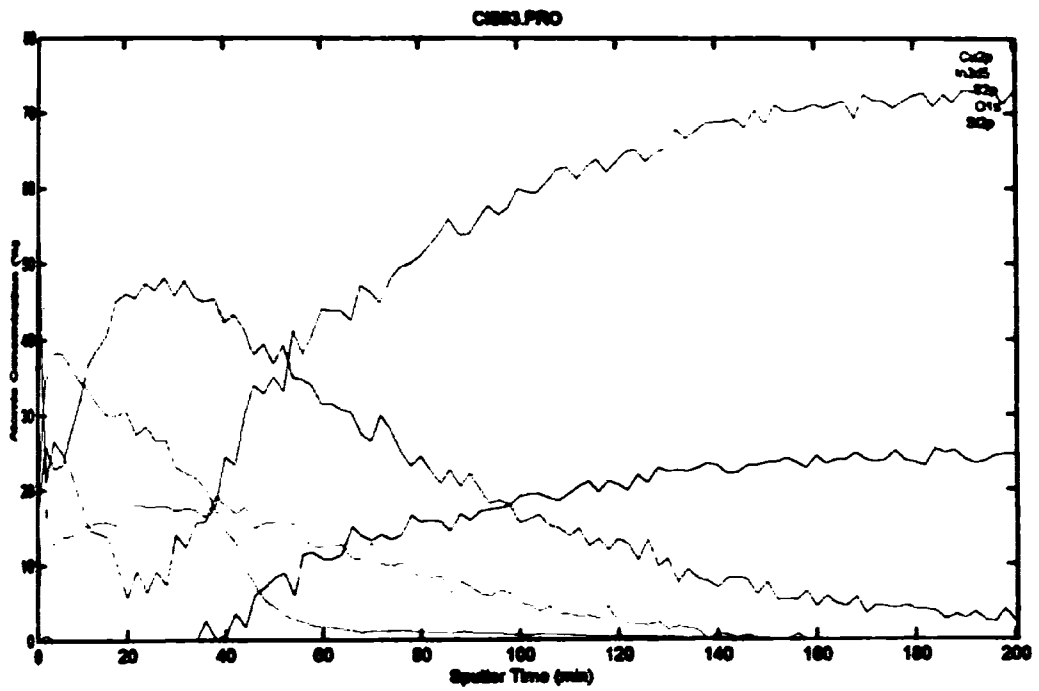


Fig.3.9c, At.conc.% vs sputter time graph of sample CIII(6)

### 3.5 Sulfurization of CuInS<sub>2</sub> films

From the results of above analyses, one can understand that it is possible to prepare CuInS<sub>2</sub> thin films by evaporating indium over chemical bath deposited Cu<sub>x</sub>S films and subsequently annealing the films. The best result was obtained for sample prepared by diffusing 400Å indium [sample CIII(4)]. The XRD spectrum matched well with standard data. XPS depth profile of the sample showed presence of Cu, In and S throughout the depth. However, atomic concentration of S was less than that of stoichiometric CuInS<sub>2</sub>. In order to increase the S content in the films, samples were annealed in sulfur vapor in an open tube at different temperatures for different durations. Again these films were characterized using the above techniques. Following section deals with the annealing of CIII(4) sample and the characterization.

### 3.6 Experimental Details

Sulfur-annealing chamber had two horizontal tubular sections; the upper one was “sample chamber” and the lower one was “sulfur-powder-chamber”. Resistive heating could be given to both sections separately. Sample chamber could be heated to 300<sup>o</sup>C and sulfur chamber to 200<sup>o</sup>C. Two thermocouples were used to measure temperature of these two chambers separately.

Sulfur chamber was maintained at a temperature of about 150 <sup>o</sup>C to obtain a sulfur flux during the process. Temperature of samples was varied as 100 <sup>o</sup>C, 130 <sup>o</sup>C, 160 <sup>o</sup>C, 200 <sup>o</sup>C, 250 <sup>o</sup>C & 300 <sup>o</sup>C keeping the annealing time constant at 1 hour. Deposition of sulfur in cold regions at the end of the chamber indicated existence of sulfur flux. When sample was annealed at temperatures below 200<sup>o</sup>C, a thin layer of S gets deposited on film surface.

When annealed at temperatures greater than 200 °C, there is a clear reduction in thickness of the film. Hence after several trials, temperature of the sample source was fixed at 200 °C and the films were annealed for different time periods. These films were again characterized.

### 3.7 Results and Discussions

#### 3.7.1 XRD

XRD spectrum of samples annealed at 200 °C in sulfur atmosphere for ¼ hour, 1 hour, 1½ hours and 2 hours (named as S¼, S1, S1½ and S2 respectively) are illustrated in Fig.3.10. After annealing for ¼ hour, peak corresponding to (112) plane became sharper, showing an improvement in the crystallinity of the films. However, on increasing the annealing time, intensity of the peak decreased.

Grain size of these films was found to increase with sulfur annealing time. For the S1 & S2 samples, grain size values were 65 nm & 118 nm respectively.

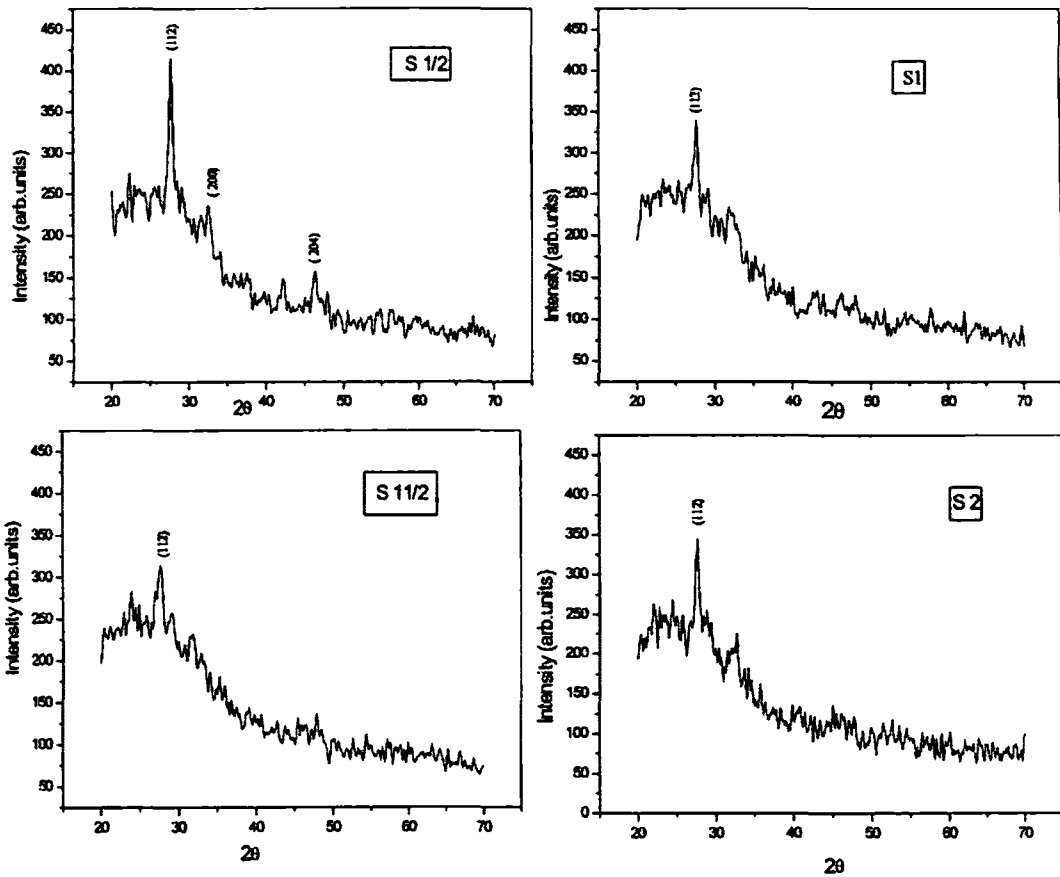


*Fig.3.10 XRD of samples annealed in sulfur atmosphere for different durations*

### 3.7.2 Electrical properties

In order to clarify effect of S annealing on resistivity and mobility of  $\text{CuInS}_2$  films, Hall effect measurement was carried out. Table-3.3 shows results of samples annealed for different time. Resistivity increased for samples annealed for a time up to 1 hour. After that, resistivity again decreased. Variation of mobility and carrier

concentration with annealing time is represented in Fig.3.11. It is evident that annealing in sulfur vapor decreases mobility and carrier density.

Table-3.3  
Hall measurement

Sample	Resistivity ( $\rho$ ) $\Omega$ cm	Mobility ( $\mu$ ) $\text{cm}^2/\text{Vs}$	Carrier density ( $\text{cm}^{-3}$ )	Hall coeff. $\text{cm}^3/\text{C}$	Type of carriers
CIII(4)	$2.56 \times 10^{-3}$	5.10	$4.77 \times 10^{20}$	0.0137	holes
S1/2	$6.52 \times 10^{-3}$	2.95	$3.25 \times 10^{20}$	$1.92 \times 10^{-2}$	holes
S1	0.2067	3.22	$9.37 \times 10^{18}$	0.6659	holes
S11/2	$6.52 \times 10^{-3}$	2.59	$3.25 \times 10^{20}$	0.0192	holes
S2	$1.12 \times 10^{-2}$	1.93	$2.89 \times 10^{20}$	$2.16 \times 10^{-2}$	holes

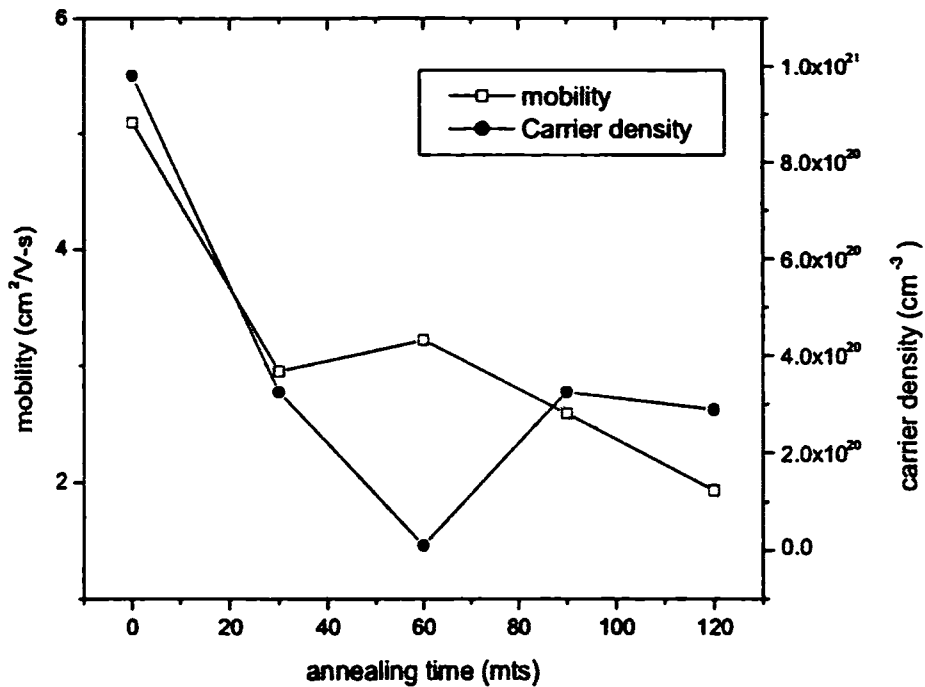
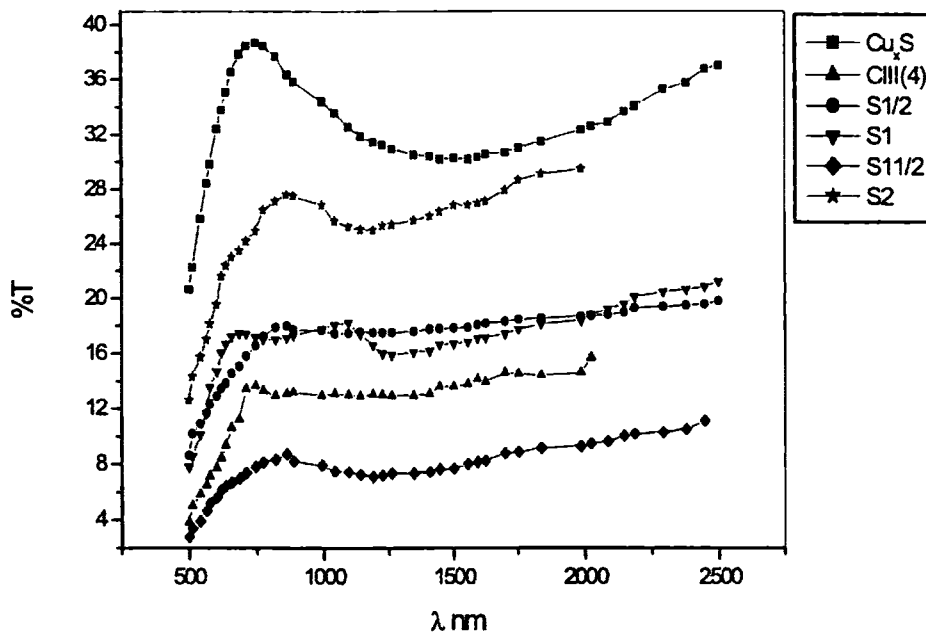


Fig.3.11 Variation of mobility and carrier density with ann. time

### 3.7.3 Optical Properties

Fig.3.12.shows transmission graph of  $\text{Cu}_x\text{S}$  film, As prepared  $\text{CuInS}_2$  [CIII(4)] and films annealed in sulfur atmosphere. As prepared  $\text{CuInS}_2$  sample (CIII(4)) has transmission around 12%. On annealing, transmission increases slightly for all samples except the one annealed for 1½ hours. For the sample annealed for 2 hours, transmission corresponds closely to the transmission of  $\text{Cu}_x\text{S}$  films. This may be due to formation of  $\text{Cu}_x\text{S}$  impurity phases in the sample. There is also a decrease in atomic concentration of indium in the sample as indicated by XPS analysis (section 3.7.5).





*Fig.3.12 Transmission spectrum of annealed samples*

Absorption spectra of these samples are illustrated in Fig.3.13 and variation in optical band gap with annealing time is represented in Fig.3.14. There is an increase in band gap with increase in annealing time. This may be due to the increase in grain size of the films with annealing time, as revealed by XRD analysis.

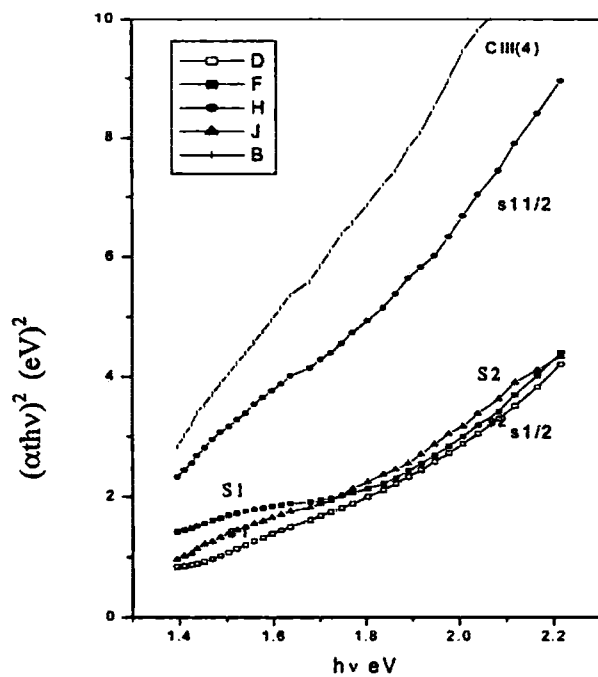


Fig.3.13 Absorption spectrum of annealed samples

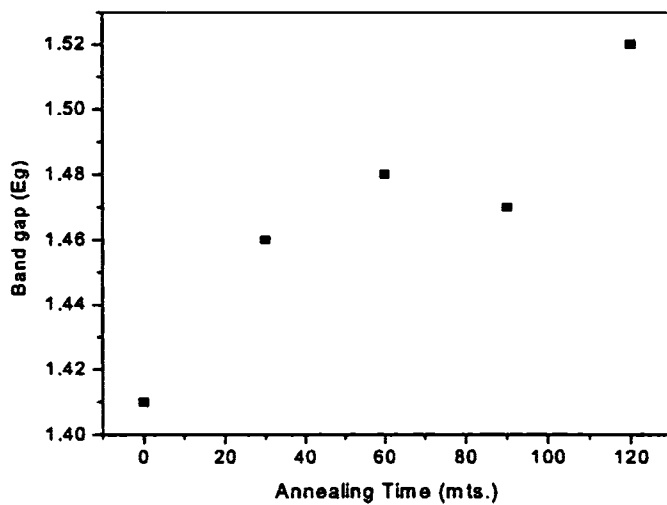


Fig.3.14 Variation in the optical band gap with annealing time.

### 3.7.4 Photosensitivity measurements

Photoelectrical properties of these samples were investigated by measuring photosensitivity (S) defined as,

$$S = \frac{(R_D - R_L)}{R_D} \times 100 \dots\dots\dots(3.9)$$

where  $R_D$  is dark resistance of the film,  $R_L$  is the resistance of the film under illumination. Photosensitivity is measured for different samples annealed in sulfur atmosphere for different periods. These samples were irradiated with white light of intensity  $40\text{mW}/\text{cm}^2$ . An I-R filter was used to remove heat content in the radiation. Variation of S with annealing time is represented in Fig.3.15. Photosensitivity is high for the samples annealed in sulfur atmosphere for 30 to 60 minutes.

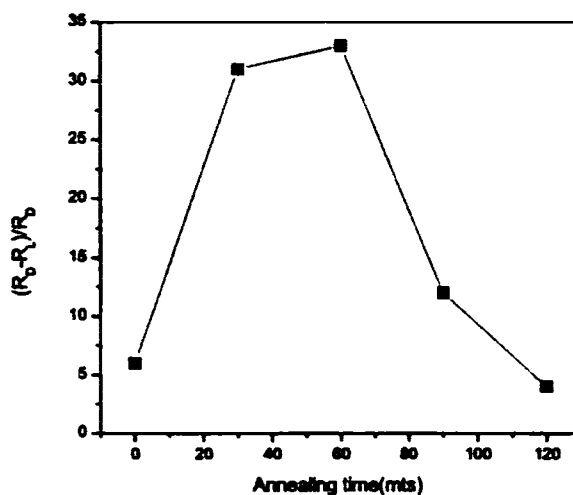


Fig.3.15. Photo response of films annealed for different time

### 3.7.5 XPS analysis

Accurate and quantitative analysis of atomic percentage in this compound is difficult to obtain using XPS because binding energies and sensitivity factors of

Cu2p and S2p are very different. (S2p = 162 eV, s = 0.44 and Cu2p<sub>3/2</sub> = 932.6 eV, s = 5.3 ) [23]. However, a qualitative analysis of CuInS<sub>2</sub> samples annealed in sulfur atmosphere for 1 hour and 2 hours was analysed using XPS. Atomic percentage (at %) vs. sputter time graph of these samples is depicted in Fig. 3.16. Table 3.4 gives approximate at % of Cu, In and S in these films. Also ratio of atomic concentration of Cu to In and the ratio of the total (Cu+In) in the film to the S content in the film is shown in the table. From this, it follows that when samples are annealed for 1 hour, there is an improvement in sulfur content in the film. (increases from 21% to 33% ) (Fig.3.16a). On increasing annealing time to 2 hours, there is no significant increase in S content compared to the one annealed for 1 hour (Fig.3.16b). On the other hand, there is decrease in atomic concentration of In. Regarding oxygen, from Fig.3.16 it is very clear that at % in the film is nearly 0% for 1 hour annealed sample. But, at % of oxygen is 3% for the sample annealed for 2 hours.

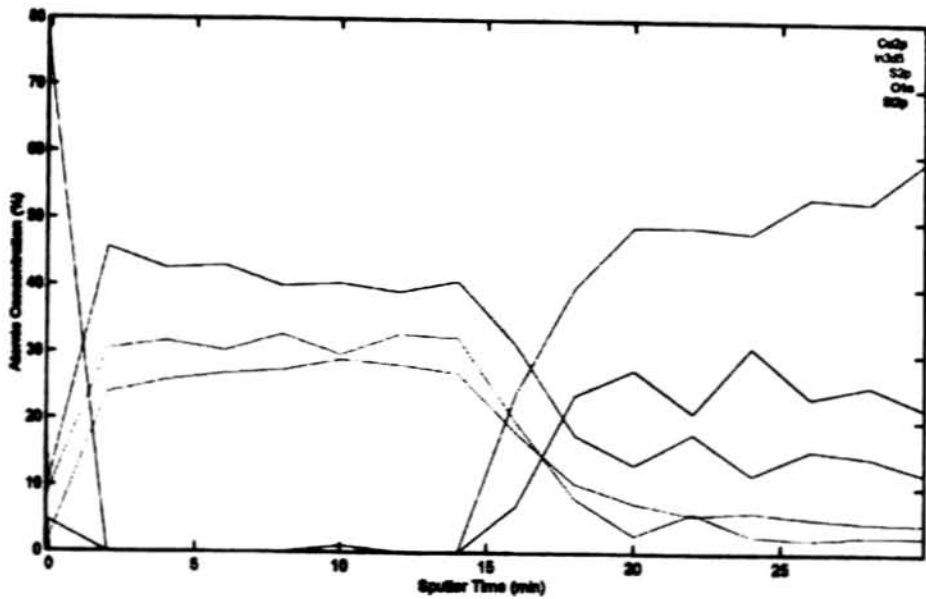


Fig.3.16a, At.conc.% vs sputter time graph of sample CIII(4), annealed for 1 hour

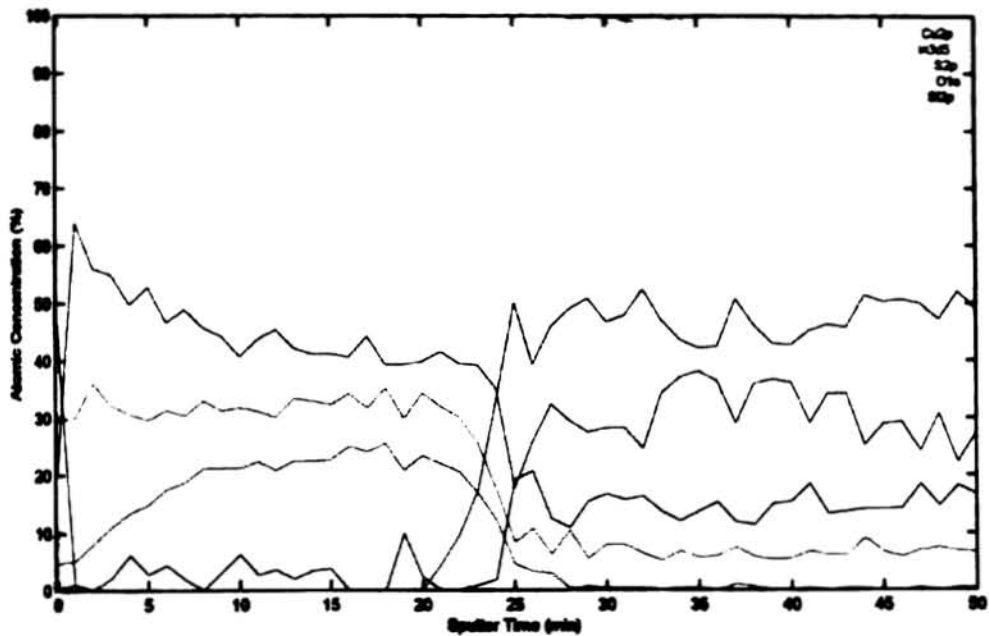


Fig.3.16b, At.conc.% vs sputter time graph of sample CIII(4), annealed for 2 hours

Table-3.4  
Atomic percentage from XPS analysis

Sample Name	Cu%	In%	S%	Cu/In in the film	(Cu+In)/S
CIII(4)	37	27	21	1.37	3.04
CIII(4)S1	40	27	33	1.48	2.03
CIII(4)S2	41	23	33	1.78	1.93
Standard CuInS <sub>2</sub> powder[23]	12	36	52	0.33	0.923

The BE values of these samples are given in Table-3.5. There are no appreciable change in the BE values due to S annealing.

Table-3.5  
*Binding Energy values of samples (in eV) annealed in sulfur atmosphere.*

Sample	Cu 2p <sub>3/2</sub>	Cu 2p <sub>1/2</sub>	In 3d <sub>5/2</sub>	In 3d <sub>3/2</sub>	S 2p
CIII(4) as prepared	952.5	932.6	452.5	445	162
S1	951.8	932.5	452.5	445	162
S2	952.5	932.5	452.5	445	162

### 3.8 Conclusion

We prepared CuInS<sub>2</sub> thin films using a new and low cost technique. The films obtained were characterized using different techniques. Even though XRD

peaks were clearly indicating the formation of  $\text{CuInS}_2$  compound, XPS analysis indicated that the films are deficient in sulfur. In order to increase sulfur content, films were annealed in sulfur atmosphere for different times. There is an increase in atomic concentration of sulfur due to annealing up to one hour. But this could not be increased above 33%. There is reduction in the at % of In with increase in the annealing time and about 3% of Oxygen is present in samples annealed for two hours.

## **Part-II $\text{CuInS}_2$ thin films from CBD CdS films**

With an aim of fabrication of  $\text{CuInS}_2$ / CdS solar cells, we tried another new procedure for the preparation of  $\text{CuInS}_2$  thin films. In the earlier part of this chapter, we saw that it is possible to prepare  $\text{CuInS}_2$  thin films by thermally diffusing indium into the  $\text{Cu}_x\text{S}$  layer. If we can convert top layer of a sufficiently thick CdS into  $\text{Cu}_x\text{S}$ , and then convert it into  $\text{CuInS}_2$ ,  $\text{CuInS}_2$ / CdS solar cells can be fabricated in an easy way. Metallurgical junction will be formed within the CdS film thereby avoiding atmospheric contamination of the interface. With this intention, we tried to prepare  $\text{CuInS}_2$  films using CBD CdS films.

### **3.9 Experimental Details**

Preparation of  $\text{CuInS}_2$  is a three-stage process, the first stage is preparation of CdS using chemical bath deposition; second is preparation of  $\text{Cu}_x\text{S}$  from CdS and the third stage is preparation of  $\text{CuInS}_2$  by evaporating indium on  $\text{Cu}_x\text{S}$  and subsequently annealing the samples.

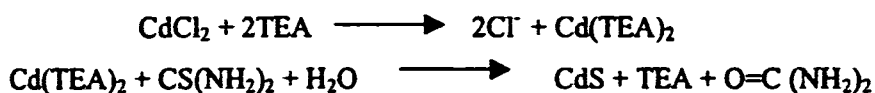
### i) Preparation of CdS thin films

Among various deposition techniques used for preparation of CdS films, chemical deposition is rather simple and inexpensive.

It yields stable, uniform, adherent and hard films with good reproducibility. These films are found to be near-stoichiometric [34].

For the present case, CdS thin films are prepared on glass substrate as well as on SnO<sub>2</sub> coated glass plates using CBD. Details of this technique are mentioned in section 3.2.1. Basic principle involved is the chemical reaction between cadmium chloride and thiourea in aqueous solution. Chemical deposition of CdS films requires slow release of Cd<sup>2+</sup> ions in aqueous medium. This is achieved by forming a complex with triethanolamine (TEA). Cd<sup>2+</sup> ions released from the Cd(TEA)<sub>2</sub> complex and S<sup>2-</sup> ions from thiourea condense on the substrate. Thus film formation is an ion-by-ion condensation process. pH of the solution is controlled by adding ammonia solution.

Chemical equation representing the above reaction is,



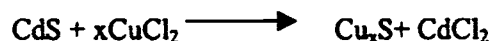
For preparing the bath, 10ml cadmium chloride (1M) was mixed with 4ml of TEA. A thick white precipitate was formed. To this, 25% ammonia solution was added slowly, till the precipitate just dissolved completely. Then 10 ml of thiourea was added. pH of the solution is around 10.5. Well-cleaned substrates were dipped in this solution and beaker containing the solution was kept in hot air oven with temperature stabilized at 80<sup>0</sup>C. No stirring was given. The arrangement was kept undisturbed for 75 minutes for deposition. Single-dipped and double-dipped films were prepared for the present study.



### ii) Preparation of $\text{Cu}_x\text{S}$ thin films

$\text{Cu}_x\text{S}$  thin films were prepared by converting CBD CdS films using the well-known Clevite process, which is widely used for  $\text{Cu}_x\text{S}$  formation in high efficiency  $\text{Cu}_x\text{S}/\text{CdS}$  solar cells [13]. Clevite process for polycrystalline cell fabrication was developed during 1970's and the most notable feature of this process is fabrication of the  $\text{Cu}_x\text{S}$  layer in CdS substrates by ion exchange. In addition, ion exchange process affects only the cations so that sulfur content of CdS remains intact [35].

In the present case, CdS samples were dipped in 0.5M  $\text{CuCl}_2$  solution (50 ml) for different periods, (<1 minute) until yellow colour of CdS film turns black. When CdS is dipped in the  $\text{CuCl}_2$  solution, Cd ions are replaced by Cu ions and thus  $\text{Cu}_x\text{S}$  is formed. Reaction can be represented by the following equation



To terminate the reaction, and to remove unreacted  $\text{CuCl}_2$ , sample was rinsed in distilled water kept at room temperature. Excess water was removed and the sample was dried in hot air.

As the time of dipping was increased in order to convert the CdS film completely to  $\text{Cu}_x\text{S}$ , cracks are developed in the film. Also, the  $\text{Cu}_x\text{S}$  film gets detached from the substrate. To reduce time of dipping, temperature of the  $\text{CuCl}_2$  solution was increased to  $95^\circ\text{C}$ . Then the time of dipping was optimized as 3 seconds for the complete conversion of the double dipped CdS film to  $\text{Cu}_x\text{S}$ .

### iii) Evaporation of In on $\text{Cu}_x\text{S}$

Pure indium (99.999%) was deposited on  $\text{Cu}_x\text{S}$  samples prepared as mentioned above. Thickness of the indium layer was varied as 100Å, 400Å, and 600Å. Then these films were annealed at  $300^\circ\text{C}$  in vacuum ( $10^{-5}$  torr) for two hours. Evaporated indium completely diffused into  $\text{Cu}_x\text{S}$  film to form  $\text{CuInS}_2$ .

## 3.11 Results and Discussions

### 3.11.1 XRD Analysis

Before conversion into a  $\text{Cu}_x\text{S}$  layer, CdS samples were investigated using X-ray diffraction studies. Fig3.17 represents the XRD pattern of CdS and the  $\text{Cu}_x\text{S}$  film formed by converting the CdS film. Table-3.6 Shows the angular position  $\theta$ , corresponding inter planar distances and (h k l) values of these films. Diffraction pattern of the as-prepared CdS film exhibits peaks corresponding to cubic CdS phase. When CdS is converted to  $\text{Cu}_x\text{S}$ , comparison of observed X-ray diffraction spectra with standard JCPDS data revealed that the  $\text{Cu}_x\text{S}$  film consists of many phases. Most of the lines were identified as those of chalcocite. Hence it was quiet impossible to give an estimation of composition (ie, value of x) of these films. Similar problem was faced by Rezig et al. who reported structural and optical properties of topotaxially-grown  $\text{Cu}_2\text{S}$  [17]. They also observed that Cu-rich chalcocite phase transforms into minor phases, when let under air-ambient atmosphere. This transformation is enhanced in the case of thin layers and it is argued that copper migration to the surface is the origin of this formation.

When 100Å indium is evaporated onto the  $\text{Cu}_x\text{S}$  film, there is slight variation in XRD pattern and it shows presence of  $\text{CuInS}_2$  phase in the sample. When In layer thickness is increased to 400 Å,  $\text{CuInS}_2$  peak appears in the XRD pattern, which shows formation of chalcopyrite  $\text{CuInS}_2$  phase with preferred orientation along the (112) plane. In addition to peaks corresponding to  $\text{CuInS}_2$ , some  $\text{Cu}_x\text{S}$  peaks are also present. But on increasing In layer thickness to 600 Å, all  $\text{Cu}_x\text{S}$  peaks disappear and  $\text{CuInS}_2$  peaks become prominent as shown in Fig3.18. The d values are listed in Table3.7.

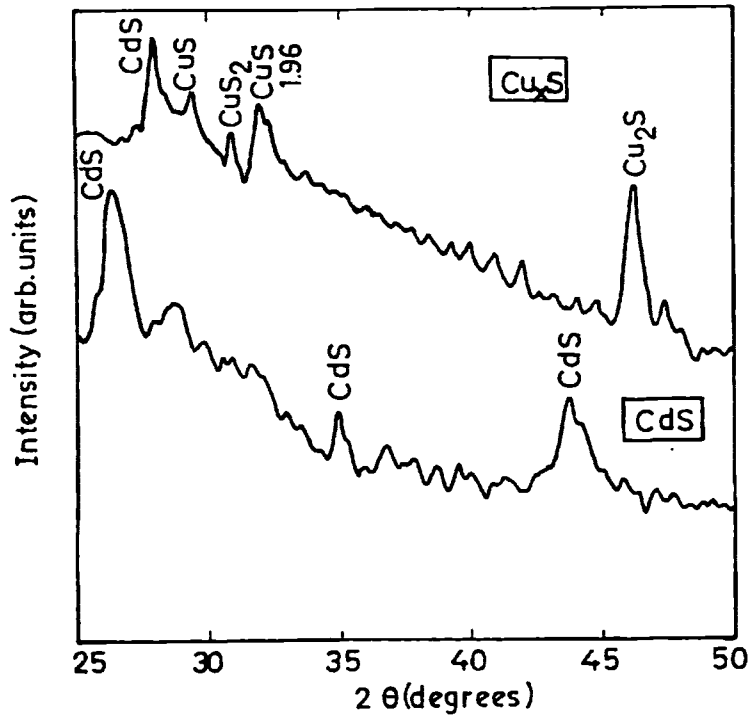


Fig.3.17. XRD pattern of CdS and  $Cu_xS$  films

Table-3.6 – XRD analysis of CdS and  $Cu_xS$

Sample	2θ	d Å		(h k l)	Phase identified
		Observed	Standard		
CdS	26.65	3.342	3.360	(111)	CdS (c)
	43.75	2.067	2.058	(220)	CdS (c)
$Cu_xS$	27.95	3.189	3.16	(101)	CdS (H)
	29.35	3.040	3.04	(102)	CuS
	31.0	2.882	2.89	(200)	$CuS_2$
	32.5	2.752	2.74	(103)	$Cu_{1.96}S$
	46.25	1.961	1.98	(060)	$Cu_2S$

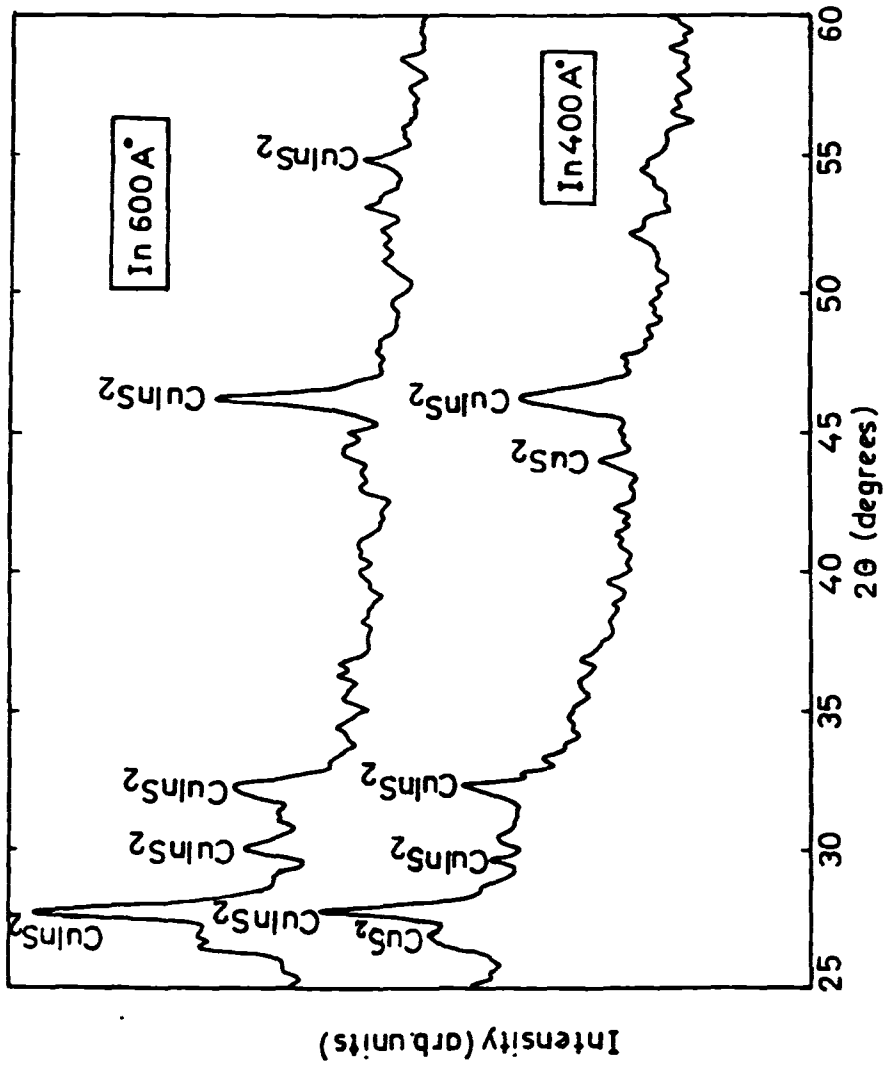


Fig.3.18 XRD of  $\text{CuInS}_2$  sample

Table 3.7

X- ray analysis data of  $\text{CuInS}_2$ 

In 400Å			In 600Å		
d(Å)	(h kl)	Phase	d(Å)	(hkl)	Phase
3.32	(111)	$\text{CuS}_2$	3.21	(112)	$\text{CuInS}_2$
3.21	(112)	$\text{CuInS}_2$	2.97	(103)	$\text{CuInS}_2$
3.03	(103)	$\text{CuInS}_2$	2.77	(200),(004)	$\text{CuInS}_2$
2.78	(200),(004)	$\text{CuInS}_2$	1.97	(220),(204)	$\text{CuInS}_2$
2.06	(220)	$\text{CuS}_2$	1.67	(312),(116)	$\text{CuInS}_2$
1.97	(220)	$\text{CuInS}_2$			

### 3.11.2 XPS Analysis

XPS analysis of the  $\text{CuInS}_2$  films was carried out by investigating Cu, In, S and C spectra, using  $\text{MgK}_\alpha$  line (1253.6 eV) for excitation. (Fig.3.19). Analysis was repeated by removing layers of the film by Ar ion sputtering for 1 minute, 2 minutes and 3 minutes. Binding energy values were corrected with reference to C 1s peak at 284.5 eV. Peaks corresponding to Cu, In & S are clearly visible at binding energies 933.01 eV & 953.4 eV for Cu  $2p_{3/2}$  & Cu  $2p_{1/2}$ , 444.75 eV & 452.42 eV for In  $3d_{5/2}$  & In  $2d_{3/2}$ , and 161.12 eV for S 2p respectively. These values are in agreement with the binding energy values of different elements in  $\text{CuInS}_2$ ; which confirms formation of  $\text{CuInS}_2$  phase.

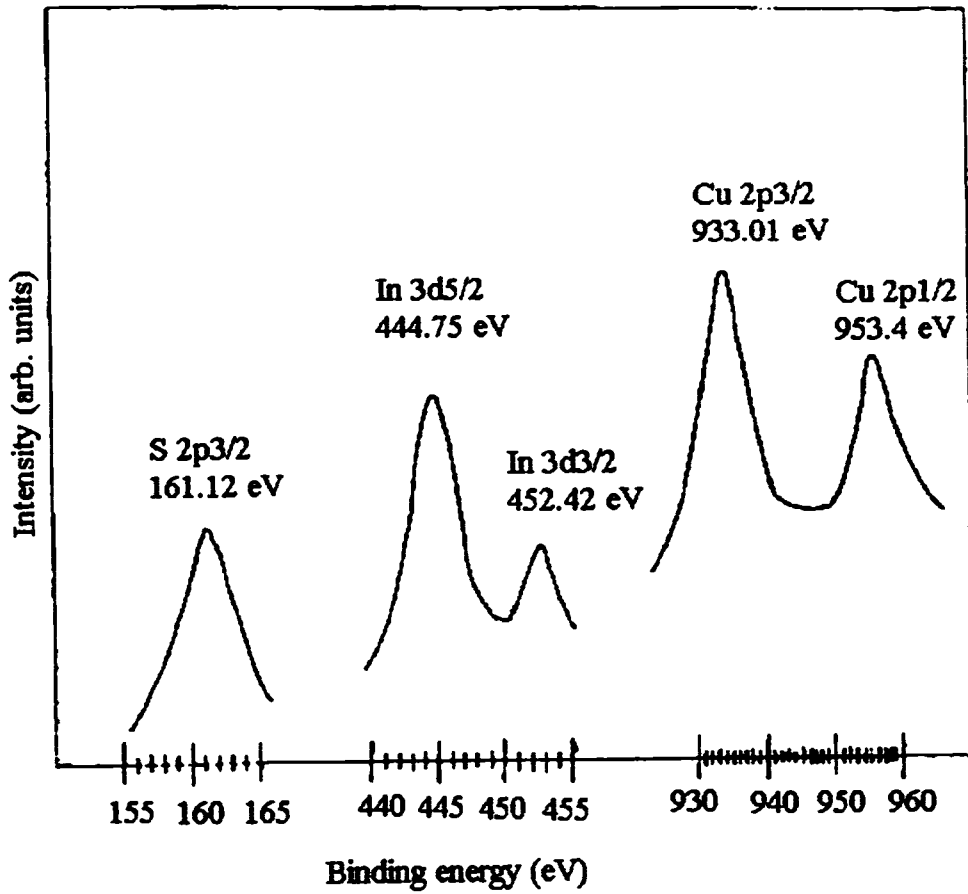


Fig.3.19 XPS of  $\text{CuInS}_2$  sample

### 3.12 Trial for the fabrication of $\text{CuInS}_2/\text{CdS}$ solar cell

In the above section, we saw that it is possible to prepare  $\text{CuInS}_2$  thin films by the thermal diffusion of indium into  $\text{Cu}_x\text{S}$  films, prepared from CBD CdS films. As mentioned earlier,  $\text{CuInS}_2/\text{CdS}$  heterojunction can be fabricated in a quite simple way if the top layer of a sufficiently thick CdS film can be converted into  $\text{CuInS}_2$ . This process has the advantage that it will avoid atmospheric contamination at the interface.

We tried to fabricate  $\text{CuInS}_2/\text{CdS}$  cell using the above-mentioned method.  $\text{SnO}_2$  coated glass plates were used as the substrate and it will serve as the back electrode of the cell. Over this, CdS films of thickness  $1.5\mu\text{m}$  (triple-dipped) were deposited using CBD. These films were then dipped in  $\text{CuCl}_2$  solution kept at a temperature of about  $90^\circ\text{C}$  for 3 seconds so that top layer is converted to  $\text{Cu}_x\text{S}$ . Then  $600\text{\AA}$  indium is evaporated over this film and is annealed at  $300^\circ\text{C}$  for 2 hours. Indium uniformly diffused into the film to form  $\text{CuInS}_2$  layer at the top and hence  $\text{CuInS}_2/\text{CdS}$  structure was fabricated. Silver was used as the top electrode. The I-V characteristic of the cell was measured at an intensity of  $40\text{mW}/\text{cm}^2$  (Fig.3.20). This junction gave a voltage of  $480\text{mV}$ ; but there was no significant current.

Low value of the photocurrent points toward the limitations of the preparation process. In this method, there is a chance of shorting during the dipping process for the preparation of  $\text{Cu}_x\text{S}$  film due to rapid diffusion of highly mobile copper ions through the imperfections in the CdS layer. Also, there may be an inhomogeneous pattern of growth of  $\text{Cu}_x\text{S}$  layer due to the sudden interruption of reaction as soon as the desired thickness is reached. In addition, this process lacks control of stoichiometry.

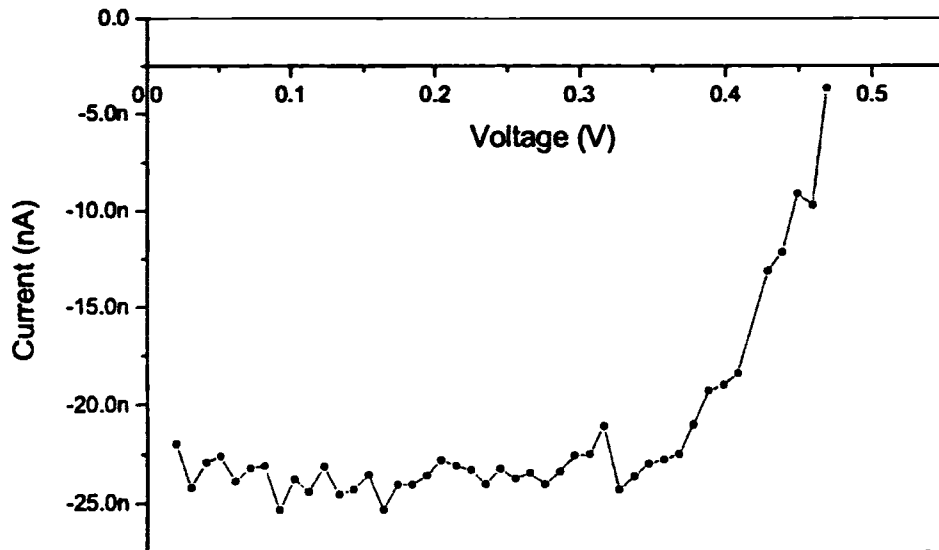


*Fig.3.20 J-V Characteristics of the cell*

### 3.13 CONCLUSION

CuInS<sub>2</sub> thin films were prepared using CBD CdS film and were characterized. Junction was fabricated by converting the top layer of CdS to CuInS<sub>2</sub>. Although open circuit voltage of this junction was quite measurable, current was very feeble.



## References

- [1] S.Bini, K.Bindu, M.lakshmi, C Sudha Kartha, K P Vijayakumar, Y.Kashiwaba, and T.Abe, *Renewable Energy*, 20 (2000) 405
- [2] Sigeyuki Nakamura and Akio Yamamoto, *Sol. Energy Mat. Sol. Cells*, 49 (1997) 415
- [3] Thin film Device Applications, K. L. Chopra and Inderjeet Kaur, Plenum Press, New York, 1983, p-2
- [4] Lakshmi M, Ph.D Thesis, Cochin University of Science and Technology, Kochi, 2001,
- [5] Bindu K, Ph.D Thesis, Cochin University of Science and Technology, Kochi, 2002
- [6] P.Hedenqvist and A.Roos, *Surface and coating Technology*, 48 (1991), L149,
- [7] Robert W. Berry, Peter M. Hall, and Murray T. Harris, 'Thin Film Technology', D.Van Nostrand company, Princeton, (1968), p-113,
- [8] K. L. Chopra and Suhit Ranjan Das, *Thin Film Solar Cells*, Plenum Press, New York, 1983,
- [9] K. L. Chopra, *Thin Film Phenomena*, Kreiger, New York, (1979)
- [10] Cristina Nascu, Ileana Pop, Violeta Ionescu, E. Indrea, and I. Bratu, *Materials Lettres*, 32 (1997); p-73]
- [11] L.D. Partain, P.S. McLeod, J.A. Duisman, T.M. Peterson, D.E.Sawyer, and C.S.Dean, *J.Appl.Phys.*, 54 (1983) 6708
- [12] Kimihiko Okamoto and Shichio Kawai, *Jpn. J. Appl. Phys.*, 12 (1973) 1130
- [13] Aperathitis, F.J. Bryant, and C.G. Scott, *Sol. Energy Mater.*, 20 (1990) 15
- [14] G. A. Armantrout, D.E.Miller, K.E. Vindelov, and T.G.Brown, *J. Vac. Sci. Technol.*, 16 (1979) 212

- [15] E. Fatas, T. Garcia, C. Ontemoyer, A. Media, E. G. Camerevo, and F. Arjona, *Mater. Chem. Phys.*, 12 (1985) 121
- [16] A. J. Varkey, *Solar Energy Mater.*, 19 (1989) 415
- [17] B. Rezig, J. Bougnot, M. El Hammouti, M. Perotin, Vu Bay , and M. Savelli, *Solar Energy Materials*, 9 (1983) 189
- [18] J.I. Pankov, 'Optical processes in semiconductors', Dover publications, New York., (1971); p-34
- [19] Paul S McLeod, Larry D Partain, Dave E Sawyer and Terry M Peterson, *Appl.Phys.Lett.*, 45 (1984) 472
- [20] L Y Sun, L L Kazmerski, A H Clark, *J. Vac. Sci. Technol.*, 15 (1978) 265
- [21] Takahiro Wada, Takayuki Negami and Mikihiko Nishitani, *Appl. Phys. Lett.*, 62 (1993) 1943
- [22] A N Tiwari, D K Pandya and K L Chopra, *Thin Solid Films*, 130 (1985) 217
- [23] M. C. Zouaghi, T. Ben Nasrallah, S. Marsillac, J. C. Bernede, and S. Belgacem, *Thin Solid Films*, 382 (2001)39
- [24] Dieter.K.Schroder, *Semiconductor Material and Device Characterization*, John Wiley & Sons, INC, New York, (1998)]
- [25] L L Kazmerski, M S Ayyagari, and G A Sanborn, *J. Appl. Phys*, 46 (1975) 4865
- [26] J.L Shay and J.H.Wernick, *Ternary Chalcopyrite Semiconductors: Growth, Electronic properties and Applications*, Pergamon Press, Oxford, (1975) p-188
- [27] J.H.Richardson and R.V.Peterson(Ed), *Systematic materials analysis, Vol-II*, Academic press, New York, (1974)
- [28] *Hand Book of Analytical Methods for materials*, (2000), *Materials Evaluation and Engineering, INC*

- [29] Malle Krunk, Valdek Mikli, Oglja Bijakina, and Enn Mellikov, *Applied Surface Science*, 142 (1999) 356
- [30] Rosenberg and Tu, 'Treatise on Materials Science and Technology', Vol-27, Academic Press, 1988, p-65
- [31] Koichi Fukuzaki and Shigemi Kohiki, *Appl. Phys.Lett.*, 73 (1998) 1385
- [32] Poolla Raja Ram, R. Thangaraj, A. K. Sharma, and O. P. Agnihotri, *Solar Cells*, 14 (1985) 123
- [33] W Gaarenstroom and N Weinograd, *J.Chem.Phys.*, 67 (1997) 3500
- [34] M. T. S. Nair, P. K. Nair, R. A. Zingaro, and E. A. Meyers, *J. Appl. Phys.*, 75 (1994) 1557
- [35] T. Sands, J. Washburn, and R. Gronsky, *Solar Energy Materials*, 10 (1984) 349

## Chapter- 4

**STUDIES ON CUINS<sub>2</sub> THIN FILMS PREPARED USING CHEMICAL SPRAY  
PYROLYSIS TECHNIQUE**

4.1 Introduction.....	143
4.2 Experimental Details.....	144
4.3 Variation of Cu/In at 400°C, keeping S/Cu = 4 .....	147
4.3.1 X- ray diffraction.....	148
4.3.2 Optical properties .....	149
4.3.3 Scanning Electron Micrograph .....	151
4.3.4 Electrical properties .....	153
4.3.5 Photosensitivity.....	153
4.3.6 XPS Analysis .....	153
4.4 Variation of deposition temperature.....	155
4.4.1 XRD .....	155
4.4.2 Optical properties .....	158
4.4.2 Electrical properties .....	160
4.4.3 Photosensitivity.....	162
4.5 Variation of (Cu+In)/S ratio, keeping Cu/In = 1.....	163
4.5.1 XRD .....	163
4.5.2 Optical properties .....	163
4.5.2 Electrical properties .....	165
4.5.4 Photosensitivity measurement.....	168
4.6 Variation in Cu/In at 300°C, keeping S/Cu = 4 .....	168
4.6.1 XRD .....	169
4.6.2 Optical properties .....	170

4.6.3 Thickness.....	172
4.6.4 Electrical properties .....	172
4.6.5 Photosensitivity .....	174
4.6.6 XPS .....	174
4.7 Variation in S/Cu ratio, keeping Cu/In = 0.5 .....	178
4.7.1 XRD .....	178
4.7.2 Optical properties .....	179
4.7.3 Electrical properties .....	181
4.7.4 XPS .....	182
4.7.4 Photosensitivity .....	186
4.8 Conclusion.....	186
References .....	191

## Chapter- 4

### STUDIES ON $\text{CuInS}_2$ THIN FILMS PREPARED USING CHEMICAL SPRAY PYROLYSIS TECHNIQUE

#### 4.1 Introduction

Two of the principal requirements for a thin film solar cell material for terrestrial applications are high optical absorption as well as quantum efficiency and low fabrication costs. Several promising materials are currently being investigated in various research laboratories to improve optical/ electrical properties and to reduce process cost.  $\text{CuInS}_2$  is one such material. Even though cell efficiency may not be as high as with competitive materials like Silicon, CdTe and  $\text{CuInSe}_2$ , a very low processing cost and eco friendly nature would allow it to be a good candidate.

Chemical Spray pyrolysis (CSP) deposition, one of the chemical techniques suitable for preparation of thin films, has been applied to deposit a wide variety of thin films. It involves spraying a solution, usually aqueous, containing soluble salts of constituents of the desired compound onto a heated substrate. It is quite suitable for depositing large area thin films using simple apparatus with good reproducibility. Major shortcoming of this technique is that some times it may make films with voids.

CSP was developed in the early 1960s by Hill and Chamberlin and preparation of thin films of certain inorganic sulfides and selenides using this technique was first reported by Chamberlin and Skarman in 1966 [1]. At present, this method is used for preparation of ternary compounds and their quaternary and quinary alloys. Spray pyrolysis of  $\text{CuInS}_2$  and other I-III-VI<sub>2</sub> compounds has been reported by Pamplin *et al.* in 1979 [2]. Electrical and structural properties of  $\text{CuInS}_2$  thin films prepared using spray pyrolysis has been reported by Gorska *et al.* [3]. Hernandez *et al.* reported structural, kinetic and optical properties of spray pyrolysed  $\text{CuInS}_2$  films [4]. Again in a

very recent paper, Marsillac et al. reported the post-annealing treatment of spray-deposited  $\text{CuInS}_2$  films [5]. An attempt to evaluate the content of chlorine, oxygen, carbon and nitrogen impurities in sprayed films was made by Krunks et al.[6].

One of the major problems with preparation of ternary chalcopyrites like  $\text{CuInS}_2$  is the control of stoichiometry, i.e., control of the excess copper content and of the copper-to-indium and metal to chalcogen ratios. Interestingly in CSP technique, ratios of the constituent elements can be easily varied by controlling their concentration in the spray solution. In the present investigation, we varied the copper-to-indium and metal to chalcogen ratio in a wide range, at different growth temperatures. By means of detailed analysis of these films, we obtained further information about film resistivity and photosensitivity as a function of the composition in the solution. This information is helpful when designing solar cells made using this material. This chapter describes preparation and characterization of  $\text{CuInS}_2$  films prepared using CSP.

## 4.2 Experimental Details

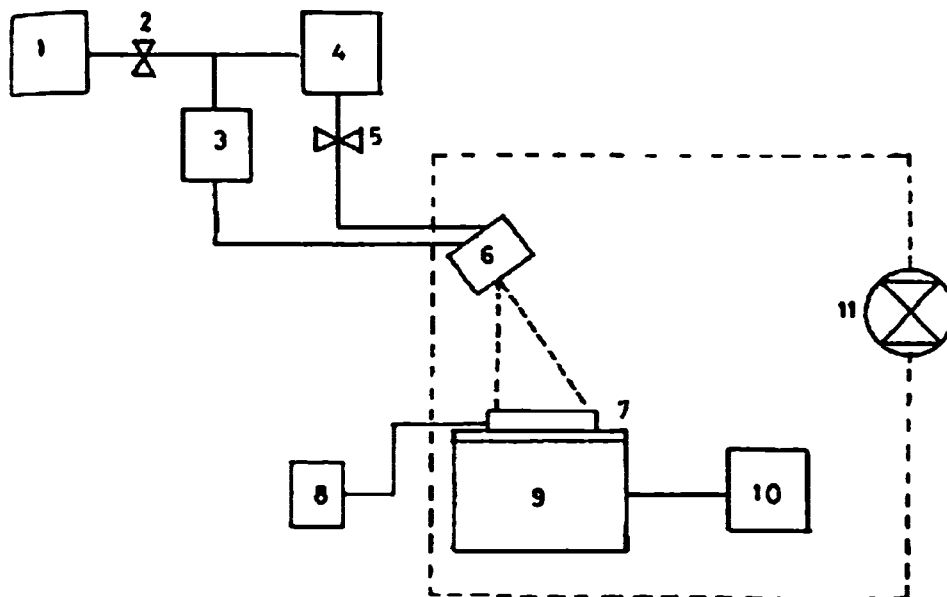
Experimental set-up for the deposition is schematically shown in Fig.4.1. Cleaned glass slides were placed on a thick iron block ( $15 \times 9 \times 1 \text{ cm}^3$ ), which can be heated to the required temperature with a controlled heater. Temperature of substrate holder was measured using a digital thermometer (Thermins, series 4000) and temperature control was achieved using a variable transformer. Spray head and heater with substrate are kept inside a chamber provided with an exhaust fan for removing gaseous by-products and vapor of the solvent (here water). During spray, temperature of substrate was kept constant with an accuracy of  $\pm 5^\circ\text{C}$ . Pressure of carrier gas was noted using a manometer and was kept at  $90 \pm 0.5$  cm. of Hg. Spray rate was 15ml/min., and distance between spray head and the substrates was  $\sim 15$ cm. In order to get uniform

composition and thickness, spray head was moved to either side manually with uniform speed.

CuInS<sub>2</sub> thin films were deposited over glass substrates from aqueous solutions of cupric chloride (CuCl<sub>2</sub>·2½H<sub>2</sub>O), indium tri chloride (InCl<sub>3</sub>), and thiourea (CS (NH<sub>2</sub>)<sub>2</sub>) using compressed air as the carrier gas. Thiourea was chosen as the source of sulfur ions in spray solution because it avoids precipitation of metallic sulfides and hydroxides since it forms complexes with copper and indium ions easily [7]. Aqueous solutions of these salts were prepared in distilled water, and Cu/In ratio and S/Cu ratio in spray solutions were varied. Substrates were kept at different temperatures in order to study its effects on the deposited films.

We varied deposition temperature from 200°C to 400°C, Cu/In ratio from 0.5 to 1.5 and S/Cu ratio from 4 to 8. Even though deposition and characterization of CuInS<sub>2</sub> thin films using spray pyrolysis was reported previously by several groups [8-10], such wide variation in composition of spray solution has not been reported yet. Structural, electrical, optical and composition analysis of all these films were done. Photosensitivity of these films were measured and obtained conditions for depositing films with good photoresponse (87%). To the best of our knowledge, such study has not been conducted for CuInS<sub>2</sub> thin films prepared from solutions with wide compositional variations. Each of these cases will be discussed in the following sections.





- |                                |                           |
|--------------------------------|---------------------------|
| 1. Air compressor              | 2. Gas flow control valve |
| 3. Manometer                   | 4. Solution reservoir     |
| 5. Solution flow control valve | 6. Spray head             |
| 7. Substrate                   | 8. Thermometer            |
| 9. Substrate heater            | 10. Heater control        |
| 11. Exhaust fan                |                           |

*Fig.4.1 Experimental set up for spray pyrolysis system*

### 4.3 Variation of Cu/In at 400°C, keeping S/Cu = 4

Cu/In ratio in the solution was varied by adding appropriate amounts of indium chloride with respect to a fixed concentration of copper in the form of  $\text{CuCl}_2 \cdot 2 \frac{1}{2} \text{H}_2\text{O}$ . At first, Cu/In molar ratio in spray solution was varied as 0.9, 1 & 1.1. It was already reported that because of loss of chalcogen during pyrolysis process, the amount of sulfur relative to copper in the spray solution should be at least double that required theoretically for stoichiometry [11]. Hence to compensate the loss of sulfur during spraying, S/Cu molar ratio was fixed at 4. The samples are named A, B, & C respectively. Composition of the spray solution was:

$\text{CuCl}_2 \cdot 2 \frac{1}{2} \text{H}_2\text{O}$  – 0.025M ; 100ml

$\text{CS}(\text{NH}_2)_2$  -0.1M ;100ml

$\text{InCl}_3$  – 0.0277M (for sample A ) , 0.025M (sample B ) , & 0.022M(sample C ) ;100ml

In all cases, pH of solution was kept at 3. The deposition temperature was 400°C. Glass slides (37.5mm×12.5mm×1.25mm) cleaned as described in section 5.2.1 were placed on the substrate holder and were heated to the required temperature. These were kept in that stabilized temperature for one hour and then solution was sprayed at a rate of 15ml/min. After completion of spray, the samples were kept at the same temperature for ½ hour and were then allowed to cool at a rate of 3°C/min.

$\text{CuInS}_2$  is formed by pyrolytic decomposition of sprayed droplets on the surface of the heated substrates. Films obtained were extremely adherent to the substrates and were homogeneous in appearance. In order to characterize these films, structural, optical and electrical studies were carried out.

### 4.3.1 X- ray diffraction

X-ray diffraction patterns of the films are shown in Fig.4.2. They show good crystallinity with preferred orientation along (112) direction. Peak intensity is maximum for sample A, but the peak is sharper for sample B. For sample C (Cu/In = 1.1), peak height is very much less than that obtained for sample A.

Grain size was calculated from the (112) peak using Scherrer's formula and is tabulated in Table 4.1. Among the three samples, sample B has the largest grain size.

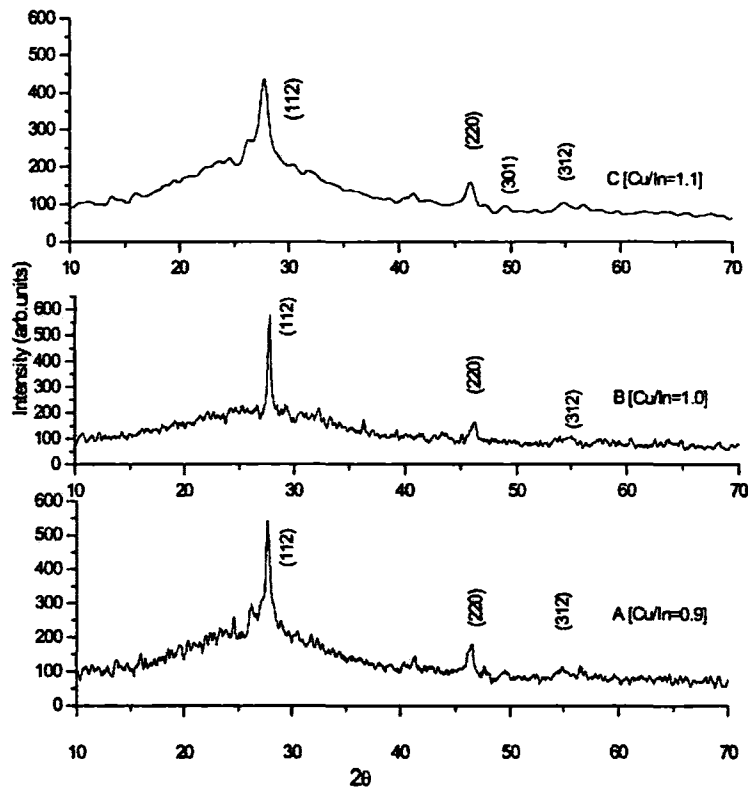


Fig.4.2 X-ray diffraction pattern of samples A, B & C

Table-4.1. Grain size of samples A,B &amp; C

Sample	A	B	C
Grain size (nm)	23	30	16

### 4.3.2 Optical properties

Figure 4.3 shows the transmission (T) as a function of wavelength for samples A, B & C. Transmission decreases sharply after a particular wavelength and onset of the decrease represents the fundamental absorption edge [12]. It was observed that this onset shifted slightly towards lower wavelength side as Cu/In ratio in the spray solution increased.

To calculate value of the bandgap, a graph with  $(\alpha h\nu)^2$  against  $h\nu$  was plotted for region near and above the fundamental absorption edge (Figure 4.4). Extrapolated intercept on  $h\nu$  axis gave value of the bandgap. From the graph, band gaps obtained for samples A & C are 1.42eV. For sample B, band gap is 1.4 eV. Band gap of sprayed films is expected to be lower than that of single crystal as a result of appearance of an exponential or nearly exponential absorption tail, due to the formation of density of states tail at band edge [8].

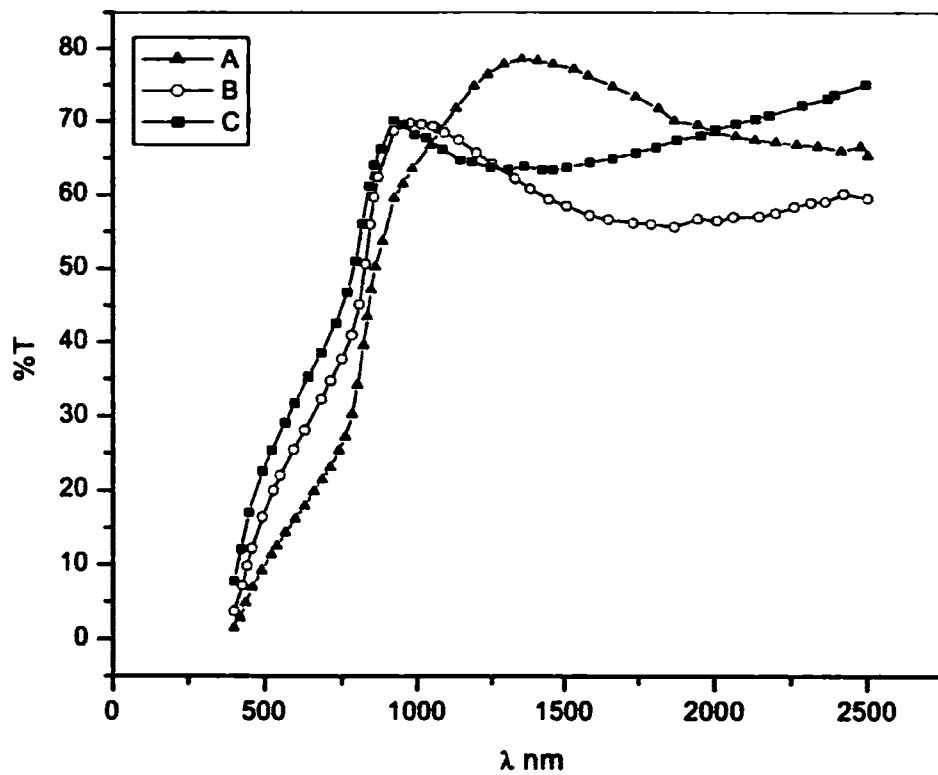


*Fig.4.3 Transmission spectra of samples A, B, & C*

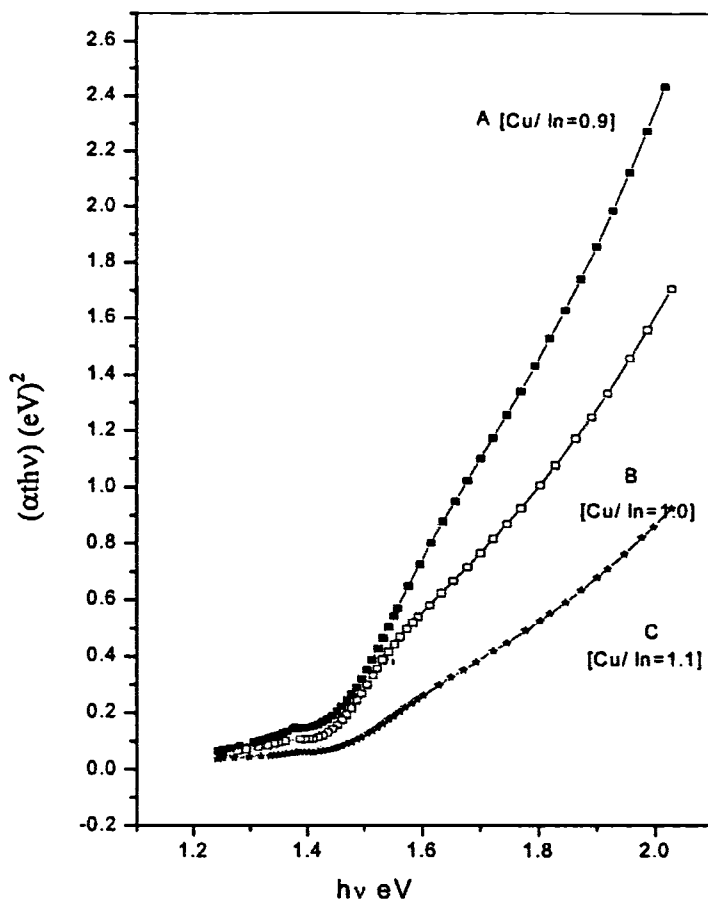
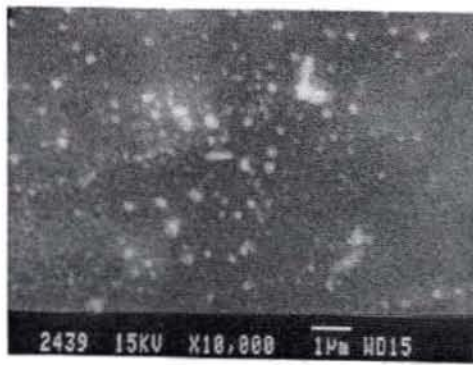


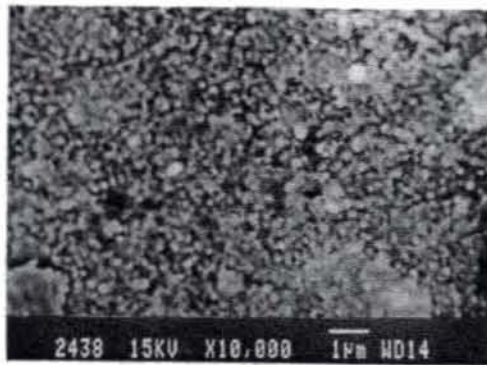
Fig.4.4  $(\alpha hv)^2$  vs.  $h\nu$  plot of A, B, & C

### 4.3.3 Scanning Electron Micrograph

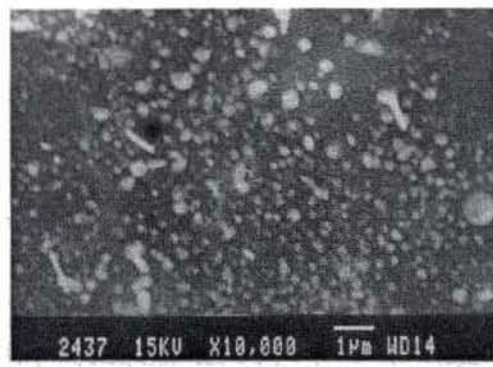
SEM micrographs of the films indicated polycrystalline nature with well-defined circular grains and are shown in Fig.4.5. Among these samples, sample B has better crystalline nature as is evident from XRD as well.



(A)



(B)



(C)

*Fig.4.5 SEM of samples A, B, & C*

#### 4.3.4 Electrical properties

Resistivity, carrier concentrations and mobility of the films were determined using Hall measurement and results are tabulated in Table-4.2. All these films were found to be p-type. Resistivity of these films varies with variation in Cu/In ratio. Sample B (Cu/In =1) had the lowest resistivity (1.21Ω cm). Sample A and C had almost equal resistivity (70 & 60Ω cm. respectively).

Table-4.2 Hall measurement results

Sample	Resistivity ( $\rho$ ) $\Omega$ cm	Mobility ( $\mu$ ) $\text{cm}^2/\text{Vs}$	Carrier density ( $\text{cm}^{-3}$ )	Type of carriers
A	70	4.73	$1.88 \times 10^{16}$	holes
B	1.21	2.24	$2.29 \times 10^{18}$	holes
C	60	103	$1 \times 10^{15}$	holes

#### 4.3.5 Photosensitivity

Photosensitivity (S) was determined from measured values of resistance of the film in darkness and under an illumination of  $40\text{mW}/\text{cm}^2$ , as described in section 3.7.4. Values obtained for samples A,B,& C are 13.8%, 14.2%, and 27.8% respectively. Here sample C was found to be better in photosensitivity.

#### 4.3.6 XPS Analysis

Atomic concentration percentage (at.%) of different elements present in these samples was compared using XPS depth profile. In all the cases, Cu/In ratio in film was found to be greater than that in spray solution. Also, these samples are found to be deficient in sulfur. Table-4.3 gives approximate atomic concentration % of different elements present in the sample. Results of XPS analysis of sample B prepared at a lower temperature of  $250^\circ\text{C}$  are also included in the table.



Table-4.3 Atomic percentage from XPS analysis

Sample	Cu %	In %	S %	O %	Cu/In	(Cu+In)/S
A	44	24	27	5	1.83	2.51
B	44	24	28	4	1.83	2.42
C	40	25	31	4	1.6	2.09
B(L.T)	35	28	35	2	1.25	1.8

From Table 4.3, it is evident that for the sample prepared at low temperature, at.% of S and Cu/In ratio is better. Depth profile of atomic concentration of sample B is shown in Fig.4.6. All the elements are almost uniformly present throughout the thickness of the sample.

Even though air was used as the carrier gas for spraying, only 2-5% of oxygen is present in these films, and for the sample prepared at low temperature, at. % of oxygen is only 2%.

Binding energy values obtained for different elements are in conformity with earlier reported values. XPS depth profile showing binding energy of one of these samples (sample B) is shown in Fig. 4.7. There is one peak corresponding to oxygen at the surface. This peak situated at binding energy of 531.75eV can be attributed to elemental oxygen due to surface contamination [10]. After etching, this contribution decreases strongly, which confirms that this is due to surface contamination itself.

Peaks corresponding to all elements are very slightly shifted as the analysis proceeds from the surface to the substrate. This is due to the influence of the substrate

as it is possible that all these elements may slightly diffuse into the glass substrate during deposition.

From above analysis, it is found that high substrate temperature does not favor better stoichiometry of  $\text{CuInS}_2$  films. In order to optimize growth temperature, sample B was prepared at different temperatures.

#### 4.4 Variation of deposition temperature

$\text{CuInS}_2$  films were prepared using CSP over glass substrates heated to different temperatures ranging from 200 °C to 400 °C, keeping composition of the spray solution same as that used for the preparation of sample B. i.e., using the solution in which  $\text{Cu/In} = 1$ , and  $\text{S/Cu} = 4$ . At 200 °C, the films formed were not uniform and had several pinholes and adhesion was very poor. Films prepared at higher temperatures (like 380°C and 400 °C) appeared thinner than those prepared at lower temperatures. Characterization of all these films was done using different techniques and these are described below

##### 4.4.1 XRD

As growth temperature increases, crystallinity of the films improves as indicated in Fig. 4.8. Good crystallinity was achieved between 350 °C and 400 °C. Preferred orientation of the crystallites is along the (112) plane. Peak corresponding to (220) plane is visible only for samples prepared above 300 °C. Grain size of these samples is listed in Table-4.4. From which, it is clear that grain size increases with deposition temperature.































































































































































